Graduate School ETD Form 9
(Revised 01/14)

PURDUE UNIVERSITY
GRADUATE SCHOOL
Thesis/Dissertation Acceptance

This is to certify that the thesis/dissertation prepared

By Masoud Vaezi

Entitled
MODELING AND CONTROL OF HYDRAULIC WIND POWER TRANSFER SYSTEMS

For the degree of Master of Science in Mechanical Engineering

Is approved by the final examining committee:

Dr. Afshin Izadian

Dr. Sohel Anwar

Dr. Likun Zhu

To the best of my knowledge and as understood by the student in the *Thesis/Dissertation Agreement. Publication Delay, and Certification/Disclaimer (Graduate School Form 32)*, this thesis/dissertation adheres to the provisions of Purdue University's "Policy on Integrity in Research" and the use of copyrighted material.

Dr. Afshin Izadian

Approved by Major Professor(s): _____

_____

Approved by: Dr. Sohel Anwar 07/28/2014

Head of the Department Graduate Program Date

MODELING AND CONTROL OF HYDRAULIC WIND POWER TRANSFER SYSTEMS

A Thesis
Submitted to the Faculty
of
Purdue University
by
Masoud Vaezi

In Partial Fulfillment of the
Requirements for the Degree
of
Master of Science in Mechanical Engineering

August 2014
Purdue University
Indianapolis, Indiana

First and foremost, I have to thank my parents for their love and support throughout my life. Thank you both for giving me strength to reach for the stars and chase my dreams. My sisters and brothers deserve my wholehearted thanks as well.

To all my friends, thank you for your understanding and encouragement in my many, many moments of crisis. Your friendship makes my life a wonderful experience. I cannot list all the names here, but you are always on my mind.

Finally, I would like to leave the remaining space in memory of Mohammad Vaezi (1970-2013), my lovely older brother.

ACKNOWLEDGEMENTS

I would like to thank Dr. Afshin Izadian for his endless academic and financial support during my research and study, and provisions above the academic contexts. I would like to thank Dr. Sohel Anwar for all his scientific and financial support during my studies. I would like to thank my committee members for their assistance and supervision in preparation of this thesis. Finally, I reserve special thanks for my family, for their boundless mental, emotional, and financial support during my hard work.

TABLE OF CONTENTS

Page

Page

LIST OF TABLES

LIST OF FIGURES

Figure Page

Figure Page

Figure Page

Figure Page

ABSTRACT

Vaezi, Masoud. M.S.M.E., Purdue University, August 2014. Modeling and Control of Hydraulic Wind Power Transfer Systems. Major Professors: Afshin Izadian and Sohel Anwar.

Hydraulic wind power transfer systems deliver the captured energy by the blades to the generators differently. In the conventional systems this task is carried out by a gearbox or an intermediate medium. New generation of wind power systems transfer the captured energy by means of high-pressure hydraulic fluids. A hydraulic pump is connected to the blades shaft at a high distance from the ground, in nacelle, to pressurize a hydraulic flow down to ground level equipment through hoses. Multiple wind turbines can also pressurize a flow sending to a single hose toward the generator. The pressurized flow carries a large amount of energy which will be transferred to the mechanical energy by a hydraulic motor. Finally, a generator is connected to the hydraulic motor to generate electrical power. This hydraulic system runs under two main disturbances, wind speed fluctuations and load variations. Intermittent nature of the wind applies a fluctuating torque on the hydraulic pump shaft. Also, variations of the consumed electrical power by the grid cause a considerable load disturbance on the system.

This thesis studies the hydraulic wind power transfer systems. To get a better understanding, a mathematical model of the system is developed and studied utilizing the governing equations for every single hydraulic component in the system. The

mathematical model embodies nonlinearities which are inherited from the hydraulic components such as check valves, proportional valves, pressure relief valves, etc.

An experimental prototype of the hydraulic wind power transfer systems is designed and implemented to study the dynamic behavior and operation of the system. The provided nonlinear mathematical model is then validated by experimental result from the prototype.

Moreover, this thesis develops a control system for the hydraulic wind power transfer systems. To maintain a fixed frequency electrical voltage by the system, the generator should remain at a constant rotational speed. The fluctuating wind speed from the upstream, and the load variations from the downstream apply considerable disturbances on the system. A controller is designed and implemented to regulate the flow in the proportional valve and as a consequence the generator maintains its constant speed compensating for load and wind turbine disturbances. The control system is applied to the mathematical model as well as the experimental prototype by utilizing MATLAB/Simulink and dSPACE 1104 fast prototyping hardware and the results are compared.

1. INTRODUCTION

1.1 Problem Statement

Renewable energies have recently received a great attention as an alternative to fossil fuels. Environmental issues, such as the excess amount of hydrocarbon in the air caused by fossil fuels, have compelled the researchers and engineers to look for new types of renewable energies as well as new ways to increase the efficiency of current renewable energy systems.

Wind power, as one of the most known and most considerable renewable energies, is the conversion of wind energy into a useful form of energy, such as using wind turbines to produce electrical power, windmills for mechanical power, wind pumps for water pumping or drainage, or sails to propel ships.

Large wind farms consist of hundreds of individual wind turbines which are connected to an electric power transmission network. For new constructions, onshore wind is an inexpensive source of electricity, competitive with or in many places cheaper than fossil fuel plants [1]. Offshore wind is steadier and stronger than on land. Offshore farms have less visual impact, but their construction and maintenance costs are considerably higher. Small onshore wind farms can feed some energy into the grid or provide electricity to isolated off-grid locations [2].

Wind power, as an alternative to fossil fuels, is plentiful, renewable, widely distributed, clean, produces no greenhouse gas emissions during operation and uses little land [3]. The effects on the environment are generally less problematic than those from other power sources.

Wind energy generation systems have been improved over the last decade, but the high capital investments and low capacity factors have not been resolved to decrease the cost of the energy [4]. Strong foundations are required to hold the forces applied by the weight of the turbine, the gearbox, and the generator and the forces applied by the wind. The typical expected lifetime of a utility wind turbine is 20 years. However, gearboxes require an overhaul in 5 to 7 years of operation, and a gearbox replacement could cost approximately 10 percent of the entire turbine [5], [6]. Conventional wind farms consist of hundreds of wind towers, each of which is equipped with a gearbox and a generator located in a nacelle on top of the tower. Recent developments in hydraulic wind power transfer technology offer several advantages over conventional wind energy transfer technologies [7]-[10].

Hydraulic Wind Power Transfer (HWPT) systems introduce several advantages over the conventional systems. First, HWPT systems replace the bulky gearbox, power electronics and the generator in the nacelle with a single pump. This replacement will reduce a great amount of implementation and maintenance cost. Moreover, the design of the hydraulic circuit in HWPT system allows for generation of fixed frequency electricity power without utilizing power electronics. This benefit will considerably shrink the capital costs and operation costs. Figure 1.1 illustrates the schematic of HWPT systems.

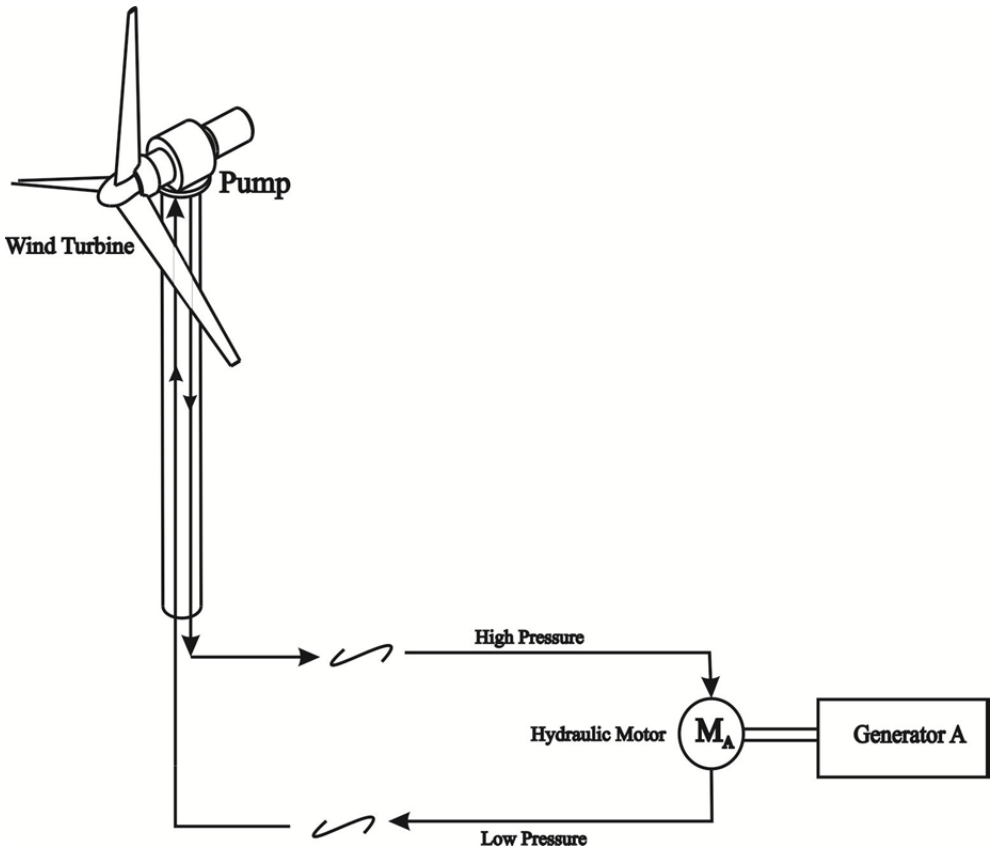

Figure 1.1 Schematic of hydraulic wind power system

Finally, the flexibility of hydraulic circuits will offer a new configuration for wind farms. In this new configuration, a single generator can be utilized for multiple wind turbines rather than implementing one generator for one wind turbine in conventional wind farms. In Addition, the generator used in HWPT systems can be located on the ground which is of high importance to decrease the capital and operation cost. Figure 1.2 shows the schematic of multi-turbine HWPT systems.

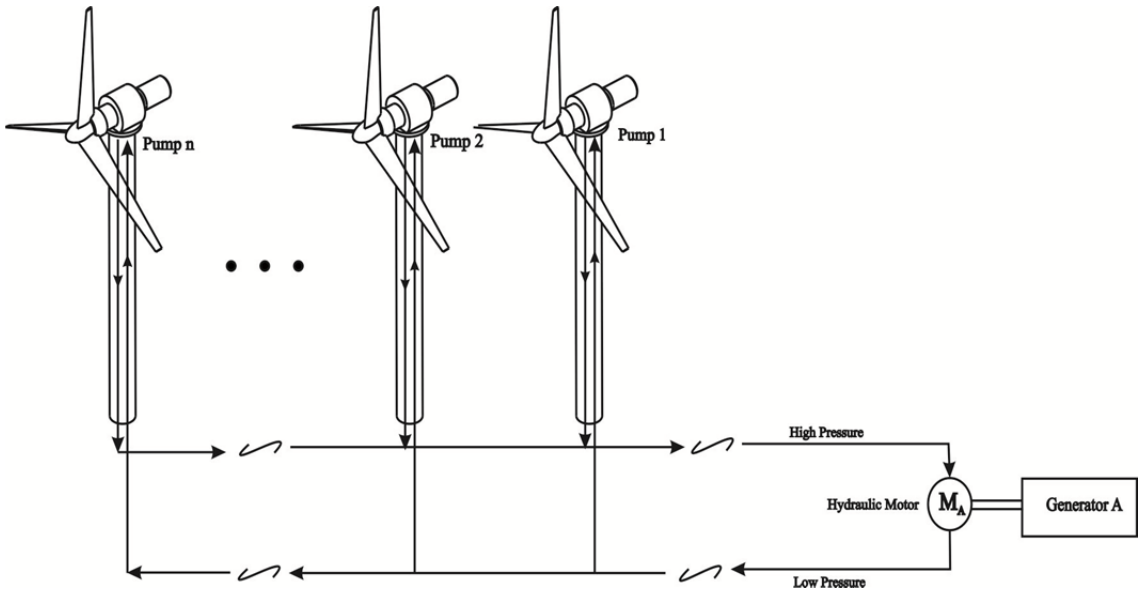

Figure 1.2 Schematic of multi-turbine HWPT systems

1.2 Previous Work

Transferring the energy via a hydraulic circuit has been considerably studied throughout recent decades. Engineering fields such as hybrid vehicles, heavy duty machines, automation, manufacturing, power systems and etc. are utilizing hydraulic circuits as mean to transfer the energy [11].

Hydraulic Transmission System (HTS) is widely spreading because of its functionality and benefits. Quick response time, decouple dynamic, easy implementation, durability are some of the advantages for these type of systems [12]. Different applications of hydraulic transmission systems include: earth moving equipment and machinery [13], oil industry [14], hydrostatic transmission systems [15], servo applications [16], and other actuation purposes [17].

1.3 Objectives

Hydraulic wind power transfer systems as a new generation of wind turbines require a great amount effort and study to be completely understood and implemented. This thesis studies modeling and control of hydraulic wind power systems in order to contribute to the ongoing research on these systems for their development and improvement.

The main objective of this project is to understand the dynamic behavior of hydraulic wind power transfer systems in order to design a control system for a better operation. The first step is to study the hydraulic components of these systems as well as their design and operation. This goal is carried out by studying dynamic principles of the hydraulic components such as hydraulic pumps, hydraulic motors, check valves, proportional valves, pressure relief valves, hoses and etc. Using these governing equations, the mathematical model of the system for different configurations is derived. Nonlinearities in the components result in a nonlinear mathematical model which needs to be well-understood and studied.

To validate the derived model by the governing equations, an experimental setup is designed and implemented as a test-bed for further research. This experimental system includes various hydraulic components and sensors. A fast prototyping hardware dSPACE 1104 is utilized to acquire the speed, flow rate, and pressure data from hydraulic system. This device also enables application of desired commands to the actuators. The implemented setup helps a better understanding of hydraulic wind power transfer systems in order to improve the design and operation.

Another objective of this thesis is to design a flawless control system to improve the operation. The intermittent nature of wind speed as well as grid load disturbances greatly affect the desired outputs. Therefore, this is essential to study the system dynamic in order to compensate for disturbances through an accurately designed controller. Moreover, nonlinearities such as hysteresis in the proportional valve make the design of the control loop more challenging. Thus, the designed controller is required to address this behavior.

1.4 About This Thesis

This thesis is organized as follows: Chapter 2 introduces the concept of hydraulic wind power transfer systems. Operation of these systems is explained and in the last section, the experimental prototype of the hydraulic system is described. System components as well as data acquisition approach are also introduce in this chapter.

Chapter 3 initially studies the governing equations of the hydraulic components. Hydraulic pumps and motors, check valve, proportional valve, and etc. are some of the components which are mathematically studied. Using the dynamic principles, next section introduces mathematical nonlinear models for both load-controlled system and valve-controlled system. In the load-controlled system, the flow is split between the primary and auxiliary motor based on the load torque on the hydraulic motors as inputs to the system. Utilizing a proportional valve in the way of flow to the generator, the system can be controlled by a command to the valve. Valve-controlled system splits the flow in respect to position of the valve spool. Derived nonlinear mathematical models are then verified by the experimental results from the prototype.

Chapter 4 makes a successful attempt to identify the valve-controlled system by running it over in different operating points. Recording and studying a large amount of experimental inputs and their correspondent outputs, the prototype as black box is identified and modeled by a bank of linear models. The existing hysteresis in the proportional valve is compensated by a new approach. Finally, the bank of model is validated by the experimental results from the prototype running in various conditions.

Chapter 5 studies the derived mathematical model for better controller design. utilizing the existing theories of linear systems, the nonlinear system is linearized by a novel algorithm. One of the challenges to linearize nonlinear systems with a wide range operating points is to find the best number of operating points as well as their effectiveness in modeling. This section proposes a new approach to come up with the optimum linearization of these systems. In the last section, the linearized models are studied by standard stability theories developed for linear systems.

Finally, Chapter 6 utilizes the linear bank of model to design an observer for the system in order to estimate some of the distorted state variables. In addition, a well-structured control system, multiple-model adaptive control, is designed and simulated for the bank of model to run the system in desired conditions. Moreover, a control system is designed and implemented for the experimental prototype to maintain the constant speed for primary motor.

2. HYDRAULIC WIND POWER TRANSFER SYSTEMS

2.1 Introduction to the Hydraulic System

Hydraulic wind power transfer technology provides a platform for lightweight wind power generation and transfer systems [8]. Figure 2.1 illustrates the hydraulic wind power transfer technology where a pump coupled with the wind turbine is used to generate high-pressure hydraulic fluid to transfer the power. The pressurized fluid, generated by the hydraulic pumps, is directed to run the generators on the ground level [18].

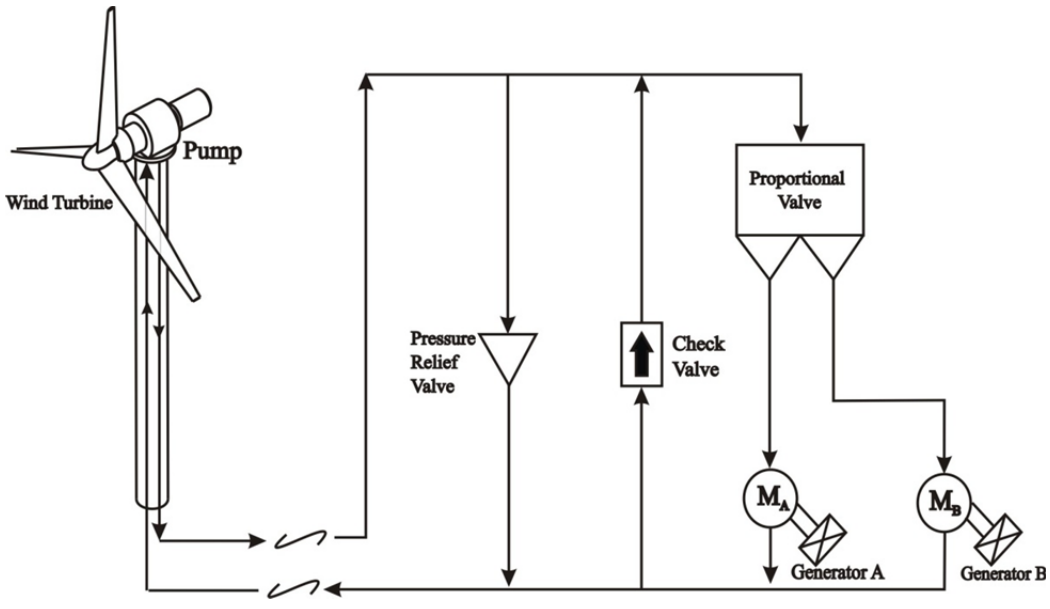

Figure 2.1 Schematic of the high-pressure hydraulic power transfer system. The hydraulic pump is a distance from the central generation unit

By distributing the flow between the hydraulic motor-generators, the energy transfer system performance can be controlled [19]. Figure 2.1 illustrates the hydraulic circuitry of a single-turbine wind power transfer system. Nonlinearities in such systems result from nonlinear components such as check valves, directional valves, and proportional valves. These nonlinearities are functions of operating conditions and cause behavioral changes and variations in the system as the wind speed varies. The intermittent nature of the wind affects the prime mover characteristics by causing fluctuations in fluid circulation, system pressure, and the generated power [20]. To control the characteristics of the generated power (e.g. the generated power and frequency) at high wind speed, different control techniques can be applied [21], [22]. At high wind speeds, the amount of generated power exceeds the system losses and is enough to maintain the fixed speed of the main generator. The auxiliary generator is used to absorb the excess power. Thus, the rated speed of the generators and the high pressure of the system keep the damping coefficients and viscous losses of the hydraulic wind energy transfer system constant. As the wind speed drops, the auxiliary motor is used to control the speed and the generated power by maintaining the fluid rate and the pressure at the main generator. As the storage connected to the auxiliary generator is exhausted, the system can no longer maintain the power to the main generator. Thus, the main generator is shut down, and the auxiliary generator is used to capture the energy of the low-speed wind. If the wind turbine's cut-in speed is decreased, the system operation at low rpms suggests a boost in the capacity factor of the power plant. However, in low wind speed, the pump shaft speed drops such that the viscosity losses and damping coefficients become dependent on the rotational speeds.

2.2 Operation of the Hydraulic System

The Hydraulic Wind Power Transfer System (HWPTS) is based on converting wind power to fluid power and then converting to electricity at the generator. HWPTS consists of a hydraulic pump, a proportional valve and hydraulic motors connected to the generator. Wind turbine harvest wind energy is the form of aerodynamical torque. This torque derives the pump and the pump provides flow to the fluid carriers, pipes, tubes or hoses [23]. The flow enters the proportional valve and is split between to branches. One branch is directed to the main hydraulic motor and the other one connects to the auxiliary motor. Safety component like pressure relief valve and check valves protect the hydraulic circuit against over pressure and undesired flow direction. Both motors and the pump have fixed displacement pump which means that certain amount of fluid is passed across them per revolution. The feature of fixed displacement makes the system economical. Since the wind turbine generates a large amount of torque at a relatively low angular velocity, a large displacement hydraulic pump is required to flow a large volume of the high-pressure hydraulics to transfer the power to the generators. The pump may also be equipped with a fixed internal speed-up mechanism. Flexible high-pressure pipes/hoses connect the pump to the piping toward the central generation unit.

The proportional valve is a flow control mechanism in hydraulic circuits. The valve splits the inlet flow between two outlets at a ratio determined by the command from the valve controller. A schematic diagram of a wind energy hydraulic transmission system is illustrated in Figure 2.1.

As the figure demonstrates, a fixed displacement pump is mechanically coupled with the wind turbine. The hydraulic motors are coupled with electric generators to

produce electric power in a central power generation unit. Electromagnetic torque of the generator imposes mechanical torque on hydraulic motor shaft which causes the pressure in the pipes or hoses to increase. The pump supplies flow under the pressure. The pump and the motors are positive displacement which means they can supply hydraulic fluid under any working pressure without remarkable flow reduction.

In this configuration, pressure relief valves are considered to protect the system components from the destructive impact of localized high-pressure fluids. In addition, check valves force the hydraulic flow to be unidirectional. Finally, the proportional valve distributes a controlled amount of flow to each hydraulic motor to be converted to the electrical power by the generators. The next section introduces the experimental prototype of the hydraulic system.

2.3 Experimental Prototype of The Hydraulic System

In order to study and analyze the hydraulic wind power transfer systems, an experimental prototype is designed and implemented. This experimental setup can operate under wide range of operating conditions to illustrate the performance of the system. Moreover, the dynamic response of the derived nonlinear mathematical model is validated utilizing the results from this experimental setup. Figure 2.2 shows the schematic diagram of the hydraulic wind power transfer system from which the setup is designed and created. Figure 2.3 depicts the overlay of the experimental hydraulic circuit.

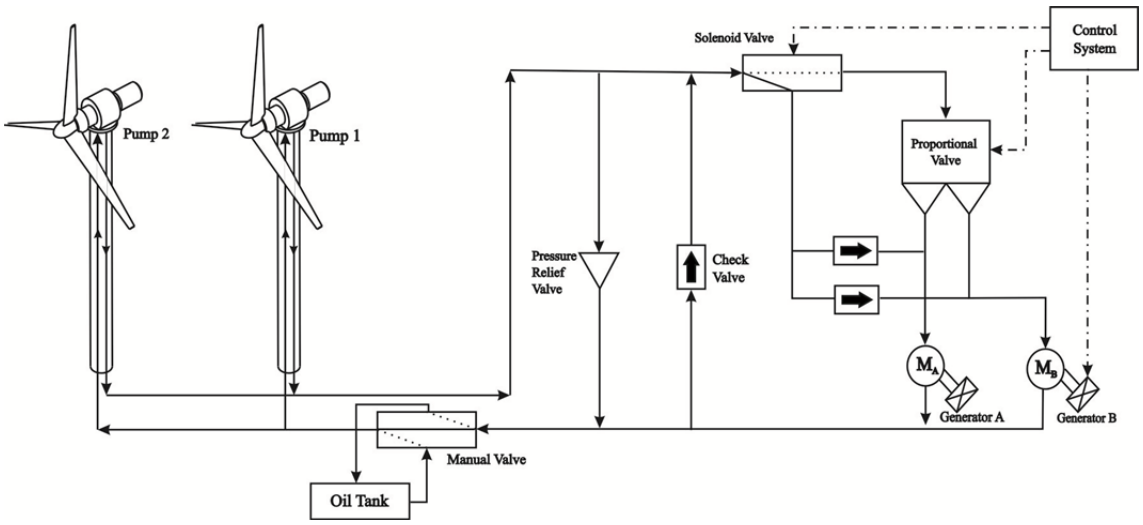

Figure 2.2 Hydraulic circuit schematic of the experimental setup

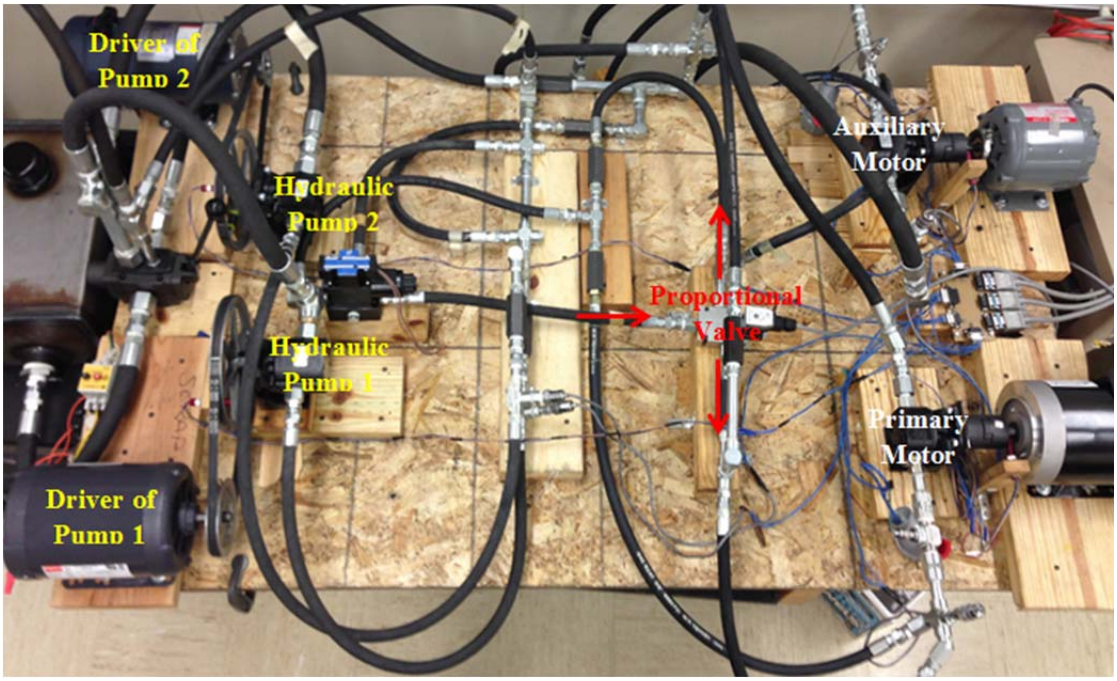

Figure 2.3 The experimental setup of the hydraulic wind power transfer system

In this experimental setup, a DC motor and a 3-phase AC motor are simulating the wind turbine blades. The generated torque by the wind on the wind turbine shaft is simulated by two drivers and a belt and pulley mechanism. This belt and pulley

mechanism is used to reduce the speed of the drivers in order to increase for a higher torque on the pump shaft. The hydraulic pump pressurizes a fluid to the circuit through hoses. The pressurized flow first passes through a 2-way manual valve which switches between open hydraulic circuit and closed hydraulic circuit. In open hydraulic circuit, there is an oil tank added to the system which ejects the trapped air by pushing additional fluid. On the other hand, when the 2-way manual valve is closed, the circuit bypasses the oil tank and presents a closed hydraulic circuit. The flow coming out of 2-way manual valve is sent to the hydraulic motors which are coupled with generators. These generators are connected to a load board which simulates the consumed electrical power by the grid.

To monitor the conditions of the system, several sensors are implemented such as speed sensors, flow sensors, and pressure sensors. The data recorded by these sensors are transmitted to an electrical board which is connected to real-time platform. dSPACE 1104 is a real-time fast prototyping hardware which exchanges the data between the computer and the experimental prototype. The controller is designed and implemented in MATLAB/Simulink which is connected to dSPACE to send the control inputs. In addition, data measured by the sensors are available to be displayed and recorded by utilizing the control desk, additional software of dSPACE. Finally, hydraulic components of the system and the information about their operation are flawlessly represented in [12].

The experimental setup is designed to run under two different configurations: 1) load-controlled configuration, and 2) valve-controlled configuration.

2.3.1 Load-controlled Configuration

The control input to the load-controlled configuration is a load on the generators. In this configuration, the pressurized flow coming out of the hydraulic pumps is split between hydraulic motors, proportional to their current resistive load. The more load is applied to a hydraulic motor; the less flow passes through it. By applying a load profile as a control input, one can regulate the system for a constant speed on the primary motor. Figure 2.4 illustrates the schematic diagram of load-controlled hydraulic circuit.

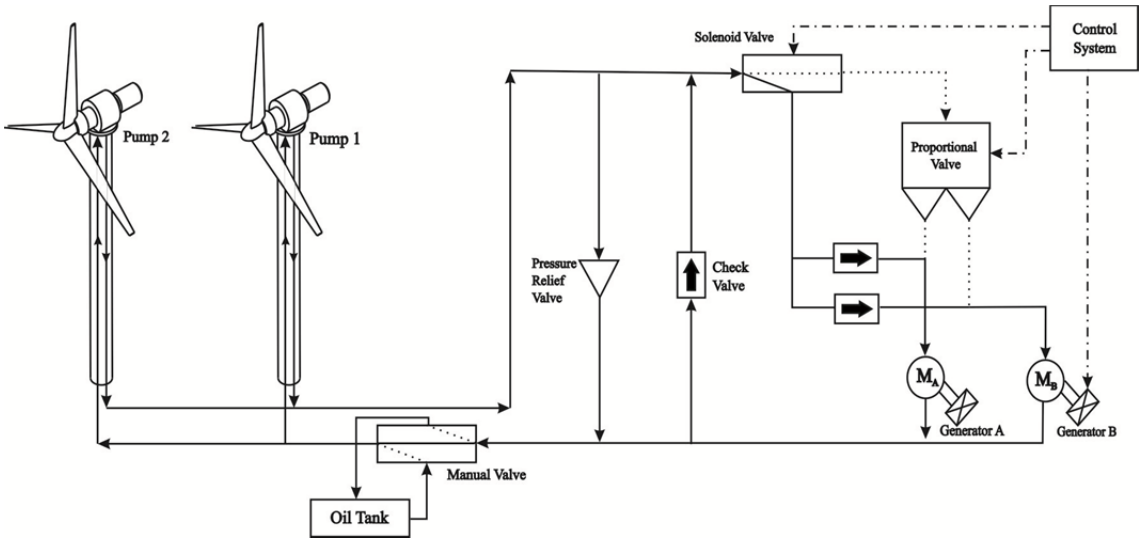

Figure 2.4 Schematic diagram of load-controlled hydraulic circuit

2.3.2 Valve-controlled Configuration

In this configuration, the pressurized flow coming out of the hydraulic pumps passes through a 3-way proportional valve. The position of the valve spool in this configuration determines the amount of flow going to each hydraulic motor. Therefore, the control input to this system is a voltage profile to the proportional. The higher voltage is applied, the less flow passes through the primary motor. A well-designed controller

can actuate the proportional valve to maintain the primary motor speed under disturbances. Figure 2.5 illustrates the schematic diagram of valve-controlled hydraulic circuit.

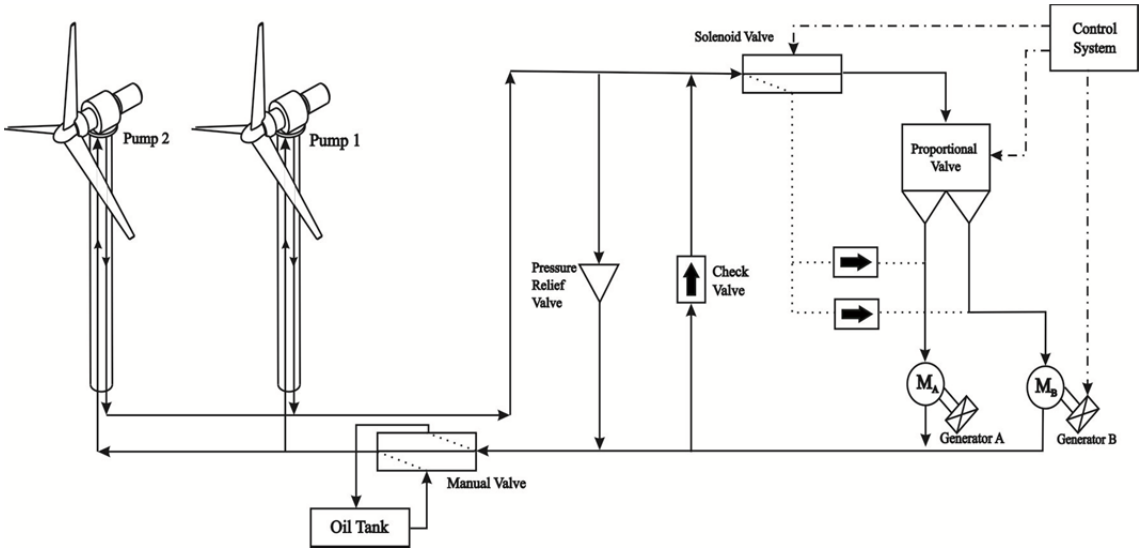

Figure 2.5 Schematic diagram of valve-controlled hydraulic circuit.

3. WHITE BOX MODELING

In this chapter mathematical model of the hydraulic wind power transfer systems is derived by utilizing the governing equations of the hydraulic components in the prototype. The introduced governing equations are put together to build the ordinary differential equations of the closed loop system. Finally, the last section validates the derived ODE model with the experimental results from prototype.

3.1 Governing Equations

To derive the state space representation of the system, the integrated configuration of the hydraulic components must be considered. This section introduces the governing equations of the hydraulic components to obtain the dynamic model of the hydraulic system. To come up with the closed loop system model, flows and torques are calculated by the governing equations of the hydraulic components.

3.1.1 Fixed Displacement Pump

Hydraulic pumps deliver a constant flow [24], [25] determined by:

$$Q_p = D_P\ \omega_P - \frac{C_{Sp}\ D_P}{\mu_p}\ P_p, \tag{3.1}$$

where, $Q_p$is the actual delivered flow, and D_p, ω_p , and P_p are the pump displacement, the angular velocity, and the differential pressure, respectively. C_{Sp} and μ_p are the slippage coefficient and absolute viscosity. As shown in equation (3.1), the actual flow is less than the theoretical flow because of the flow slip in the pump's moving parts. The slippage coefficient is determined by the architecture of the pump and has a great correlation with the clearance of the moving parts. The coefficient is obtained experimentally and is a cubed function of the moving parts' clearance [26]. Therefore, hydraulic manufacturers design the internal mechanism of pumps and motors with minimum clearance of the moving parts and suggest certain operating regions e.g. high rotational speeds. The torque delivered from a pump can be calculated as [24]:

$$T_p = D_p P_p / \eta_{mech,p} \tag{3.2}$$

where $\eta_{mech,P}$ is the pump mechanical efficiency expressed as a function of volumetric $\eta_{vol,P}$and the total efficiency $\eta_{total,P}$ is:

$$\eta_{mech,p} = \eta_{total,p} / \eta_{vol,p} \tag{3.3}$$

3.1.2 Fixed Displacement Motor

The flow and torque equations are derived for the hydraulic motor using the motor governing equations. The hydraulic flow supplied to the hydraulic motor can be obtained by [24]:

$$Q_m = D_m \omega_m + \frac{C_{Sm} D_m}{\mu_m} P_m, \tag{3.4}$$

where D_m, C_{Sm} and μ_m are the motor displacement, the slippage coefficient, and the absolute viscosity. Q_m, ω_m, and P_m are the actual flow passing the motor, the motor velocity, and the differential pressure across the motor terminals.

$$T_m = D_m P_m \eta_{mech,m} \tag{3.5}$$

where $\eta_{mech,m}$ is the mechanical efficiency of the motor and is expressed as:

$$\eta_{mech,m} = \eta_{total,m} / \eta_{vol,m} \tag{3.6}$$

The total torque produced in the hydraulic motor is expressed as the sum of the torques from the motor loads and is given as [24]:

$$I_m \frac{d\omega_m}{dt} = D_m\ P - C_{mv}\ D_m\ \mu\omega_m - C_{mf}\ D_m\ P - T_b - T_L, \tag{3.7}$$

where, T_L and T_b are the net load torque and the breakaway torque and C_{mv}, C_{mf} are the viscous drag coefficient and the mechanical friction (coulomb friction) coefficients. In equation (3.7) all possible retarding torques are considered. C_{mv}, C_{mf}, T_b are the related coefficients to these retarding torques, which are calculated experimentally. Specifically, C_{mv} is a function of the inverse of the clearance between moving parts [26]. For simplicity, the retarding torque elements are lumped into one element represented as a function of motor speed. Hence, equation (3.7) can be re-written as:

$$D_m P_m - B_m \omega_m - T_L = I_m \frac{d\omega_m}{dt}, \tag{3.8}$$

where B_m is the lumped coefficient that includes all retarding torque coefficients.

3.1.3 Hose Dynamics

The dynamics of a hydraulic hose is related to the existing compression through it. The governing equation of the flexible hose is derived from the principles of mass conservation and also bulk modulus and fluid compressibility regarding the system limits. The fluid compressibility model can be expressed as follows [24]:

$$Q_c = (V/\beta)(dP/dt), \tag{3.9}$$

where V is the fluid volume subjected to the pressure effect, β is the fixed fluid bulk modulus, P is the system pressure, and Q_c is the flow rate of the fluid compressibility expressed:

$$Q_c = Q_e - Q_b, \tag{3.10}$$

where Q_b and Q_e are the flow rates at the beginning and the end of the hose, respectively. Thus, we can combine the two equations as follows:

$$\frac{dP}{dt} = \left(Q_e - Q_b\right)\frac{\beta}{V} \tag{3.11}$$

3.1.4 Pressure Relief Valve

The pressure relief valve is a type of valve used to control or limit the pressure in a system or vessel which can build up by a process upset, instrument or equipment failure, or fire. The pressure is relieved by allowing the pressurized fluid to flow from an auxiliary passage out of the system. The relief valve is designed or set to open at a predetermined set pressure to protect pressure vessels and other equipment from being

subjected to pressures that exceed their design limits. Reference [24] represents a simple model for pressure relief valve in opening and closing states:

$$Q_{prv} = \begin{cases} k_v(P - P_v), P > P_v \\ 0 \quad , P \le P_v \end{cases}, \tag{3.12}$$

where K_v is the valve slope coefficient, P is the system pressure, and P_v is the valve's preset opening pressure.

3.1.5 Check Valve

A check valve, clack valve, non-return valve or one-way valve is a valve that normally allows fluid (liquid or gas) to flow through it in only one direction. Check valves are two-port valves, meaning they have two openings in the body, one for fluid to enter and the other for fluid to leave. There are various types of check valves used in a wide variety of applications. For a spring preload check valve [27], the flow rate passing through the check valve can be obtained by:

$$Q_{cv} = \begin{cases} Cl_b \dfrac{(P - P_v)A_{disc}}{k_s}, P > P_v \\ 0 \quad , P \le P_v \end{cases}, \tag{3.13}$$

where Q_{cv} is the flow rate through the check valve, C is the flow coefficient, l_b is the hydraulic perimeter of the valve disc, P is the system pressure, P_v is the valve opening pressure, A_{disc} is the area in which the fluid acts on the valve disc, and K_s is the stiffness of the spring. The dynamics of the pressure relief valves and check valves are not included in the model, as their effects are negligible.

3.1.6 Proportional Valve

Proportional valve is designated to regulate the outlet flow from the pump. These valves impose resistance against the entering flow and thus the flow rate changes at the outlet. When the power is taken from a wind turbine to run an electric generator, the speed needs to be maintained regardless of the load and input power fluctuations. Therefore, a proportional valve is placed between the pump and the motors to control the flow of the primary motor. In a conventional hydraulic system using a proportional valve when inlet flow exceeds the rated flow to the controlled outlet the upstream pressure increases and the surpass flow is bypassed to the tank through a pressure relief valve. To avoid from such energy wasting, a proportional valve with two outlets can be used so that the excess energy is directed to an auxiliary motor. This motor runs to charge a battery or store the energy in a hydraulic accumulator.

Flow from a proportional valve is controlled by its orifice area. Since the valve splits the flow between two outlets, the orifice areas of the outlets are complementary. It means that when one area opens the other one closes. The flow out of an orifice in a proportional valve is calculated using [25]:

$$Q = C_D A \sqrt{\frac{2\Delta P}{\rho}} \tag{3.14}$$

where A is the orifice area and ΔP is the pressure differential across the orifice. C_D and ρ are discharge coefficient and fluid density. Since the area of the orifice for each outlet is proportional to the valve spool position, the area of each outlet orifice can be expressed as a linear function of the spool displacement, thus an equation can be obtained for the

control flow to the primary motor (motor A) and the excess flow to the auxiliary motor(motor B):

$$Q_{pvA} = C_D \frac{A_{\max}}{h_{\max}} h_i \sqrt{\frac{2}{\rho}(P_p - P_{mA})}$$
$$Q_{pvB} = C_D \frac{A_{\max}}{h_{\max}} (h_{\max} - h_i) \sqrt{\frac{2}{\rho}(P_p - P_{mB})} \quad (3.15)$$

where Q_{PvA} is the flow out of the proportional valve to primary motor and Q_{PvB} is the flow to the auxiliary motor, A_{Max} is the maximum area of the outlet port of the valve and has the same value for both ports, h_i is the spool displacement and h_{Max} is maximum spool displacement [28].

3.2 Load-Controlled Hydraulic System

As mentioned earlier, load-controlled hydraulic system is one of the possible configurations of the hydraulic wind power transfer systems which is controlled by the external loads on the hydraulic motors. This section introduces the mathematical modeling of this configuration using the governing equations of the hydraulic components from the previous section.

3.2.1 Mathematical Modeling

Consider a simplified hydraulic power transfer system where the pump flow is distributed between two hydraulic motors based on the natural characteristics and geometry of the hydraulic circuit, namely the natural flow split [29]. In this configuration, the resistance of each hydraulic motor determines the incoming flow. The more load is

applied to the motor; the less flow passes through it. Utilizing this characteristic, one can maintain a desired speed for each motor. Figure 3.1 illustrates the load-controlled configuration.

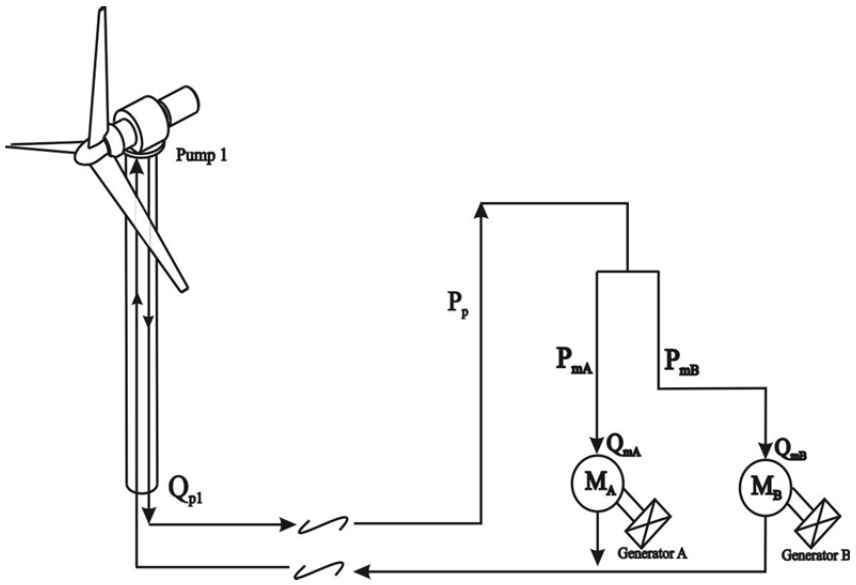

Figure 3.1 Schematic of load-controlled configuration

According to the dynamic equations from the previous section, the flow of the hydraulic pump and motors is as follows:

$$\begin{aligned} Q_p &= D_p\omega_p - k_{L,p}P_p \\ Q_{mA} &= D_{mA}\omega_{mA} + k_{L,mA}P_{mA} \\ Q_{mB} &= D_{mB}\omega_{mB} + k_{L,mB}P_{mB} \end{aligned} \tag{3.16}$$

The subscript m_A and m_B correspond to hydraulic motor A and hydraulic motor B, respectively. Also, properties of the pump is represented by the subscript *p*.

Based on the compressibility of the flow in hoses, we have:

$$Q_c = (V/\beta)(dP/dt), \tag{3.17}$$

$$Q_c = Q_p - Q_{mA} - Q_{mB} \tag{3.18}$$

Therefore:

$$dP_p/dt = (Q_p - Q_{mA} - Q_{mB})(\beta/V_p) \tag{3.19}$$

Replacing the equation (3.16) into equation (3.19):

$$dP_p/dt = (D_p\omega_p - k_{L,p}P_p - (D_{mA}\omega_{mA} + k_{L,mA}P_{mA}) - (D_{mB}\omega_{mB} + k_{L,mB}P_{mB}))(\beta/V_p) \tag{3.20}$$

Pressures of the hydraulic motors, P_{mA} and P_{mB} are identical to the pressure of the pump, P_p, if there is no loss in the hoses and hydraulic components such as check valves and solenoid valve. This pressure drop through the hydraulic circuit is proportional to the squared of upstream flow:

$$\Delta P = L * Q_p^{\,2} \tag{3.21}$$

Thus,

$$P_{mA} = P_p - L_{mA} * Q_p^{\,2} \tag{3.22}$$

$$P_{mB} = P_p - L_{mB} * Q_p^{\,2} \tag{3.23}$$

where L_{mA} and L_{mB} are the loss coefficients for motor A and motor B hydraulic lines, respectively.

Based on the equation (3.7), we have four different types of torques on the hydraulic motor shaft. Prime mover torque, DP, external load torque, T_L, and loss torques (frictions and breakaway torque, T_b:

$$T_{friction} = C_{mv}\, D_m\, \mu\omega_m - C_{mf}\, D_m\, P + T_b \tag{3.24}$$

According to [24], one can consider the loss torque as a second degree polynomial of the shaft speed:

$$T_{friction} = C_1 \omega_m^2 + C_2 \omega_m + T_b \tag{3.25}$$

Rephrasing the (3.7):

$$I_m \frac{d\omega_m}{dt} = D_m \ P - (C_1 \omega_m^2 + C_2 \omega_m + T_b) - T_L \tag{3.26}$$

Thus, for both primary and auxiliary motors:

$$\frac{d\omega_{mA}}{dt} = [D_{mA} \ P_{mA} - (C_{1A} \omega_{mA}^2 + C_{2A} \omega_{mA} + T_{bmA}) - T_{LmA}] / I_{mA}, \tag{3.27}$$

$$\frac{d\omega_{mB}}{dt} = [D_{mB} \ P_{mB} - (C_{1B} \omega_{mB}^2 + C_{2B} \omega_{mB} + T_{bmB}) - T_{LmB}] / I_{mB} \tag{3.28}$$

Consequently, equation (3.20), equation (3.27) and equation (3.28) represent the nonlinear state space model. The system and output functions of the nonlinear system can be obtained from the general nonlinear model as

$$\begin{aligned} \dot{x} &= f(x) + g(x)U \\ y &= h(x) \end{aligned} \tag{3.29}$$

where *x* is the state vector, *y* is the output vector, *U* is the input vector, *f(x)*, *g(x)*, and *h(x)* are the system function, input function, and output function, respectively. These functions are dependent on hydraulic pump angular velocityω_p and T_{LmA}, T_{LmB} the external load torques on the motors. The state variable *x* includes the pump pressure, the primary motor angular velocity, and the auxiliary motor angular velocity. The system functions and variables are illustrated as follows:

$$x=\begin{bmatrix} P_p \\ \omega_{mA} \\ \omega_{mB} \end{bmatrix},\quad U=\begin{bmatrix} \omega_p \\ T_{LmA} \\ T_{LmB} \end{bmatrix},\quad y=\begin{bmatrix} P_p \\ P_{mA} \\ P_{mB} \\ \omega_{mA} \\ \omega_{mB} \end{bmatrix}.$$

Therefore, the nonlinear model of the load-controlled system is as follows:

$$f(x)=\begin{Bmatrix} (-k_{L,p}P_p-(D_{mA}\omega_{mA}+k_{L,mA}P_{mA})-(D_{mB}\omega_{mB}+k_{L,mB}P_{mB}))(\beta/V_p) \\ [D_{mA}\ P_{mA}-(C_{1A}\omega_{mA}^2+C_{2A}\omega_{mA}+T_{bmA})]/I_{mA} \\ [D_{mB}\ P_{mB}-(C_{1B}\omega_{mB}^2+C_{2B}\omega_{mB}+T_{bmB})]/I_{mB} \end{Bmatrix} \tag{3.30}$$

$$g(x)=\begin{bmatrix} D_p\,\beta/V_p & 0 & 0 \\ 0 & -1/I_{mA} & 0 \\ 0 & 0 & -1/I_{mB} \end{bmatrix} \tag{3.31}$$

$$h(x)=\begin{Bmatrix} P_p \\ P_p-L_{mA}*Q_p^{\,2} \\ P_p-L_{mB}*Q_p^{\,2} \\ \omega_{mA} \\ \omega_{mB} \end{Bmatrix}. \tag{3.32}$$

In this section the load-controlled system configuration was modeled. This system is controlled by the loads on the hydraulic motors. Next section validates the model structure with the experimental results.

3.2.2 Model Verification with Experimental Data

In this section the nonlinear mathematical model of the load-controlled system configuration is verified with experimental setup. First, the mathematical model is

implemented in MATLAB/Simulink using the same parameters as the experimental setup listed in Table 3.1.

Parameters such as pump and motors displacements, pump and motors leakage coefficients, hydraulic motors friction loss coefficients, loss coefficients of the hydraulic lines, and etc. are experimentally estimated through numbers of experiments on the prototype.

Table 3.1 List of Prototype Parameters Used in Simulation

Symbol	Quantity	Value	Unit
D_p	Pump Displacement	0.7178	in^3/rev
D_{mA}	Primary Motor Displacement	0.258	in^3/rev
D_{mB}	Auxiliary Motor Displacement	0.5343	in^3/rev
K_p	Pump Leakage	0.0017	
K_{mA}	Primary Motor Leakage	0.0057	
K_{mB}	Auxiliary Motor Leakage	0.0050	
I_{mA}	Primary Motor Inertia	32	$lb.in^2$
I_{mB}	Auxiliary Motor Inertia	21	$lb.in^2$
L_{mA}	Primary Motor Line Loss	13.2	
L_{mB}	Auxiliary Motor Line Loss	7.5	
T_{bmA}	Primary Motor breakaway	11.8	lb.in
T_{bmB}	Auxiliary Motor breakaway	14.3	lb.in
μ	Absolute viscosity	1.85×10^{-7}	
β	Fluid Bulk Modulus	183695	psi
ρ	Fluid Density	0.0305	lb/in^3
υ	Fluid Viscosity	15.9869	cSt

A prototype with the parameters listed in Table 3.1 is used to implement the hydraulic wind power transfer technology. The mathematical model developed for load-controlled operation of the prototype and the experimental data are compared in this section to evaluate the accuracy of the model. An electric motor was used to drive the hydraulic pump through the pulley and belt to reduce the pump shaft speed. The system

operating conditions, such as angular velocity and pressures, were precisely measured by fast prototyping in dSPACE 1104 hardware.

For the purpose of validation, a same arbitrary pump shaft speed profile (wind speed input on the system) is applied to both the mathematical model in MATLAB/Simulink and to the experimental setup. No external load is considered to be applied on the hydraulic motors for the simplicity of measurement.

Figure 3.2 attempts to simulate the fluctuation of the wind and as a result, fluctuation of the incoming flow to the hydraulic motors in order to challenge the performance of the parameter estimation and modeling. With this flow fluctuation, pressures of the hydraulic motors and pump as well as hydraulic motors shaft speeds are subject to considerably vary. Figure 3.3 to Figure 3.7 represents the comparison of the results between the derived mathematical model and experimental data measured by the sensors.

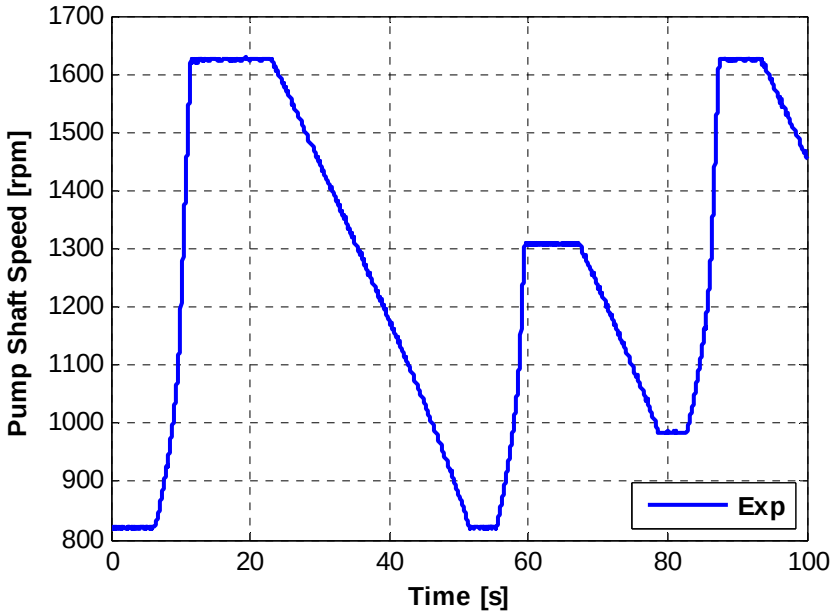

Figure 3.2 Pump shaft speed profile applied to the system and mathematical model

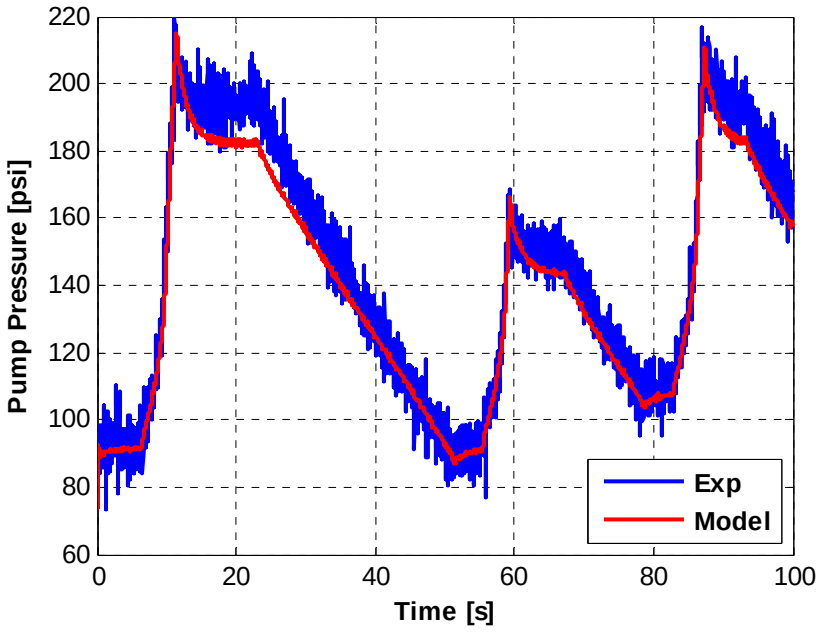

Figure 3.3 Comparison between the pump pressure of the model and experimental results in load-controlled system

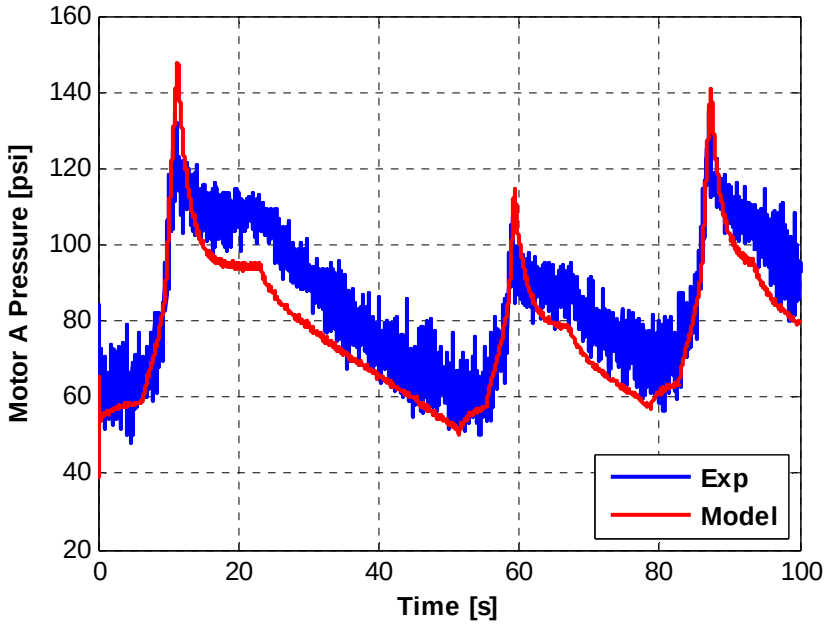

Figure 3.4 Comparison between the motor A pressure of the model and experimental results in load-controlled system

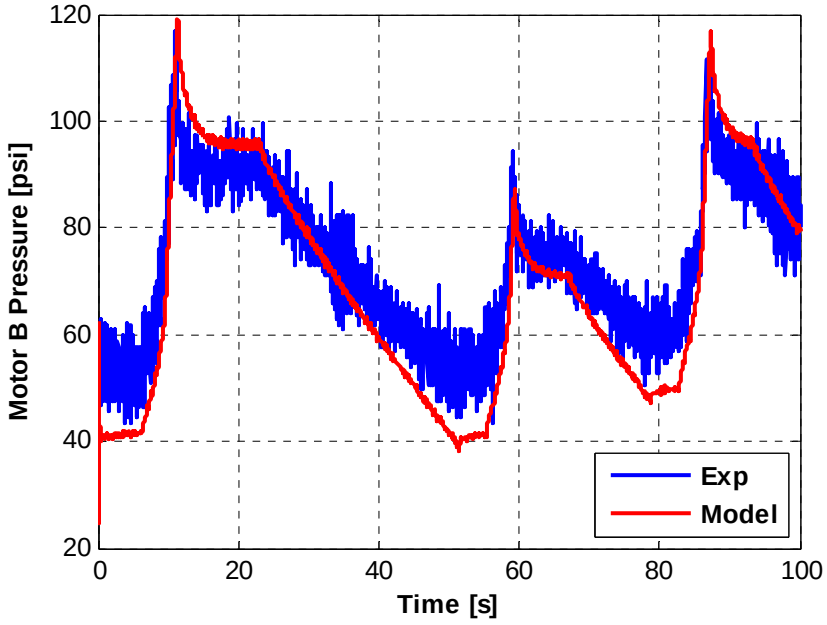

Figure 3.5 Comparison between the motor B pressure of the model and experimental results in load-controlled system

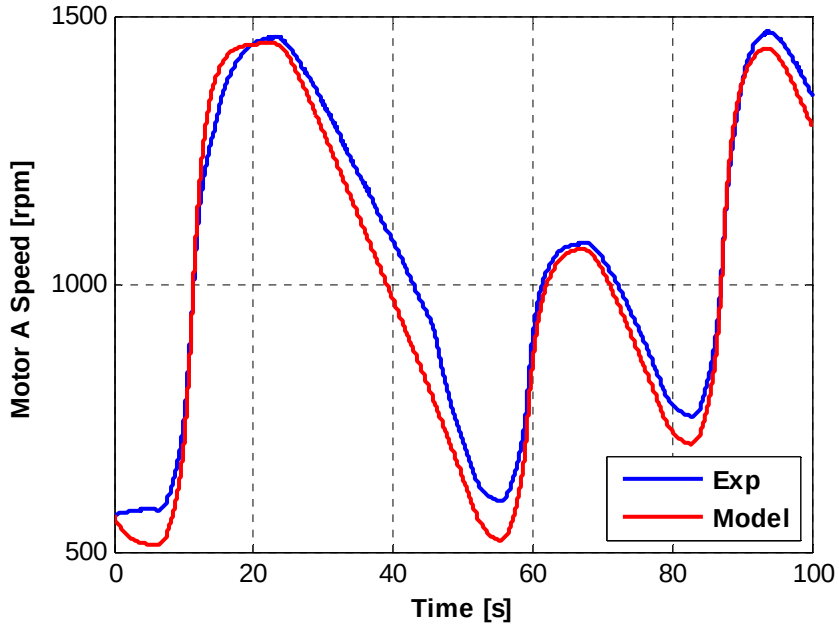

Figure 3.6 Comparison between the motor A speed of the model and experimental results in load-controlled system

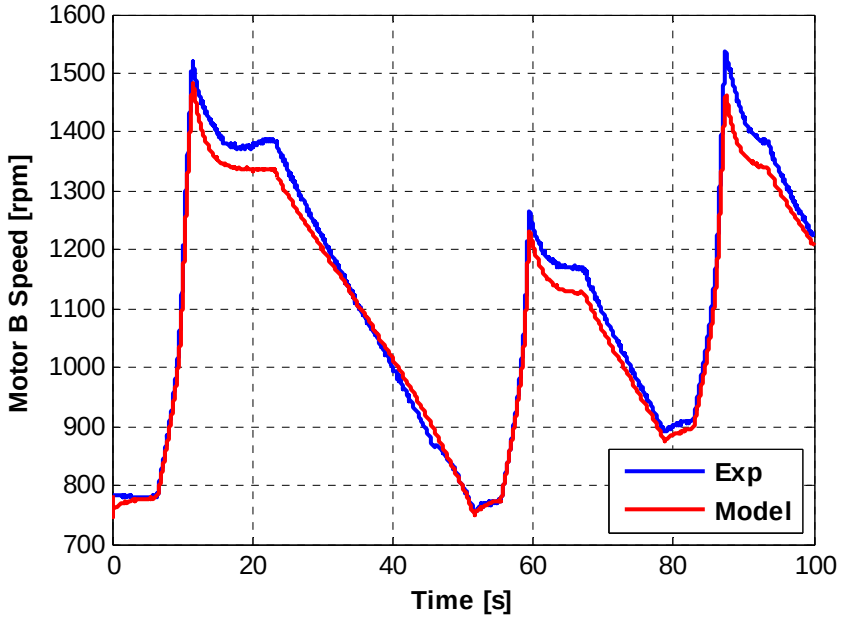

Figure 3.7 Comparison between the motor B speed of the model and experimental results in load-controlled system

This section utilized the mathematical model structure along with the estimated parameters to represent the model of a load-controlled system configuration. Results from the figures show a reasonable match between the model and the real setup. However, the unmolded nonlinearities always cause some discrepancies in the result which is negligible.

3.3 Valve-Controlled Hydraulic System

The main characteristic of the valve-controlled system configuration is the proportional valve used in it. By utilizing a proportional valve in the way of upcoming flow from the pump, the system can be controlled differently. 3-way proportional valve splits the inlet flow into two outlets, primary motor and auxiliary motor, by moving its spool.

3.3.1 Mathematical Modeling

The control system applies a voltage to the valve to move the spool as well as changing the flow rate ratio between the outlets. In this configuration, one can maintain a constant speed for primary motor by actuating the proportional valve other than exerting loads on the hydraulic motors. Figure 3.8 illustrates the schematic of valve-controlled system.

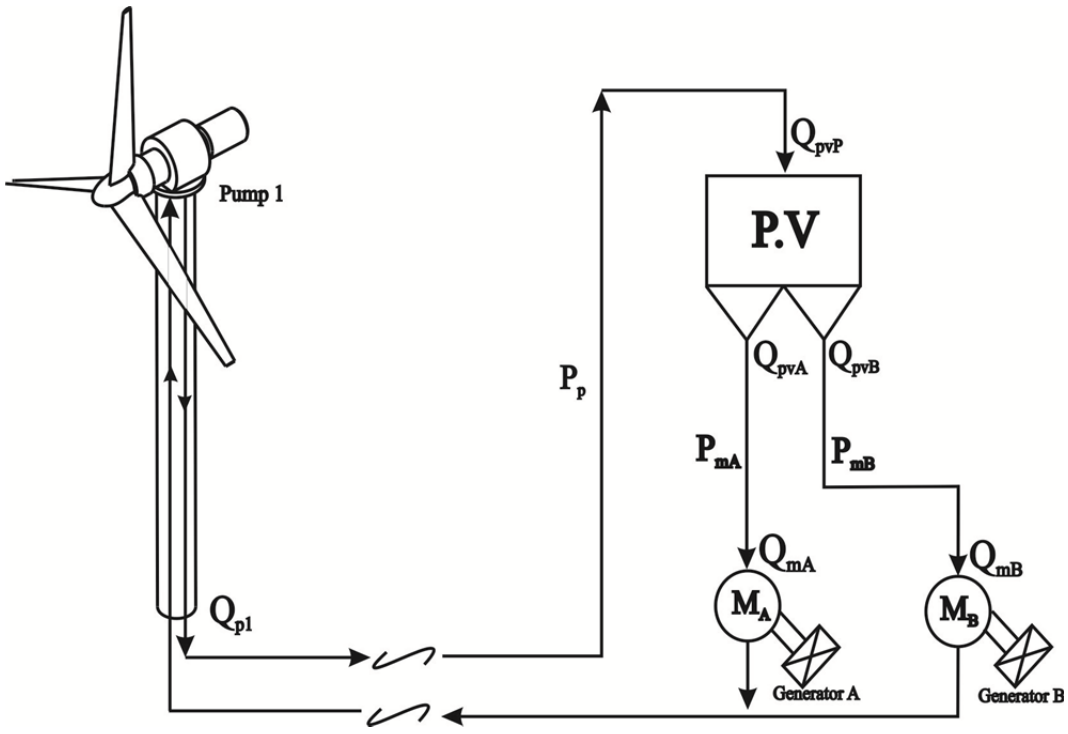

Figure 3.8 Schematic of valve-controlled configuration

The previous section considered the governing equations of the hydraulic components to derive the nonlinear state space representation. The key advantages of the state space representation comprise of a detailed mathematical demonstration of the system that incorporates the initial conditions into the solution.

In load-controlled system the variation of the pressure in the circuit was considered to be the same for the whole system. Pressure of the pump was a state. However, pressures of the hydraulic motors were a combination of states as the final output. Utilizing a proportional valve in the system causes independent pressure variations in each line. Therefore, in this configuration, there would be 5 states including pressure of the hydraulic motors.

The pressure in each section of the high-pressure line is separated, and the stored energy variation is studied. Considering the high-pressure line shown Figure 3.8, three compressibility equations can be written to demonstrate the energy stored in the line between the pump and the input port of the valve and the energy stored in each of the valve outlets and the hydraulic motors. Considering the individual speed variation of each hydraulic motor, the total state space equations reach five and are described as follows. The flow in each section of the high pressure line can be extracted from equation (3.1), equation (3.4) and equation (3.15). In addition, the mass conservation principle reveals the flow rate difference in each branch of the high pressure line (Figure 3.8) as follows:

$$Q_{C_p} = Q_p - Q_{pvP} \tag{3.33}$$

$$Q_{C_{mA}} = Q_{pvA} - Q_{mA} \tag{3.34}$$

$$Q_{C_{mB}} = Q_{pvB} - Q_{mB} \tag{3.35}$$

where Q_{c_p}, $Q_{c_{mA}}$, and $Q_{c_{mB}}$ are the flow rate differences between the inlet and the outlet of the high pressure lines which are pumped to the proportional valve, the proportional valve to motor A, and the proportional valve to motor B. Also, $Q_{pvP} = Q_{mA} + Q_{mB}$ represents the summation of outlet flows. Accordingly, the pressure variation in each section of the high pressure line can be obtained as follows:

$$dP_p/dt = (Q_p - Q_{pvP})(\beta/V_p) \tag{3.36}$$

$$dP_{mA}/dt = (Q_{pvA} - Q_{mA})(\beta/V_{mA}) \tag{3.37}$$

$$dP_{mB}/dt = (Q_{pvB} - Q_{mB})(\beta/V_{mB}) \tag{3.38}$$

Replacing the equations for the flows:

$$dP_p/dt = (D_p\omega_p - \frac{C_{pS}\ D_P}{\mu}P_p - (C_d\frac{A_{\max}}{h_{\max}}h_i\sqrt{\frac{2}{\rho}(P_p - P_{mA})}) - (C_d\frac{A_{\max}}{h_{\max}}(h_{\max} - h_i)\sqrt{\frac{2}{\rho}(P_p - P_{mB})}))(\beta/V_p)$$

(3.39)

$$dP_{mA}/dt = ((C_d\frac{A_{\max}}{h_{\max}}h_i\sqrt{\frac{2}{\rho}(P_p - P_{mA})}) - (D_{mA}\omega_{mA} + \frac{C_{mS}\ D_{mA}}{\mu}P_{mA}))(\beta/V_{mA})$$

(3.40)

$$dP_{mB}/dt = ((C_d\frac{A_{\max}}{h_{\max}}(h_{\max} - h_i)\sqrt{\frac{2}{\rho}(P_p - P_{mB})}) - (D_{mB}\omega_{mB} + \frac{C_{mBS}\ D_{mB}}{\mu}P_{mB}))(\beta/V_{mB}).$$

(3.41)

The hydraulic motor speed states are the same as load-controlled modeling.

Consequently, equation (3.39), equation (3.40), equation (3.41), equation (3.27) and equation (3.28) represent the nonlinear state space model. The system and output functions of the nonlinear system can be obtained from the general nonlinear model as:

$$\begin{aligned}\dot{x} &= f(x) + g(x)U\\ y &= h(x)\end{aligned}$$

(3.42)

where *x* is the state vector, *y* is the output vector, *U* is the input vector, *f(x)*, *g(x)*, and *h(x)* are the system function, input function, and output function, respectively. These functions are dependent on hydraulic pump angular velocity ω_p, the proportional valve position h_i, and T_{LmA}, T_{LmB} the load torques on the motors. The state variable *x* includes the pressures, the primary motor angular velocity, and the auxiliary motor angular velocity. The system functions and variables are illustrated as follows:

$$x=\begin{bmatrix} P_p \\ P_{mA} \\ P_{mB} \\ \omega_{mA} \\ \omega_{mB} \end{bmatrix},\quad U=\begin{bmatrix} h_i \\ \omega_p \\ T_{LmA} \\ T_{LmB} \end{bmatrix}. \tag{3.43}$$

Therefore, the nonlinear state space model of valve-controlled system configuration will be as [30]:

$$f(x)=\begin{Bmatrix} \left(-\frac{C_{pS}\ D_P}{\mu}P_p-\left(C_d A_{\max}\sqrt{\frac{2}{\rho}(P_p-P_{mB})}\right)\right)(\beta/V_p) \\ -\left(D_{mA}\omega_{mA}-\frac{C_{mAS}\ D_{mA}}{\mu}P_{mA}\right)(\beta/V_{mA}) \\ \left(\left(C_d A_{\max}\sqrt{\frac{2}{\rho}(P_p-P_{mB})}\right)-\left(D_{mB}\omega_{mB}-\frac{C_{mBS}\ D_{mB}}{\mu}P_{mB}\right)\right)(\beta/V_{mB}) \\ [D_{mA}\ P_{mA}-(C_{1A}\omega_{mA}^2+C_{2A}\omega_{mA}+T_{bmA})]/I_{mA} \\ [D_{mB}\ P_{mB}-(C_{1B}\omega_{mB}^2+C_{2B}\omega_{mB}+T_{bmB})]/I_{mB} \end{Bmatrix} \tag{3.44}$$

$$g(x)=\begin{bmatrix} \left(-C_d\frac{A_{\max}}{h_{\max}}\sqrt{\frac{2}{\rho}(P_p-P_{mA})}+C_d\frac{A_{\max}}{h_{\max}}\sqrt{\frac{2}{\rho}(P_p-P_{mB})}\right)(\beta/V_p) & D_p(\beta/V_p) & 0 & 0 \\ \left(C_d\frac{A_{\max}}{h_{\max}}\sqrt{\frac{2}{\rho}(P_p-P_{mA})}\right)(\beta/V_{mA}) & 0 & 0 & 0 \\ \left(-C_d\frac{A_{\max}}{h_{\max}}\sqrt{\frac{2}{\rho}9P_p-P_{mB})}\right)(\beta/V_{mB}) & 0 & 0 & 0 \\ 0 & 0 & -1/I_{mA} & 0 \\ 0 & 0 & 0 & -1/I_{mB} \end{bmatrix} \tag{3.45}$$

This section represented the nonlinear model valve-controlled system based on the governing equations of hydraulic components.

3.3.2 Model Verification with Experimental Data

Similarly to the load-controlled system validation, the nonlinear model of the system is implemented in MATLAB/Simulink and the same inputs are sent to both mathematical model and experimental prototype to compare the outputs.

The schematic diagram of the hydraulic wind power transfer and the circuit configuration are shown in Figure 3.8. A proportional valve controls the amount of flow directed to each hydraulic motor through a pulse width modulated (PWM) command.

For the first experiment, a PWM signal of 100 Hz with 90% duty cycle was used to control the proportional valve and to direct the flow toward the primary motor. The step response of the system was generated by applying step voltage to the DC motor to accelerate the hydraulic pump from zero to 450 rpm. After reaching the steady state, a second step was applied to speed up the system from 450 to 550 rpm, followed by a step-down to 450 rpm to analyze the undershoots. The experimental recorded pump speed profile that was also used in system simulations is shown in Figure 3.9. The pump speed variation resulted in a change in the output of the primary motors. Figure 3.10 to Figure 3.12 represent the comparison of the results between the derived mathematical model and experimental data measured by the sensors for the first experiment.

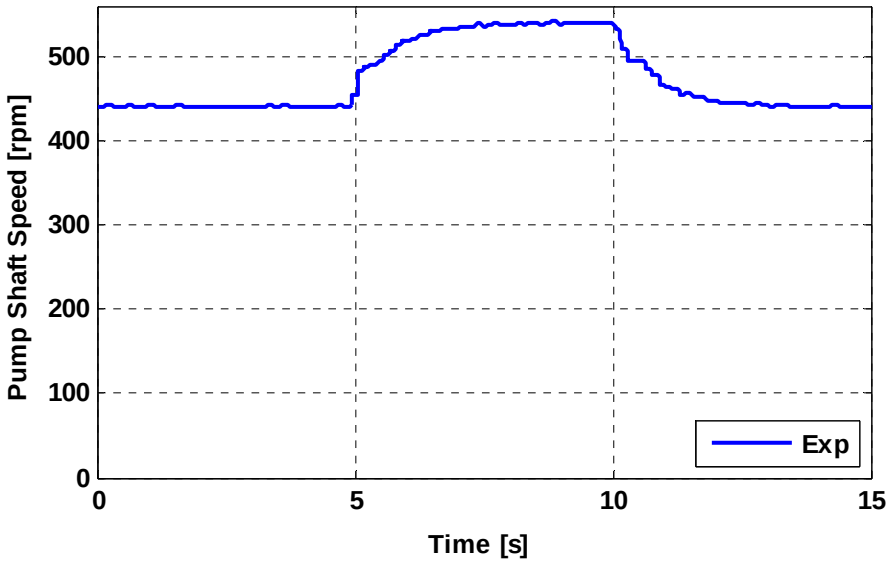

Figure 3.9 Hydraulic pump shaft speed profile in valve-controlled system for the first experiment

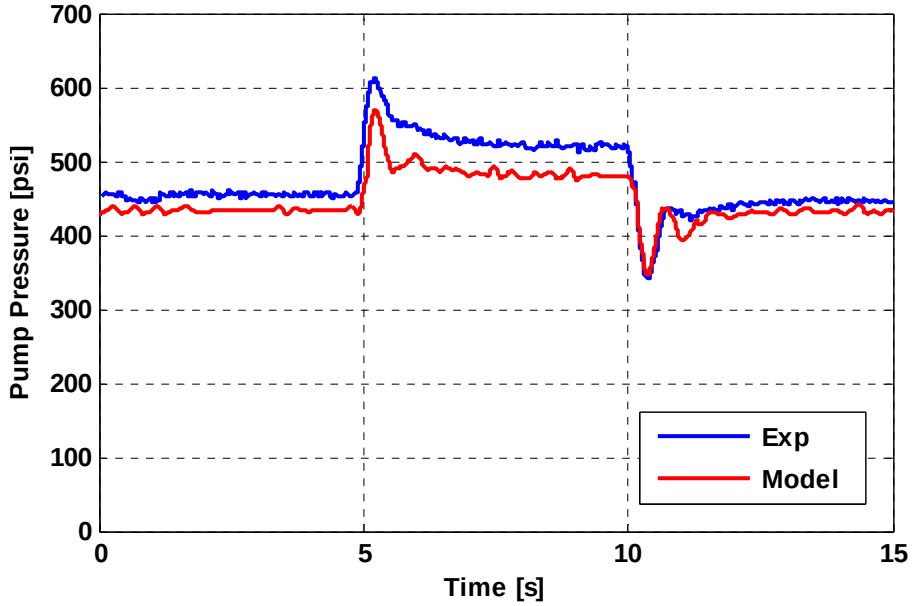

Figure 3.10 Comparison between the pump pressure of the model and the experimental results in valve-controlled system for the first experiment

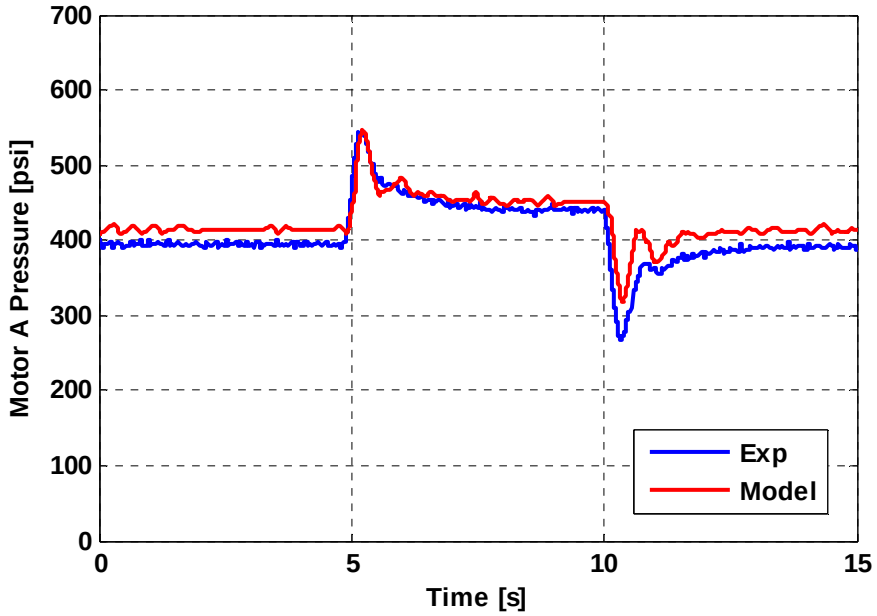

Figure 3.11 Comparison between the motor A pressure of the model and the experimental results in valve-controlled system for the first experiment

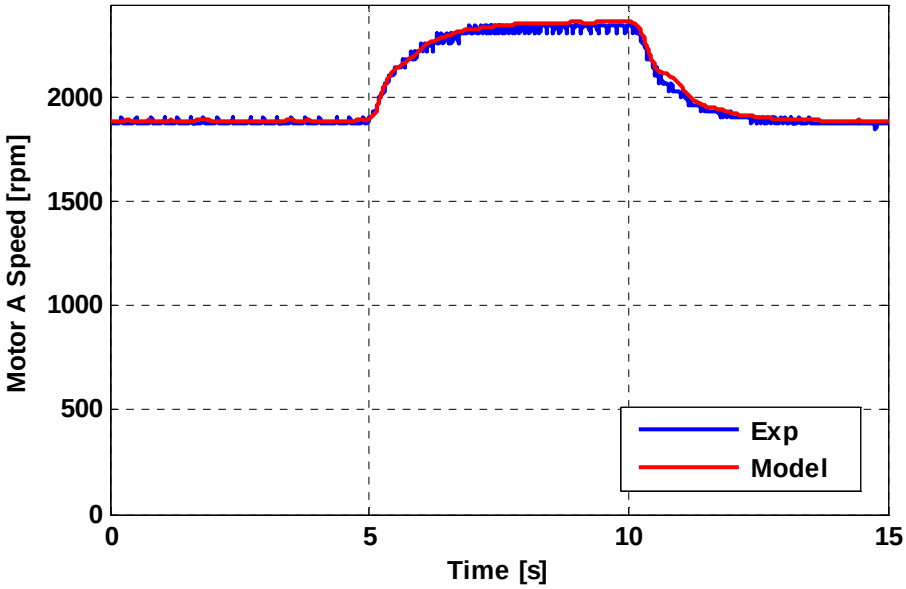

Figure 3.12 Comparison between the motor A speed of the model and the experimental results in valve-controlled system for the first experiment

Figure 3.12 shows the angular velocity of the primary motor obtained from the mathematical model and the experimental setup. As the figure demonstrates, the theoretical and actual velocities are in good agreement when the damping coefficient of the system is considered a speed-dependent variable. A slight difference between the theoretical and actual values was the result of geometry differences in the prototype and the mathematical model.

In the second experiment, a PWM signal of 100 Hz with 1% duty cycle was used to control the proportional valve to direct the flow toward the auxiliary motor. The same procedure was considered for the pump by applying step voltage to the DC motor to accelerate the hydraulic pump from zero to 400 rpm. After reaching the steady state, a second step was applied to speed up the system from 400 to 500 rpm, followed by a step-down back to 400 rpm to analyze the undershoots. The velocities were slightly lower than the one used in the main motor experiment to prevent the auxiliary motor excessive acceleration. The velocity profile shown in Figure 3.13 was recorded from the experimental setup and was used in the mathematical modeling. Figure 3.14 to Figure 3.16 represent the comparison of the results between the derived mathematical model and experimental data measured by the sensors for the first experiment.

In this section, the pressure and angular velocity dynamics demonstrated a close agreement in both the transient and the steady state. Results of the mathematical model were verified with those obtained from the prototype experimental setup [30], [31].

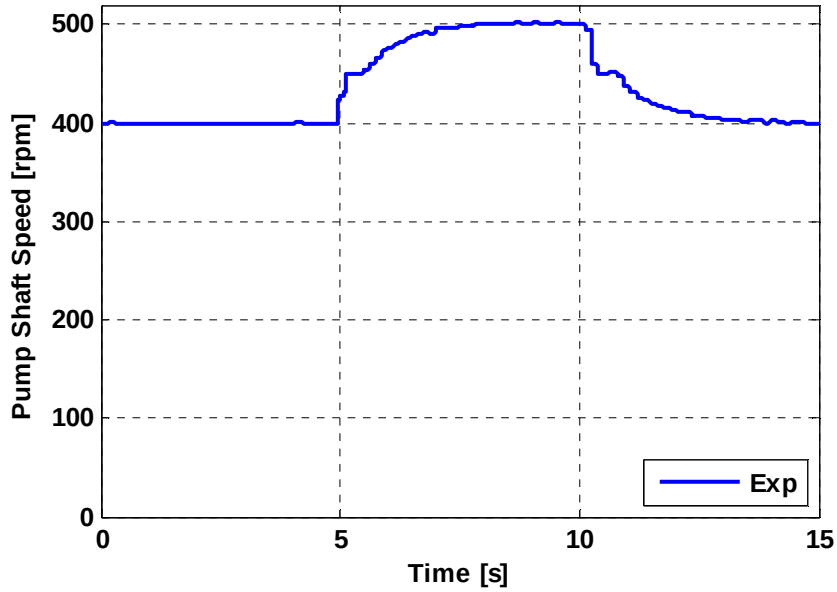

Figure 3.13 Hydraulic pump shaft speed profile in valve-controlled system for the second experiment

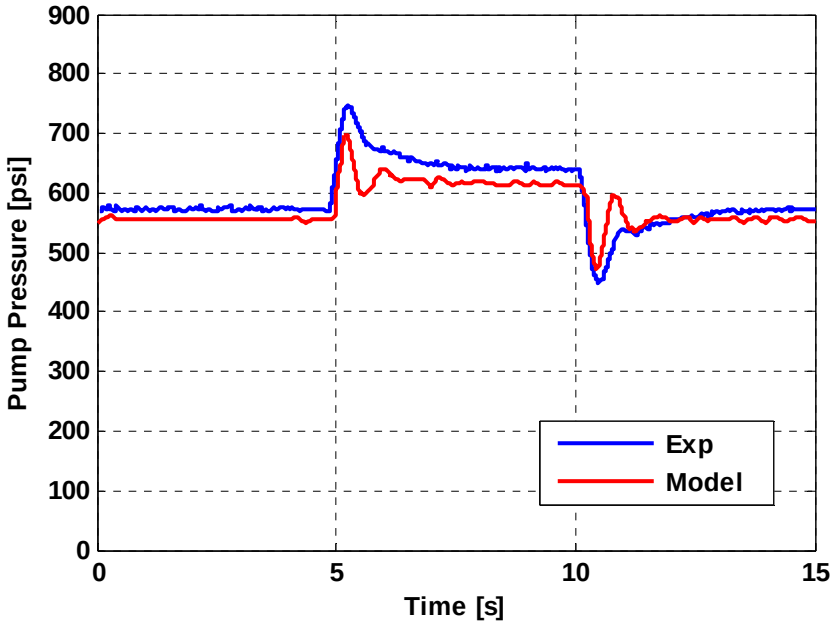

Figure 3.14 Comparison between the pump pressure of the model and the experimental results in valve-controlled system for the second experiment

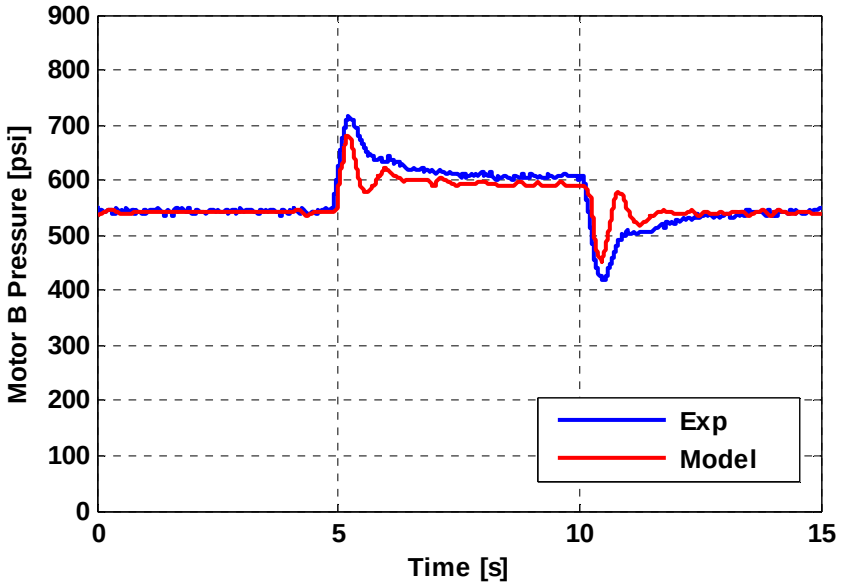

Figure 3.15 Comparison between the motor B pressure of the model and the experimental results in valve-controlled system for the second experiment

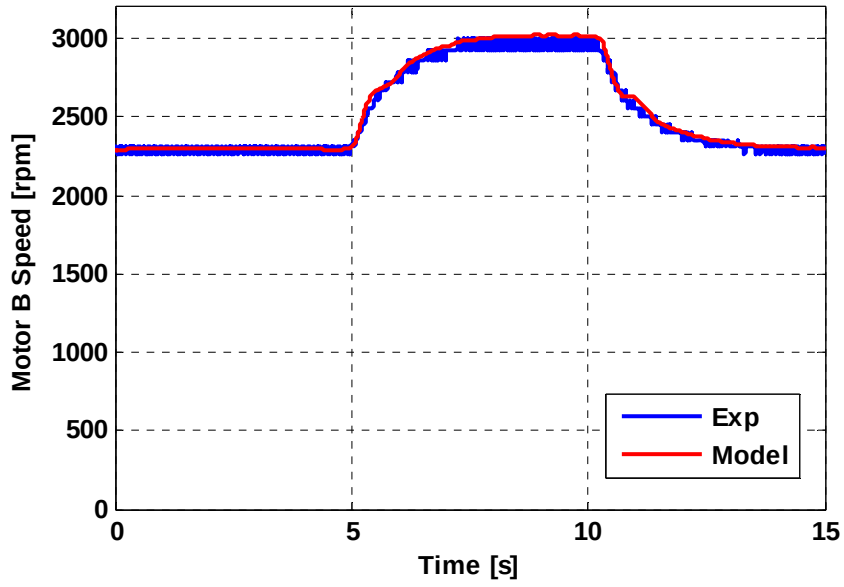

Figure 3.16 Comparison between the motor B speed of the model and the experimental results in valve-controlled system for the second experiment

4. BLACK BOX MODELING

Hydraulic wind power transfer systems exhibit a highly nonlinear dynamic influenced by system actuator hysteresis and disturbances from wind speed and load torque. This chapter presents a system identification approach to approximate such a nonlinear dynamic.

To reach desired operating objectives from a hydraulic transmission system, the system needs to be controlled appropriately. The speed control of hydraulic wind power systems is challenging, since it is a nonlinear system under random disturbances such as wind speed [19] and load torque. The nonlinearities in such system are originated from nonlinear behavior of components such as check valves, directional valves and more importantly the proportional valve. These nonlinearities will cause behavioral changes and variations in the system. Therefore, the speed control of the system would require an in-depth modeling. The controller's structure and performance depends on the accuracy of state variable approximation while the system is influenced by large input variations in a wide operating range. Proper controllers can be designed using the linear models [32].

Implementing a flawless control loop for nonlinear systems with wide range of operating points requires sufficient knowledge about the system dynamic by either a mathematical modeling or system identification as well as information about all states. As the mathematical modeling was carried out in previous section, another promising

way to address those needs is to approximate the nonlinear system with piecewise affine system (PWA). This method provides a bank of linear models each of which describe the nonlinear system in specific operating region or cluster. A comprehensive model can be obtained utilizing a switching rule among the linearized models [33]-[36].

The precision of piecewise linear models selected in the bank of models directly influences the approximation, estimation and control performances [37]-[38]. The model bank can be obtained by: 1) piecewise affine system identification [39], 2) piecewise linearization of nonlinear mathematical models [40] which will be studied in the next chapter. In the previous chapter, the governing equations of valve-controlled hydraulic transmission systems were obtained. In these models, hydraulic parameters of pumps, motors and valves were considered to develop a comprehensive nonlinear mathematical model of the system. In this chapter, the nonlinear model which is operating on a wide range is identified to construct the linear model bank. This enables an accurate estimation of a highly nonlinear system for more effective modeling and control techniques. Experimental results are used to verify the modeling performance and validate the simulation results.

4.1 Piecewise Affine System Identification

For the purpose of system analysis or a desired state control, a well-developed piecewise affine model can be obtained and utilized. However, this requires that the linearized system represent the nonlinear behavior of the system with a limited error on a large domain [41]. These types of nonlinear systems with wide range of operating points are usually represented using multiple linear models for the whole system.

The technique used in this chapter is to identify a local linear model for desired operating points. Piecewise affine system is therefore developed to cover the entire operating conditions. Each model should satisfactorily describe the plant in a specific domain. Each linear model will have an effective range, in which the system generates minimum deviation from the original plant. Out of this domain, the model's performance is reduced hence a new plant with shifted operating conditions is required. Number of models in piecewise affine systems highly affects the stability of the modeling and control as well as the amount of computations. This variable is often determined by the range of disturbances on the system.

Piecewise affine (PWA) systems are those whose state and input space is partitioned into a finite number of non-overlapping convex polyhedral regions, and whose individual subsystem in the different regions is linear or affine [42], [43]. If the subsystem in each region displays an ARX (Auto Regressive systems with eXogenous inputs) type of input output characteristics, then the system is called Piecewise affine ARX (PWARX) system [44]. A growing interest in the study of PWA systems has been witnessed over the past decades because they are equivalent to several classes of hybrid models [45]. Thus, they can be used to obtain hybrid models from data. Typical examples of hybrid systems include manufacturing systems, telecommunication networks, traffic control systems, digital circuits, and logistic systems. Another advantage of PWA models is that they can be used to approximate nonlinear dynamical systems by switching among several linear/affine models, depending on the operating regions [42], [44] and [46]. Therefore, they can be used for a simpler controller design of nonlinear system – linear controllers for the linear subsystems can be first designed according to any of the well-

known linear control synthesis methods. Then, based on the operating region of the nonlinear system, the controllers would switch from one to another.

A switching system in regression form can be described [47] as follows:

$$y_k = \varphi_k' \theta_{\sigma(k)} \tag{4.1}$$

where $\varphi_k \in R^d$ is the regression vector and $'$ denotes for transpose, $y_k \in R$ is the output, $\sigma(k) \in \{1,\ldots,s\}$ is the discrete mode, and s is the number of subsystems. $\theta_i \in R^d, i = 1,\ldots,s$, are the parameter vectors defining each subsystem.

The regression vector φ_k could, for instance, be any function of past inputs and outputs. In the following, the focus will be on systems in equation (4.1) where φ_k is formed as follows:

$$\varphi_k = [y_{k-1} \cdots y_{k-n_a} u_{k-1}' \cdots u_{k-n_b}' 1]' \tag{4.2}$$

and $u_k \in R^p$ is the input to the system. Such systems represent a subclass of the piecewise affine systems in state space form, and can be easily transformed into that form by defining the state vector as:

$$x_k = [y_{k-1} \cdots y_{k-n_a} u_{k-1}' \cdots u_{k-n_b}']' \tag{4.3}$$

The last entry of φ_k is set equal to 1 in order to allow for a constant term in equation (4.1) If the constant 1 is omitted in equation (4.2), φ_k coincides with x_k, and the system becomes piecewise linear. In the following, the vector x_k will be referred to as the *standard* regression vector, and φ_k will be called the *extended* regression vector, since it can be written as $\varphi_k = [x_k' \quad 1]'$. As for the systems in state space form, the evolution of the discrete mode σ_k can be described in a variety of ways. In PieceWise affine

AutoRegressive eXogenous (PWARX) systems, the switching mechanism is determined by a polyhedral partition of the set $\chi \subseteq R^n$ where equation (4.1) is valid. The discrete mode $\sigma(k)$ can be defined as :

$$\sigma(k) = i \quad \text{if} \quad x_k \in \chi_i, \; i = 1, \ldots, s \tag{4.4}$$

where $\{\chi_i\}_{i=1}^{s}$ is a complete partition of the regressor set χ, and each region χ_i is a convex polyhedron represented as follows:

$$\chi_i = \{x \in R^n \,|\, \overline{H}_i x + g_i \leq 0\} \tag{4.5}$$

with $\overline{H}_i \in R^{q_i \times n}$ and $g_i \in R^{q_i}, i = 1, \ldots, s$. By letting $H_i = [\overline{H}_i g_i], i = 1, \ldots, s$, and by introducing the piecewise affine map, $f : \chi \to R$ can be written as:

$$f(x) = \begin{cases} \varphi_k' \theta_1 & \text{if} \quad H_1 \varphi \leq 0 \\ \vdots & \vdots \\ \varphi_k' \theta_s & \text{if} \quad H_s \varphi \leq 0 \end{cases}, \quad \varphi = [x' \quad 1]' \tag{4.6}$$

Equation (4.1) can be alternatively rewritten as follows:

$$y_k = f(x_k) \tag{4.7}$$

PWARX systems defined by equation (4.3), equation (4.6) and equation (4.7), can be considered as a collection of ARX systems connected by switches that are determined by a polyhedral partition of the regressor set.

PWA system identification concerns obtaining a piecewise affine model of a system from experimental data. PWA models represent an attractive model structure for identification purposes, since they are the “simplest” extension of linear models but can nevertheless describe nonlinear processes with arbitrary accuracy. PWA models are also capable of handling hybrid phenomena. Given the equivalence between PWA systems

and several classes of hybrid, PWA identification techniques can be used to obtain hybrid models.

PWARX models are suitable for input-output data analysis, since they provide an input-output description of PWA systems. Consider a collection *D* data points out of N data points from the real system, as follows:

$$D = \{(y_k, x_k),\ k = 1, \ldots, N\}, \tag{4.8}$$

where $y_k \in R$ is the *measured* output of the system, and $x_k \in R^n$ is the regression vector in equation (4.3) for fixed orders n_a and n_b. A PWARX model is defined as follows:

$$y_k = f(x_k) + \varepsilon_k, \tag{4.9}$$

where $\varepsilon_k \in R$ is an error term, and *f* is the PWA map in equation (4.6).

The considered identification problem consists in finding the PWARX model that best matches the given data according to a specified fitting criterion. It involves the estimation of [47]:

- Segmentation:
  - The number of discrete modes s.
  - The coefficients $H_i = 1, \ldots, s$, of the hyperplanes defining the partition of the regressor set.
- Regression:
  - The order of submodels, n_a and n_b.
  - The parameters $\theta_i = 1, \ldots, s$, of the affine submodels.

This issue also underlies a classification problem such that each data point is associated to one region, and to the corresponding submodel. The simultaneous optimal

estimation of all the quantities mentioned above is hard, and a computationally intractable problem. To the best of our knowledge, no satisfactory formulation in the form of a single optimization problem has been provided. One of the main difficulties is the choice of the number of discrete modes s. For instance, if a perfect fit is attained by $s = N$, it means one submodel is required per data point, which is clearly an inadequate solution. Constraints on s must hence be introduced to keep the number of submodels minimal and to avoid over-fit. Heuristic and suboptimal approaches that are applicable, or at least related to the identification of PWARX models, have been proposed in the literature. Most of these approaches either assume a fixed s, or adjust s iteratively (e.g., by adding one submodel at a time) in order to improve the fit [47].

4.2 Hydraulic Wind Power System Identification

Considering various disturbances in the nonlinear model of hydraulic wind power system, operating point regions of such a system is remarkably wide. Therefore, describing the whole system linearly, requires multiple linear models. As mentioned earlier, one can linearize the nonlinear mathematical model in different operating points to obtain the linear models. However, this method requires enough knowledge about the best operating points of the model which is really challenging for wide range operating systems such as hydraulic wind power systems [48]. Another promising method, in control system applications, is piecewise affine system identification. This approach searches for the best linear regions as well as estimation of model parameters which advances the linear modeling of hydraulic wind power system.

Considering the sensitivity of the system to the parameters and inputs, it is seen that the valve position and the wind speed disturbance have a great influence on the behavior of the system. Thus, the piecewise affine system identification of such nonlinear system with different operating points must be performed. These models are specified by different control input (valve position) and disturbance input (wind speed). In our experimental setup, wind speed as one of the factors to determine the operating points varies from 200 rpm to 1000 rpm. The other input, valve position, is directly related to the applied voltage which ranges from 1.2 V to 3.8 V. Each combination of these values would result in a different operating point. However, a partial group of these operating points can be included in the domain of a single linear model.

For the simplicity of system identification, the most important state, motor A (main) speed, is considered as the desired output to be controlled. Therefore, the problem of a piecewise affine system identification for a 5-state 2-input hydraulic wind power system reduces to a multi input-single-output (MISO) system identification, which is also graphically representable.

4.2.1 Hysteresis Compensation on Data Recording

As mentioned earlier, the proportional valve consists of one inlet and two outlet orifices and a spool which changes the flow passage area of the outlet orifices. Governing equation of flow rate for each outlet is obtained in equation (3.14) which relates the pressure differential across an orifice and the passage area to the flow rate.

In the proportional valve, the hysteresis band is the widest separation observed on the spool displacement when the coil current is uniformly increasing from when it is

uniformly decreasing. Another words, hysteresis is the difference between the valve position on the upstroke and its position on the down stroke at any given input signal. To analyze this nonlinearity, steady state response of the system in all operating point is experimentally derived for both increasing valve voltage and decreasing valve voltage. Figure 4.1 depicts the behavior of the system in each case. Also, the normalized difference between surfaces in Figure 4.1 is shown in Figure 4.2.

In order to compensate for this multi-valued nonlinearity, an averaging method can be utilized. An average of those two surfaces (shown in Figure 4.1) can provide more reliable data for system identification. This averaged surface is illustrated in Figure 4.3.

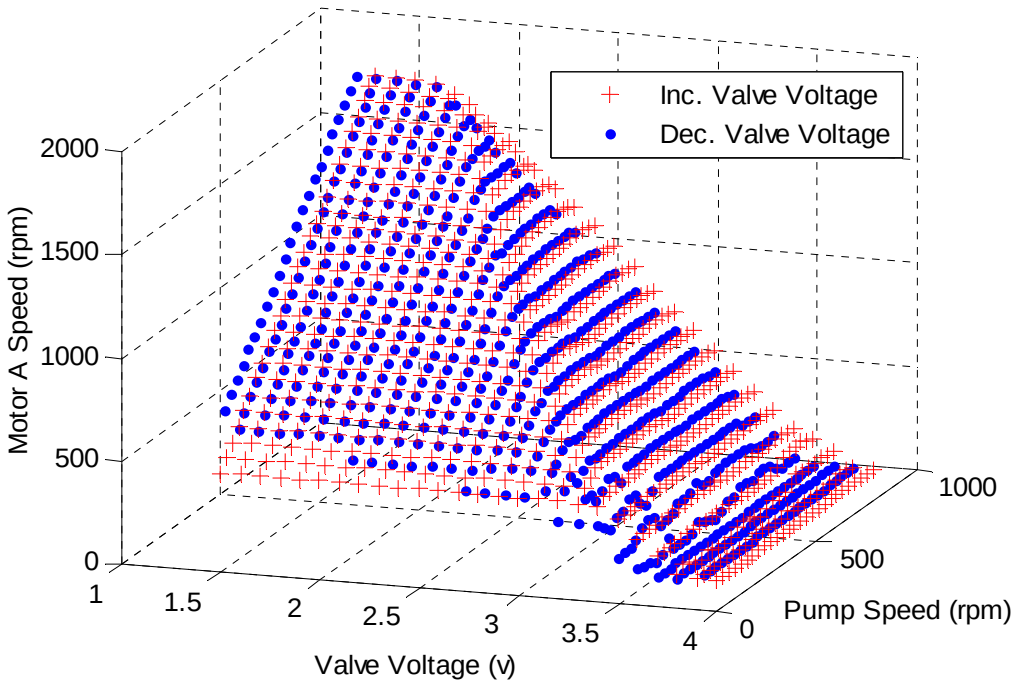

Figure 4.1 Experimental steady state system response in all operating point for increasing valve voltage and decreasing valve voltage, (2187 datapoints)

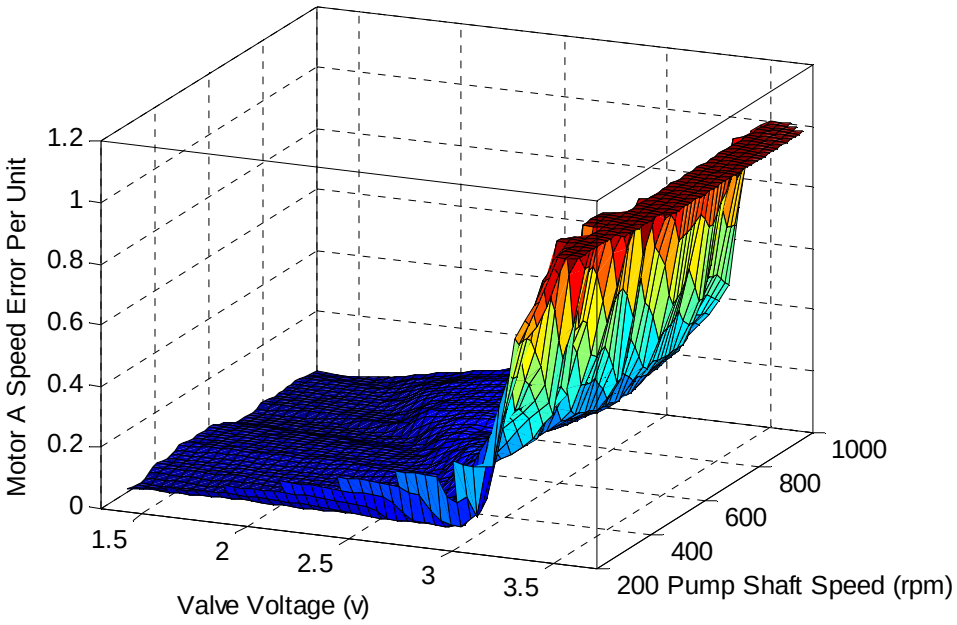

Figure 4.2 Normalized difference between increasing valve system response and decreasing valve system response

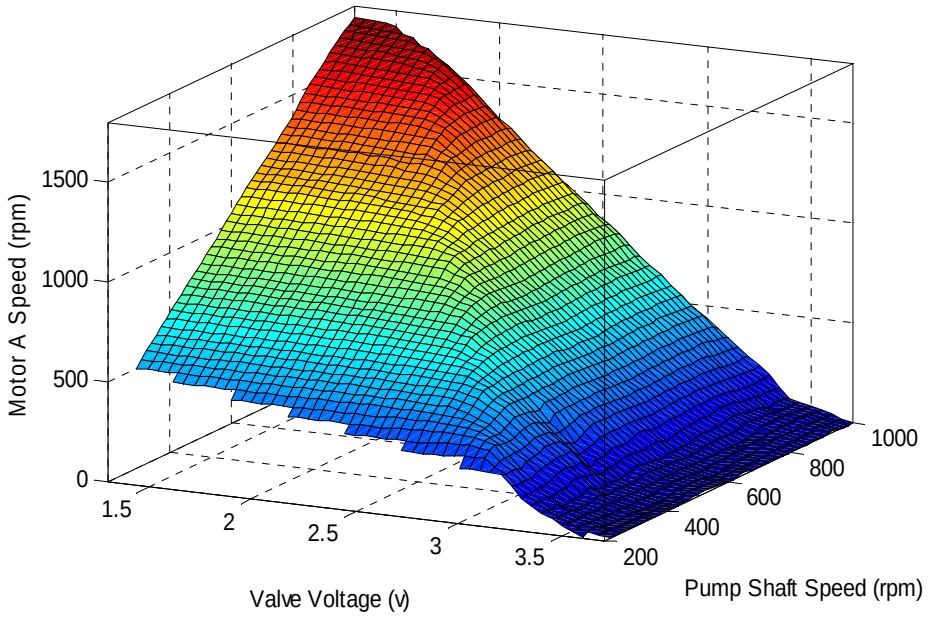

Figure 4.3 Averaged steady state response of the system in all operating points

4.2.2 Segmentation

In a practical sense, finding a balance between the number of model partitions and the overall accuracy of the estimation is of interest. To explore this relationship, different methods of partitioning are introduced such as “average” [49], “z-score” [50], and “k-means” [51]. The average method considers all observed data in one region, and thus identifies one affine model for the entire system. This approach is the base for a dynamical system. The z-score method divides the observations into two partitions based on the empirical likelihood of the observation. Finally, k-means clustering aims to partition n observations into k clusters in which each observation belongs to the cluster with the nearest mean value. Also, some advanced methods optimize the segmentation stage simultaneously with other system identification stages such as regressors estimation [39].

For convenience, heuristic approach is employed in this thesis based on system’s steady state response surface. By careful consideration of the averaged surface in Figure 4.3, it can be concluded that three linear submodels can reasonably approximate the nonlinear system. This observation determines the number of discrete modes $s = 3$. Figure 4.4 shows these submodels.

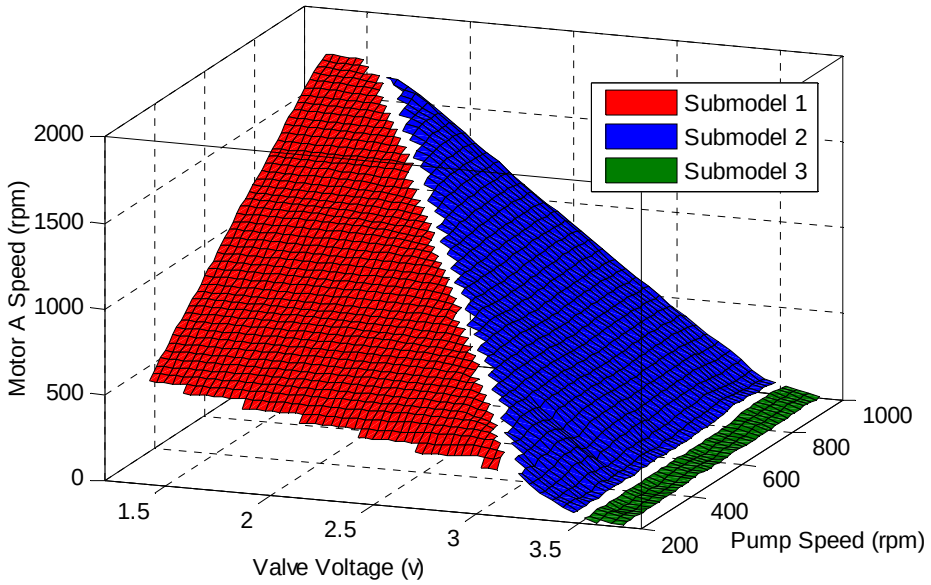

Figure 4.4 All three submodels of the system derived from steady state response

Next step is segmentation which is looking for the coefficients $H_i = 1,\ldots,s$, of the hyperplanes defining the partition of the regressor set. Averaged surface in Figure 4.3 embodies a fracture which can be described by a space line using two data points on a narrow band. Considering two operating points in the 3D system as x, y, and z coordinates, (2.95, 328, 489.5) and (1.8, 904, 1566), the space line equation can be derived as follows:

$$\begin{aligned} &\text{Valve Voltage } (h_i) = 1.25t + 1.75 \\ &\text{Pump Speed } (\omega_p) = \text{-}608t + 904 \\ &\text{Motor A Speed } (\omega_{mA}) = \text{-}1149t + 1572 \end{aligned} \tag{4.10}$$

Projection of this space line on the x-y plane results in H_i coefficients which is used for partitioning of submodels described as follows:

$$\omega_p = \text{-}486.41h_i + 1755.2 \tag{4.11}$$

Figure 4.5 depicts the fitted space line and its projection on the x-y plane. In addition, the valve voltages higher than 3.5 V specify the third cluster which is shown in red solid line.

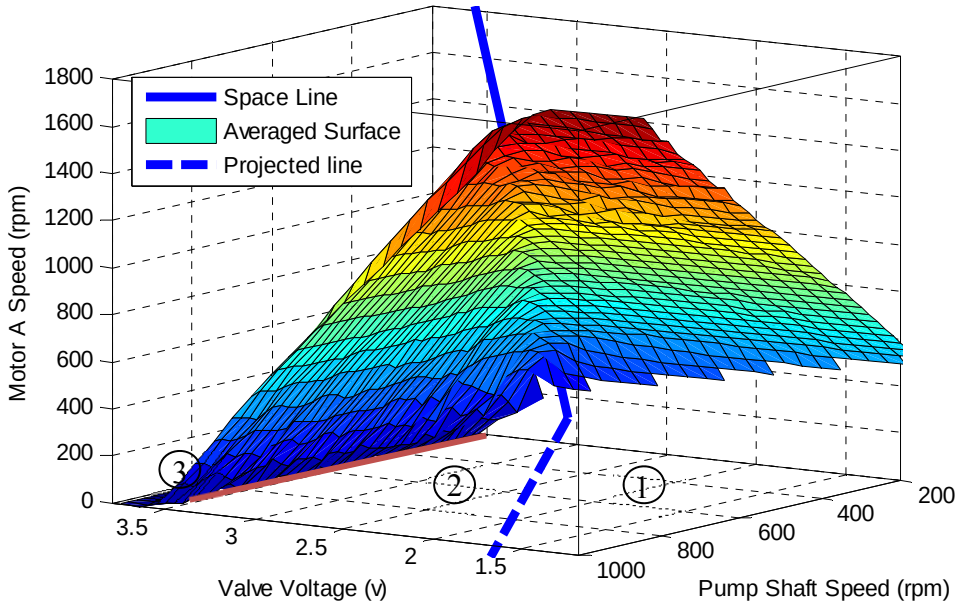

Figure 4.5 Fitted space line and its projection on xy-plane. All three clusters of the operating points

4.2.3 Regression

Studying the nonlinear mathematical model of the proposed hydraulic wind power system specifies the order of the submodels. This system contains 5 poles and 3 zeros which determines $n_a = 5$ and $n_b = 4$.

Once the data (operating points) are segmented, the dynamics of each region of the observed data is estimated using least square technique. Here, the aim is to classify the data points into clusters and to estimate an affine submodel for each cluster.

Assuming that N data points (y_k, x_k) are given, with $y_k \in R$ and $x_k \in R^n, k = 1,\ldots,N$, for a fixed *s,* the considered problem can be formulated as follows [47]:

$$\lambda_{ki} = \begin{cases} 1 & if\ x_k \in \chi_i \\ 0 & otherwise \end{cases}, \quad k = 1,\ldots,N, \qquad i =,\ldots,s$$

$$\min_{\theta_i} \frac{1}{N} \sum_{k=1}^{N} \sum_{i=1}^{s} (y_k - \varphi_k' \theta_i)^2 \lambda_{ki} \tag{4.12}$$

Solving the equation (4.12) for θ_i s will result in submodels as follows:

$$\begin{aligned} \omega_{mA}(k) = {} & 0.3333\omega_{mA}(k-1) + 0.3333\omega_{mA}(k-2) \\ & +0.3333\omega_{mA}(k-3) - 6.177\omega_{mA}(k-4) \\ & +1.666\omega_{mA}(k-5) - 22.25h_i(k) \\ & +7.417h_i(k-1) + 7.417h_i(k-2) \qquad if \quad \omega_p \ll \text{-}486.41h_i + 1755.2 \\ & +7.417h_i(k-3) + 1.769\omega_p(k) \\ & -0.5897\omega_p(k-1) - 0.5897\omega_p(k-2) \\ & -0.5897\omega_p(k-3) \end{aligned}$$

$$\begin{aligned} \omega_{mA}(k) = {} & 0.3333\omega_{mA}(k-1) + 0.3333\omega_{mA}(k-2) \\ & +0.3333\omega_{mA}(k-3) + 1.722\omega_{mA}(k-4) \\ & -8.598\omega_{mA}(k-5) - 896h_i(k) \\ & +298.7h_i(k-1) + 298.7h_i(k-2) \qquad if \quad \omega_p \geq \text{-}486.41h_i + 1755.2 \\ & +298.7h_i(k-3) + 0.0178\omega_p(k) \\ & -0.005933\omega_p(k-1) - 0.005933\omega_p(k-2) \\ & -0.005933\omega_p(k-3) \end{aligned}$$

$$\omega_{mA}(k) = 0 \qquad if \quad h_i \geq 3.5 \tag{4.13}$$

4.3 Model Verification with Experimental Data

Obtaining submodels of the nonlinear system in equation (4.13) and their region of operation, a piecewise affine system with switching rule can be implemented. To verify the performance of the identified model, several experiments have been carried out

using different input profiles at the experimental prototype. Then the experimentally recorded input profiles were applied to the piecewise affine system and the results were compared. Figure 4.6 to Figure 4.9 illustrate the comparison of the results. As the system had two input variables, four cases were considered. In case one, a fixed valve voltage was applied. In case two a step valve voltage was considered. In case three, a triangle valve voltage was applied, and in case four a sinusoidal valve voltage and pump speed variation was applied to mimic the practical wind speed and valve voltage.

In Figure 4.6.a valve position is fixed and a step pump speed disturbance is applied to the system. Figure 4.6.b shows the experimental and the model output. As it can be seen, piecewise linear model matched the experimental results accurately.

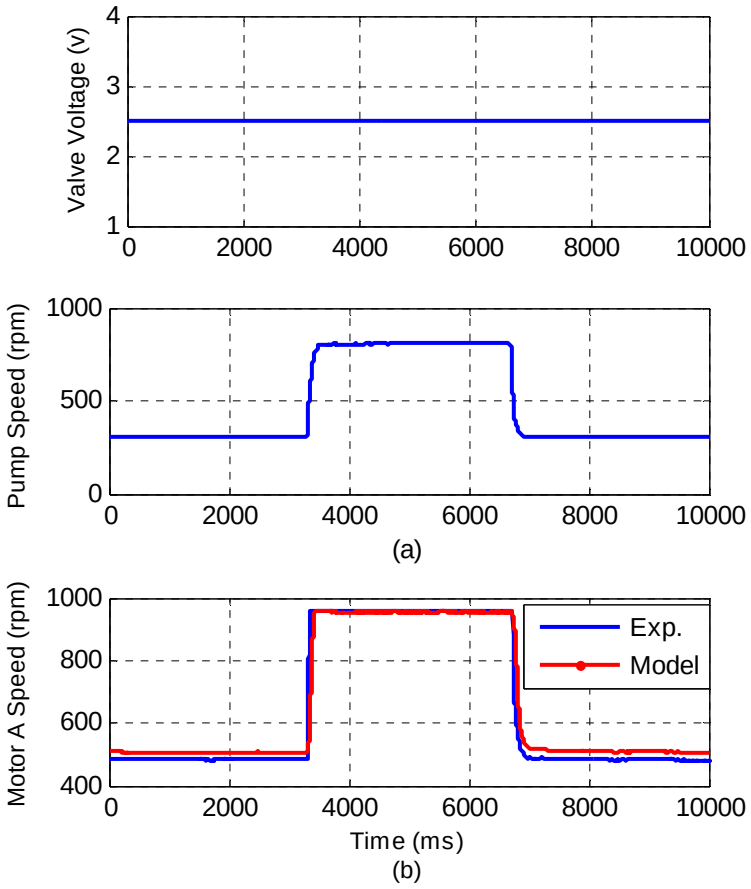

Figure 4.6 (a) inputs to the setup and model (constant valve voltage, step pump speed) (b) comparison of setup output and model

For the second experiment, Figure 4.7, a step valve position profile is applied to the system which ranges from fully open to fully closed. As the system load changed, the speed droop caused a slight speed drop at the pump. As it can be demonstrated from the figure, the proposed model output matched the experiment at 92% accuracy.

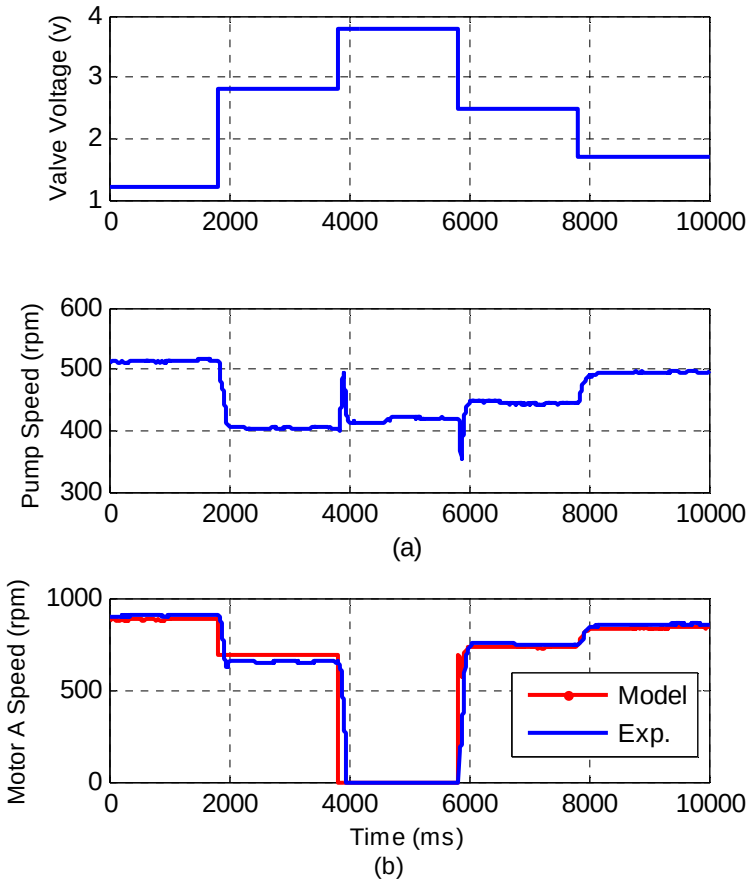

Figure 4.7 (a) inputs to the setup and model (step valve voltage, step pump speed) (b) comparison of setup output and model

To evaluate the effect of model averaging and analyze the performance of the proposed modeling, a triangle valve voltage was applied to the valve. The voltage uniformly increased from 1.5 V to 3.5 V and then uniformly decreased to 1.5 V. Figure 4.8 shows the valve input excitation voltage. In this case, the valve experienced an operation cycle as a gradual closing from fully open to fully closed and to fully open position. As a result (shown in Figure 4.8) the pump speed dropped from 600 rpm to around 500rpm and then increased to 600 rpm. The motor A speed followed the same

pattern and decreased from 1000 rpm to 200 rpm and then increased to 1000 rpm. Simulations results closely follow the experimental results and validate the approach taken to model the surfaces and the switching logic. A 93% match was observed from mathematical modeling and experimental results. A slight deviation in the model output was observed when the valve started moving from fully closed position towards fully open.

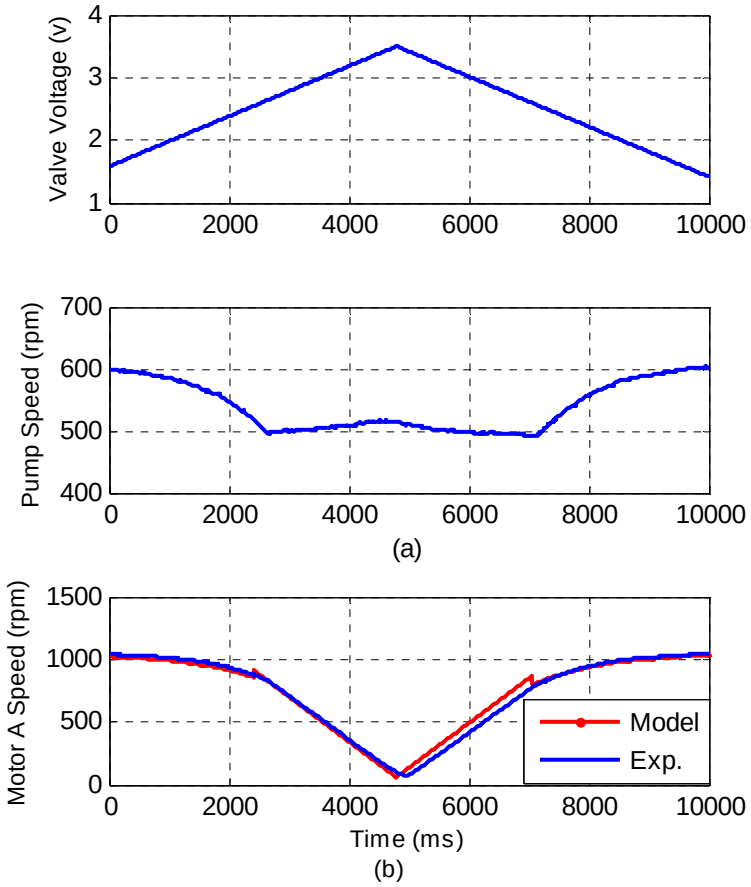

Figure 4.8 (a) inputs to the setup and model (ramp valve voltage, ramp pump speed) (b) comparison of setup output and model

Finally, in case four, both input variables were strongly varying. Figure 4.9 illustrates each of the applied inputs. A sinusoidal voltage variation for valve voltage command and step speed variations for wind turbine were considered. Output comparison of the experiment and the simulation shows a close match with an accuracy of 91%. Discrepancies occurred in transients were the result of non-ideal affine parameter estimation.

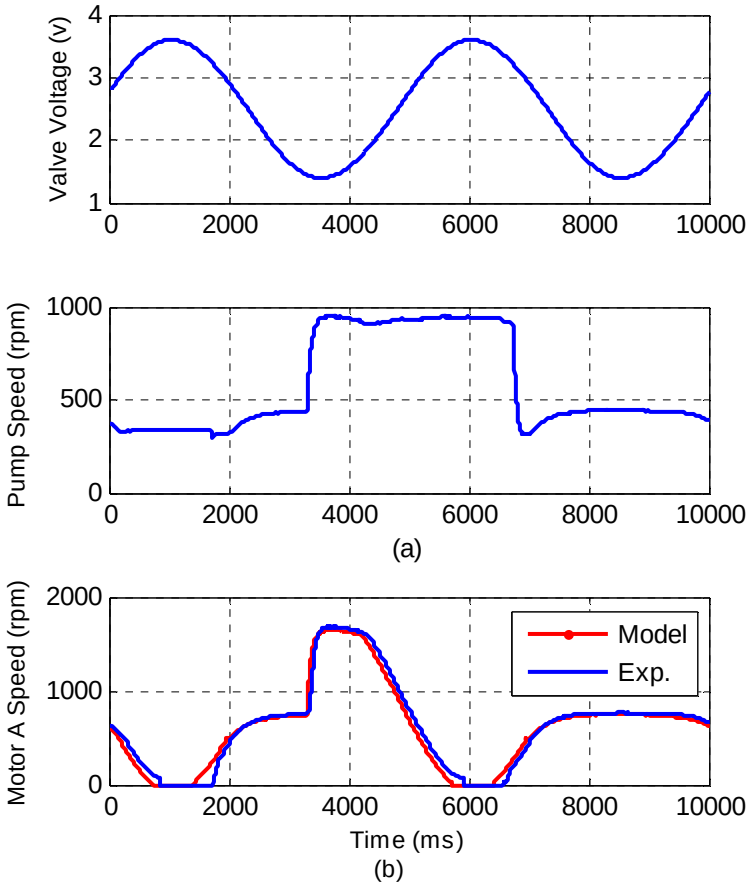

Figure 4.9 (a) inputs to the setup and model (sinusoidal valve voltage, step pump speed) (b) comparison of setup output and model

It can be seen that the piecewise affine system described a highly nonlinear dynamic of a hydraulic wind power transfer. Experimental results on different operating points and transients verified the mathematical modeling approach proposed through piecewise affine systems. Figure 4.6 to Figure 4.9 illustrated the accuracy of the model which was above 91% match.

Piecewise affine system identification of a hydraulic wind power system was presented in this chapter. Hysteresis in the proportional valve was compensated by using averaging method on the response of the system on different operating point. A graphical approach of nonlinear system modeling was presented and found to be an effective modeling tool and finally, experimentally derived submodels described the nonlinear systems [52].

5. LINEARIZATION AND ANALYSIS

To analyze the system behavior or to control the original nonlinear system, a well-developed linear model can be used through the linearization of nonlinear system. This provides an approximation of the system's dynamical behavior within a neighborhood vicinity of variables and operating conditions.

5.1 Piecewise Linearization

5.1.1 Literature and Problem Statement

Linearization of nonlinear systems allows for the use of established linear system analysis and control techniques such as Laplace transform, Fourier transform, and superposition principles [53]. General approach in linearization of a nonlinear system can be categorized into two major groups of exact linearization and approximate linearization. This category and some of their existing approaches are listed in Figure 5.1.

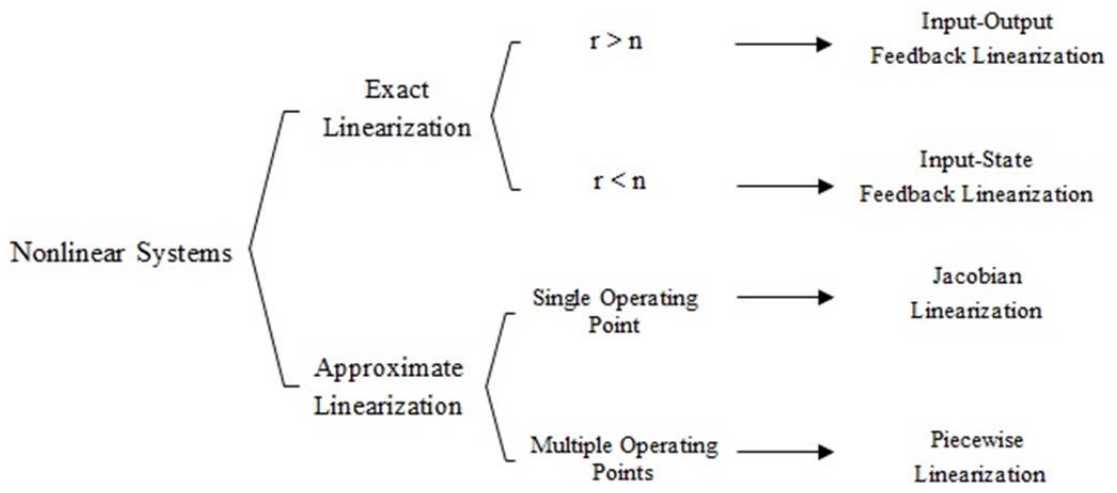

Figure 5.1 Various linearization techniques for exact and approximate results.

Exact linearization [54] can be obtained using feedback linearization [55], state space linearization [56], optimal linearization [57] and fuzzy linearization [58]. The approach is to algebraically transform nonlinear system dynamics into (fully or partly) linear models. The zero dynamics of these systems must be stable. The main drawbacks are the need for an accurate system model, as well as the need to solve potentially difficult nonlinear partial differential equations.

Linear approximations, on the other hand, can approximate nonlinear models in a certain region within a given tolerance [59]. The extent of these intervals depends on the nonlinearity of the original model. To obtain a linear approximation of a nonlinear model with a wide range of operating points, piecewise linearization can be employed. This approach captures nonlinearities around equilibrium points [60]. Various methods of piecewise linearization have been proposed in the literature [61]. Approximation of strongly nonlinear systems around multiple operating points using Taylor expansion also

leads to the piecewise linearization [62]. The resulting linear models have lower complexity, fit into well-established tools for linear systems and are capable of representing arbitrary nonlinear mappings. Examples include, complexity reduction for finding the inverse of nonlinear functions [63], distortion mitigation techniques such as predistorters for power amplifier linearization [64], approximation of nonlinear vector fields obtained from state equations [65], obtainment of approximate solutions in simulations with complex nonlinear systems [66] such as Mixed-Integer Linear Programming (MILP) models [67], search for canonical piecewise linear representations in one and multiple dimensions [68] with different goals such as black box system identification, approximation or model reduction [66].

Hydraulic wind power systems operate under wide range of conditions due to various disturbances such as wind speed, valve position and load on the generators. From the equation (3.14), it can be inferred that the pressure differential variation disturbs the flow through valve's orifices. Thus, for maintaining the flow rate, specifically through the main motor, the proportional valve's spool displacement must be adjusted to compensate for this disturbance. Intermittent wind speed imposes variable pump speed and consequently varies the flow rate in the valve's inlet.

Even if the valve maintains the main motor's flow rate constant, the speed can deviates from synchronous speed due to pressure variations and load torques. The governing equation for motor flow and delivered toque to the load are:

$$I_m \frac{d\omega_m}{dt} = D_m P_m - C_v D_m \mu \omega_m - T_L \tag{5.1}$$

$$Q_m = D_m \omega_m + K_{ms} P_m \tag{5.2}$$

This type of nonlinear systems with wide range of operating points can be linearized using multiple linear models to represent the entire system dynamics. The linearization technique used in this chapter is to utilize a local linear model for each of the different plant's operating conditions.

For a wide range of operation, piecewise linearization technique can be used to cover the entire possible operating conditions. Each model should satisfactorily describe the plant in a region around a specific operating point. This linearized plant will have an effective range of linearization, in which the system generates limited deviation from the original plant. Operating points out of this range result in reduced performance as the output deviates from the nonlinear model. Hence, a new plant with shifted operating conditions is required. A 2-D or higher order inputs impose larger selection regions and consequently the linearized models may show overlap in some areas and no coverage on others. One solution might be the introduction of a new model for un-covered areas. This will increase the number of linearized models, and might consequently increase the overlapped areas. Hence, selection of operating points and effective consideration of overlapped areas in pricewise linearization becomes critical.

Satisfactory performance of piecewise linearization algorithms depends on 1) the number of linear models required to represent a nonlinear model, and 2) the location of operating points to obtain maximum coverage and continuity.

Some methods [69] and [70] suggest equal partition of the operating points and selection of fixed number of models which has generated sub-optimal results. A simple and common linearization strategy consists of building a linear interpolation between samples of the nonlinear function over a uniform partition of its domain. A tradeoff

between increasing the approximation accuracy and simplifying the approximation by the minimum number of linearized sectors can be obtained using Genetic Algorithms [71]. Simplified models may be obtained using descent methods [72], dynamic programming [73] or heuristics such as genetic [71] as means to optimize target approximation errors.

Next section proposes a novel adaptive piecewise linearization algorithm to optimize the location of operating points, preserve continuity of nonlinear system, and determine the number of piecewise linear models such that the maximum number of operating points are covered with minimal error. The algorithm is formulated for the hydraulic wind power system.

5.1.2 Adaptive Optimum Piecewise Linearization

Wide operating range of hydraulic wind power requires several linearized models. An effective model selection is required to cover entire operating points of the system with best matching on overlapped areas. An algorithm is proposed to optimally locate the operating points of the system and determine the number of piecewise linearized models. The optimization algorithm is as follows:

Step 1: In the first step, entire range of operating conditions can be divided into individual nodes with proper dimensions that is determined according to the number of inputs and desired outputs. The maximum dimension of nodes can be obtained as:

$$N = \#_{input} + \#_{output} \tag{5.3}$$

Step 2: Each operating point (node) potentially forms a linearized model. This model can be used for other neighboring nodes if the error is less than a desired threshold.

The domain of each model is determined by examining the operating points and obtaining the error between the original model and that of the linearized model. For instance, the nodes $i_{1\times N}$ or $j_{1\times N}$ form domains D_{mi} or D_{mj} in which the error is less than ε (shown in Figure 5.2). Domain of a general node *x* can be expressed as:

$$D_{mx} = \left\{ \forall x_{1\times N} \left\| f(x) - \bar{f}(x) \right| < \varepsilon \right\} \tag{5.4}$$

where $f(x)$ is the nonlinear function and $\bar{f}(x)$ is the piecewise linearized function around node *x*.

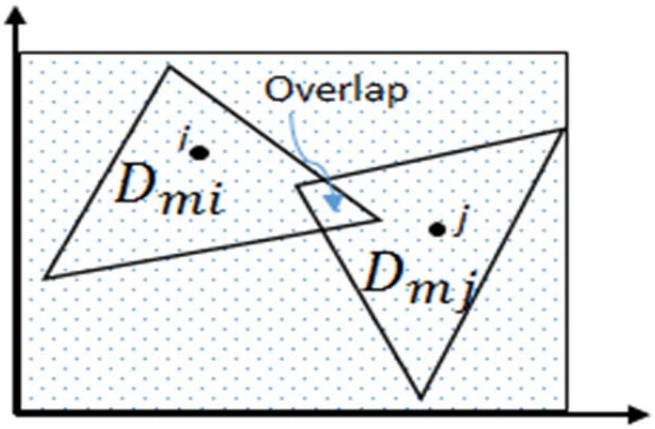

Figure 5.2 Overlap between two model domains. Shared nodes in overlap area can be modeled by both models

Step 3: Each operating point *x* is weighed by ω_x according to the number of models, *n,* that include this node in their domain D_{mn} as follows:

$$\omega_x = \sum_{n|x\in D_{mn}} n \tag{5.5}$$

A node with more weigh is less valuable as it can be expressed with more possible piecewise linearized models. The weight for each node is scaled to generate proper resolution for distinct recognition as follows:

$$\Gamma_x = \alpha \frac{1}{\omega_x^{\beta}} \tag{5.6}$$

where parameters α and β are control parameters and are selected to create the desired weight resolution.

Step 4: Model weighing. Each model is weighed according to the summation of the node weights ω_x in its domain:

$$\Gamma_{\bar{f}_i} = \sum_{x \in D_{mx}} \Gamma_x, i = 1,2,...n \tag{5.7}$$

Step 5: The models are ranked according to their weights. The maximum weighted-model is selected as one of the piecewise linearized models as follows:

$$\bar{f}_i = \sup\left\{\Gamma_{\bar{f}_i}\right\}, i = 1,2,...,n \tag{5.8}$$

Step 6: The nodes associated with this model are nullified (weighed zero) and the models will be re-ranked:

$$\left\{\forall x \in D_{mx}, \Gamma_x = 0\right\} \tag{5.9}$$

Step 7: Domain index criterion. Repeat step 6. Model selection stops if the number of added operating points per added model is less than the domain index δ.

The scaling factor generates a convex weighting profile to select the optimal number of models. When the scaling function is saturated, the function weight variation

becomes saturated resulting low value added to the number of model increase. The model selection will exit condition is as follows:

$$\left(if \frac{D_{i+1}}{\sum_{n=1,2,\ldots,(i+1)} D_n} < \delta \Rightarrow f_{i+1} = \varnothing \right) \tag{5.10}$$

Depending upon the criterion determined in step 6, there might be nodes that do not belong to any of the piecewise linearized models' domains. There is also the possibility that some nodes belong to more than one piecewise linearized model.

5.1.3 Piecewise Linearization of Hydraulic System Nonlinear Model

Hydraulic wind power transfer system is largely sensitive to valve position and the wind speed disturbances. The system operation due to the existence of the proportional valve is highly nonlinear. The system pressure variations due to valve position and the wind speed is shown in Figure 5.3. The surface shows a nonlinear response of the system while the load is constant. As the load changes, the system response also changes and consequently affects the rotational speed of wind turbine. This indicates that the system requires to be linearized around multi-dimensional operating points. Total number of possible operating points can be unlimited as the surface may contain viable nodes with domains that involve a large group of operating points. Finding suitable nodes with large domain is of interest as this optimizes the number of piecewise linearized models.

As mentioned in the model selection section, the criteria to include a possible node to a particular domain is the error and its weight which is inversely proportional to the number of system domains claiming the node in their domain, i.e. as a particular node belongs to more domains it loses its value.

In small signal model of a linearized system, the system behavior and its linearized counterpart behave similar, generating little deviation in their response in small enough distance from neighboring nodes. A piecewise linearized model of the nonlinear system (Figure 5.3) is shown in Figure 5.4. The linearized system has many operating points that may also be influenced by disturbances in form of measurement and system noise. In this case, the linearized model's output deviates more from the nonlinear model behavior. This discrepancy between linearized model and the nonlinear model increases when the operating point moves further away from the linearized model.

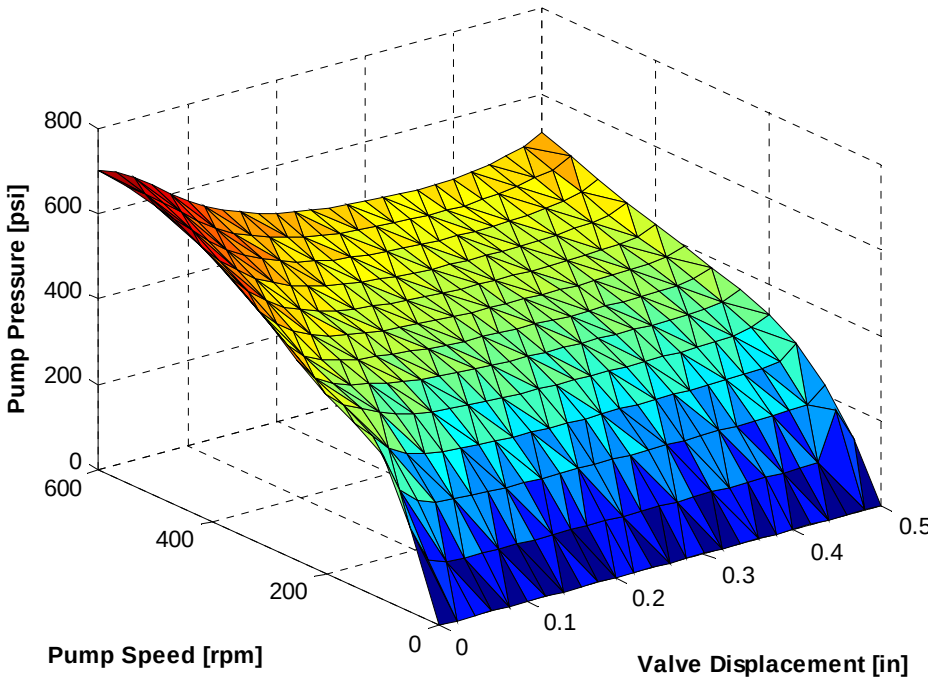

Figure 5.3 Nonlinear model of hydraulic wind power transfer system for a fixed load

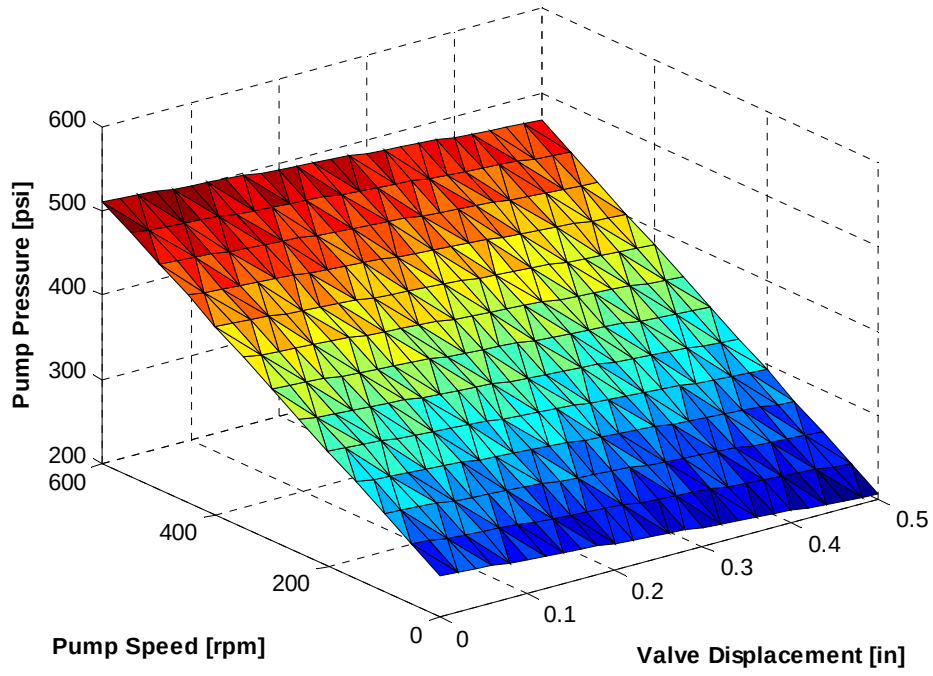

Figure 5.4 Linearized model of hydraulic wind power system around all possible operating points

Considering an acceptable deviation range between the linearized and nonlinear model determines the domain of each piecewise linearized model.

A count on the number of models that share a particular node determines the weight of the node. Among all possible nodes to be considered as operating point, an optimum number with optimum location must be selected to minimize the number of piecewise linearized models and maximize the matching and coverage.

The range of variables in the input of hydraulic wind power system is 200 to 600 rpm for shaft speed (in some systems between 10-30 rpm), and valve position from 0 to 0.5 inches. The piecewise linear modeling is formulated for hydraulic wind power in two major steps as: 1) selection of optimum model number, 2) selection of operating points.

In the first step to optimally select the models, node values must be calculated. The node values are the likelihood of the node to belong to nearby model domains. The more models cover a node the less worthy the node becomes. Figure 5.5 shows the value of each node based on the number of models that cover it. Scaling factor was used to select the optimum nodes. Two factors from equation (5.6) result in various values. Table 5.1 illustrates the effect of various choices for α and β. Through a trial and error, values of 100 and 1 can be selected for α and β respectively. These values result in enough resolution to select models. Models are valued based on the weight of nodes in their domains. Model with the highest rank covers an optimum number of nodes. Therefore, the model with highest rank is selected as a candidate for piecewise linearized model.

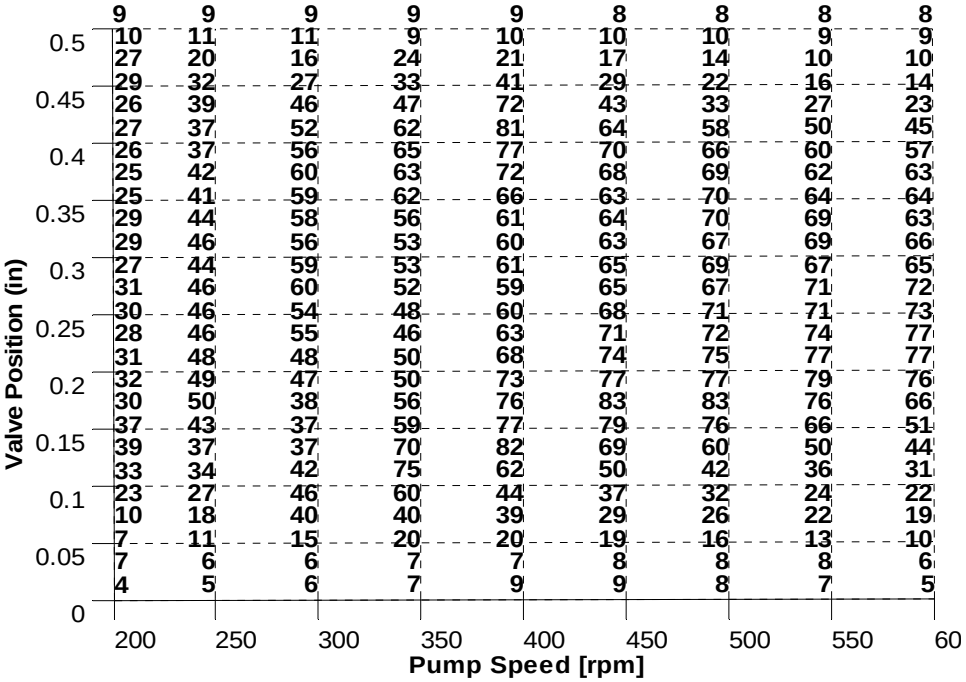

Figure 5.5 Number of models that cover a node. For instance a 9 shows that the node belongs to 9 piecewise linearized models

Table 5.1 Scaling Factor Selection

Scaling Variables	Model Ranks	Scaling Factor
$\alpha = 1$ $\beta = 1$	1	1.249
	2	0.7357
	3	0.7581
	4	0.3527
$\alpha = 1$ $\beta = 3$	1	0.0387
	2	0.0155
	3	0.0053
	4	0.0040
$\alpha = 100$ $\beta = 1$	1	124.9603
	2	73.5714
	3	75.8166
	4	35.2784
$\alpha = 100$ $\beta = 3$	1	3.8782
	2	1.5511
	3	0.5318
	4	0.4073

The nodes that configure the domain of all selected models are eliminated from weighing process and models are continued to be optimized, ranked and selected as candidates in piecewise linearization process. As each model is optimized to contain the highest node weights, the model selection is inherently optimized. The model ranking and iteration process is illustrated in Table 5.2. As the table demonstrates, the first four models are ranked in each iteration and the model associated to the highest rank was selected. As the nodes were eliminated from the domains, the weight of other iterations decreased such that the ratio of weight to number of nodes (domain index) an added model covered became a small value. At some point adding a model did not add enough domain to the overall coverage of the system. Table 5.3 illustrates the decreasing number of nodes added to overall coverage in each iteration.

Therefore, 5 iterations were sufficient for this system and 6 models fulfill the system requirements. Table 5.3 shows the number of added over total covered nodes in each iteration, the domain index.

Table 5.2 Model Ranking in Each Iteration

	Model Rank	Model Weight
Initial weigh	1	147.42
	2	145.99
	3	145.62
	4	145.30
Iteration 1	1	145.62
	2	130.35
	3	130.35
	4	124.96
Iteration 2	1	124.96
	2	124.96
	3	121.14
	4	119.96
Iteration 3	1	121.14
	2	114.66
	3	114.66
	4	113.46
Iteration 4	1	105.55
	2	105.55
	3	105.55
	4	105.55
Iteration 5	1	97.39
	2	94.42
	3	94.42
	4	91.51
Iteration 6	1	88.65
	2	83.63
	3	81.82
	4	81.64

Table 5.3 Number of Added Covered Nodes in each Iteration, Domain Index

Iteration	# of Covered Nodes per Model	Cumulative # of Nodes	Domain Index (Added/Cumulative)
1	93	93	93/93=1
2	22	115	22/115=0.191
3	17	132	0.128
4	26	158	0.164
5	12	170	0.070
6	7	178	0.039<0.04→Stop

Based on the Table 5.3 and the considered criteria, it seems that the first 6 selected models can describe the nonlinear system reasonably. Those 6 models are presented in appendix A and utilized for further analysis and simulations.

5.1.4 Results and Discussion

For better comparison, the proposed piecewise linear modeling is compared with an arbitrary model selection.

5.1.4.1 Arbitrary Model Selection

For the first step, the value of operating points was determined through an even distribution on the node domains. Selecting 6 models, a limited error with maximum deviation was achieved. Figure 5.6 illustrates all the nodes that are associated to each model. Piecewise linearized models and their operating points are also listed on the figure. The figure also illustrates the domain each model contains. Clearly, overlapping and no coverage node are shown with double, triple or no signs. Figure 5.7 demonstrates the arbitrary piecewise linearization model errors and their deviation from the nonlinear model. Dark areas illustrate higher errors and white areas demonstrate nodes out of the linearization domain and coverage [48].

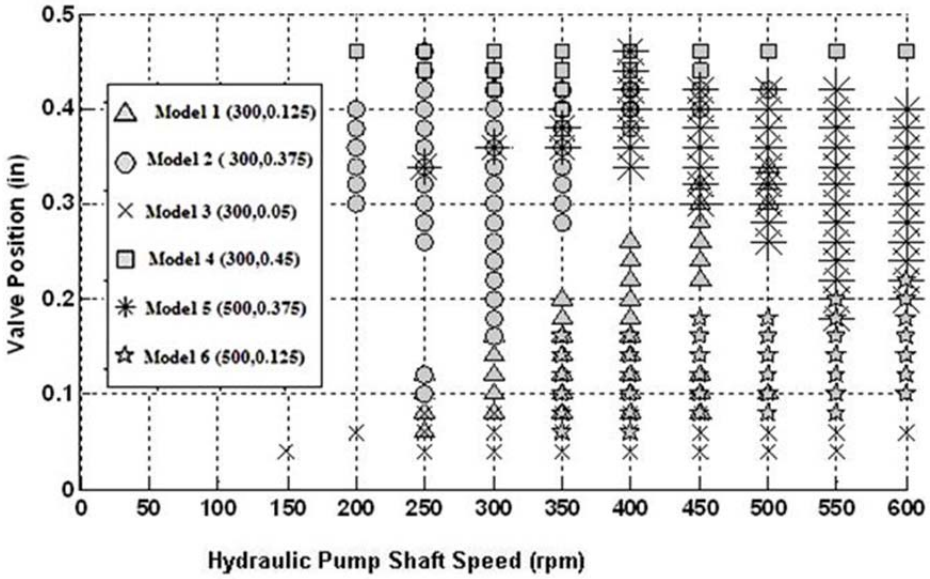

Figure 5.6 The domain associated to each piecewise linearized model

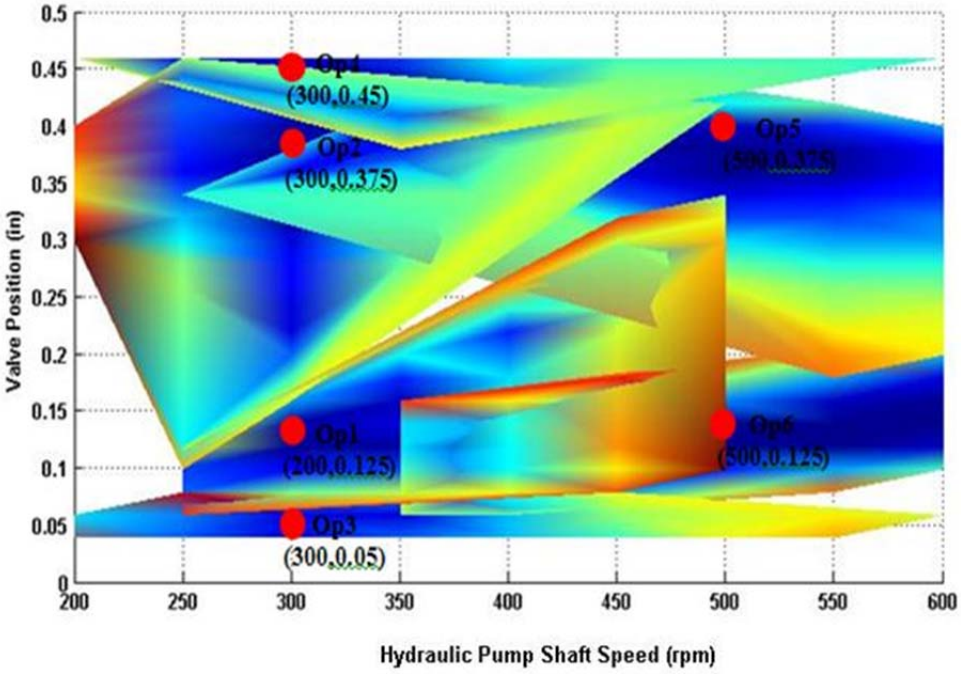

Figure 5.7 Acceptable domain for each of the piecewise linearized models

Two inputs as proportional valve position and the hydraulic motors' shaft rotational speed were used to determine the piecewise linearized models. Limiting the maximum modeling error to 7%, combination of linear models improved the node coverage to 80.75% of all nodes. Figure 5.8 illustrates the smooth coverage of the nodes.

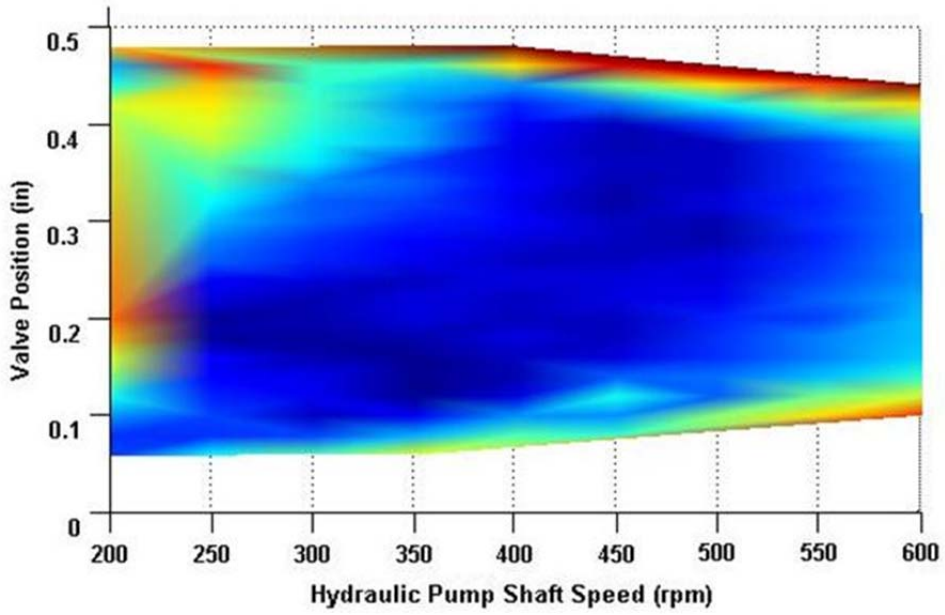

Figure 5.8 Effect of model mixing on overall model estimation and error. Red areas contain nodes with higher error

5.1.4.2 Adaptive Model Selection

The selected optimum piecewise linearized models are shown in Figure 5.9. These models cover 86.2 % of the entire domain and generate errors less than 7%. Considering the combination system to optimize the coverage and minimize the overall error, Figure 5.10 is obtained.

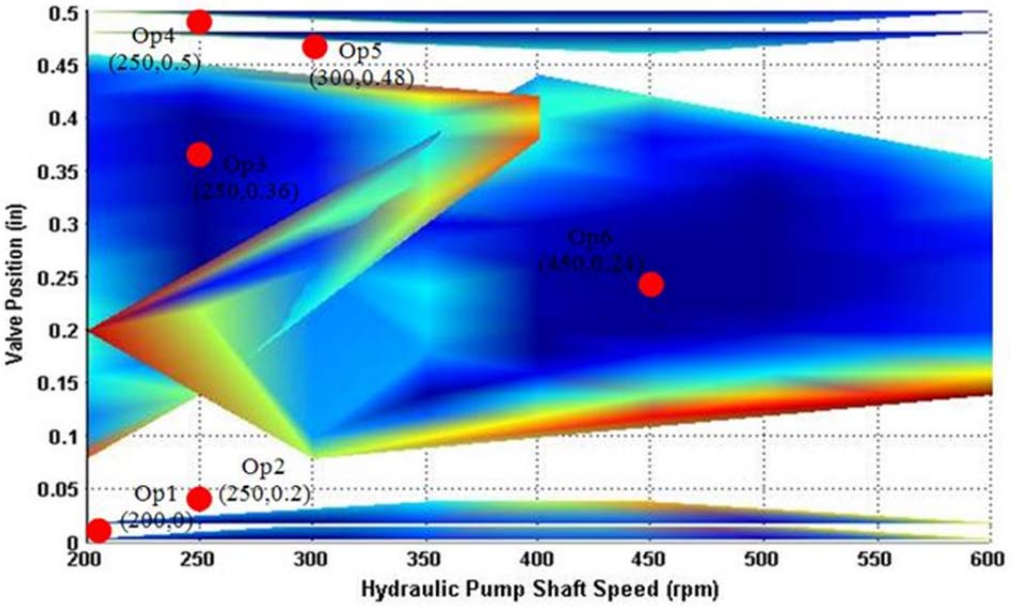

Figure 5.9 Acceptable domain for each of piecewise linearized models selected through the proposed algorithm

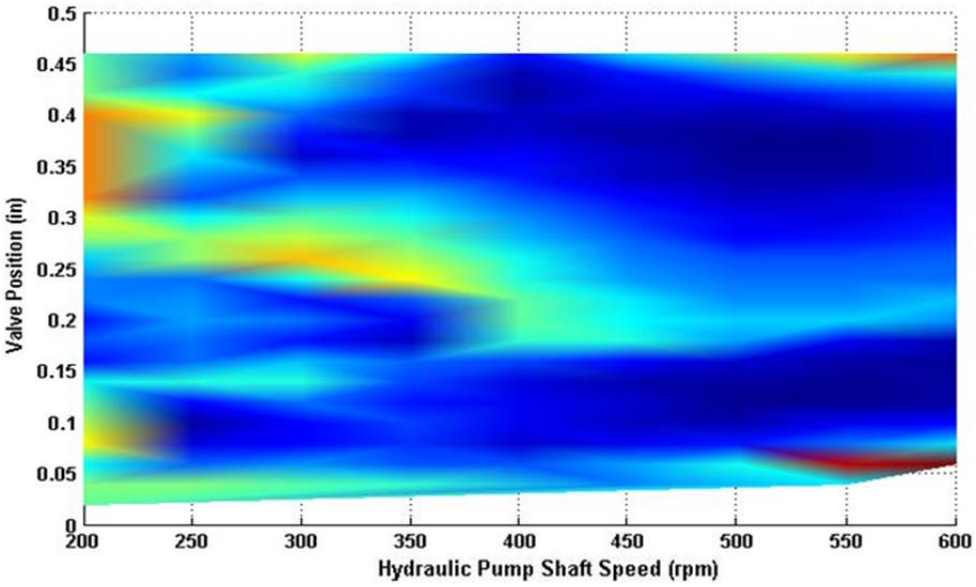

Figure 5.10 Model mixing increased the entire area coverage and reduced the overall error in modeling of non-covered nodes

As it can be seen by selected models from the proposed algorithm, the overall accuracy has been increased by 5.45%. Also by comparing the colors of Figure 5.8 and Figure 5.10, it can be concluded that besides the increase in overall coverage of the node domains, the error between nonlinear system and the multiple model adaptive estimation was optimized. These improvements are observed in the accuracy increase of the state variable estimation as an important measure in linearization.

This section introduced an automatic algorithm to select optimum operating point for piecewise linearization of n-D systems. Combination of models was effectively used to increase the coverage of each linearized model and estimate linear combination of all models for overlapped nodes. The proposed technique was successfully implemented for hydraulic wind power transfer system. The proposed method resulted in better selection of operating points and adaptive piecewise linearization process [74].

5.2 Linear Model Analysis

In control engineering, a state space representation is a mathematical model of a physical system as a set of input, output and state variables related by first-order differential equations. To abstract from the number of inputs, outputs and states, the variables are expressed as vectors. Additionally, if the dynamical system is linear and time invariant, the differential and algebraic equations may be written in matrix form. The state space representation (also known as the "time-domain approach") provides a convenient and compact way to model and analyze systems with multiple inputs and outputs.

This section studies the stability of the 6 optimally-selected linear models from previous section. Stability analysis of linear models is less challenging than the nonlinear models. Therefore, in previous sections, an attempt was made to linearize the nonlinear mathematical model. This approach considerably facilitates the study of the system dynamics.

The state space representation of a linear dynamic system is as follows:

$$\begin{aligned} \dot{x} &= Ax + BU \\ y &= Cx + DU \end{aligned} \tag{5.11}$$

The state space representation of the system could be transformed into transfer function representation by:

$$H(z) = C(sI - A)^{-1}B + D \tag{5.12}$$

where s is the Laplace operator, and I is an identity matrix with the same dimension as A.

For a SISO system with transfer function H(z) = N(z)/D(z) the poles and zeros are straightforward to define:

- Poles are the roots of D(z)
- Zeros are the roots of N(z)

Poles of a system are the frequencies of the eigensolutions not driven by U but still appearing in y, i.e., they are generated by the system. In a state space model $\dot{x} = Ax + BU$, these are the solutions of the standard eigenvalue problem $A\upsilon = \lambda\upsilon$.

One of the first things to do is to analyze whether the open-loop system (without any control) is stable. The eigenvalues of the system matrix, A, (equivalent to the poles of the transfer function) determine the stability. The eigenvalues of the A matrix are the values of s where $\det(sI - A) = 0$.

Poles of the 6 derived discrete linear models indexed in Appendix are listed in Table 5.4.

Table 5.4 List of Discrete Linear Models Poles

Model	Poles
Model 1	0.0088 0.9246 0.9947 + 0.0079i 0.9947 - 0.0079i 0.9975
Model 2	0.0059 0.7430 0.9952 + 0.0077i 0.9952 - 0.0077i 0.9990
Model 3	0.0766 0.4850 0.9949 + 0.0078i 0.9949 - 0.0078i 0.9985
Model 4	0.0349 0.8595 0.9944 + 0.0078i 0.9944 - 0.0078i 0.9975
Model 5	0.0886 0.8194 0.9951 + 0.0077i 0.9951 - 0.0077i 0.9986
Model 6	0.2220 0.6758 0.9953 + 0.0076i 0.9953 - 0.0076i 0.9991

Theorem: A discrete-time linear time-invariant system is asymptotically stable if and only if all eigenvalues are strictly inside the unit circle. As it shown in Table 5.4, all the poles of linear models are in the unit circle which determines the stability of the linear models.

6. OBSERVATION AND CONTROL

This chapter utilizes the mathematical models from previous chapters as well as linearized models and their stability analysis to observe the states of the system and also design a controller. The main function of the designed controller is to maintain a constant speed for primary motor under the load and wind disturbances.

In the first section, an observer and an adaptive control system is designed and simulated for the proposed linear models. In the second section a control system is designed and implemented for the experimental setup to validate the mathematical models and analysis.

6.1 Mathematical Model

6.1.1 Multiple-Model Adaptive Estimation

Nonlinear model of a hydraulic wind power system operates on a wide spectrum of operating points such as random wind speed disturbances and applied control commands. Thus, one way to linearize this model is to use multiple linear models representing the whole range of operating points. This section utilizes the linearized models derived by piecewise linearization in a multiple model adaptive estimation

(MMAE) framework to reduce the state estimation error. System parameters such as pressures of the pump and motors can be estimated while the overall error in entire operating points is reduced. The algorithm is composed of a bank of Kalman filters, each of which is modeled to match particular real world operating condition. Simulation results demonstrate that the adaptive approach can optimally estimate the state variables in a wide range of operating points.

6.1.1.1 Introduction and Literature Survey

Hydraulic wind power systems are new type for the wind power harvesting which offers several advantages over geared power transfer system counterparts. In this method, the gearbox is replaced with a hydraulic pump, which is coupled with the wind turbine to generate high-pressure hydraulic fluid in the system. This flow can be used to drive a number of generators. When controlled, the hydraulic flow is distributed between two hydraulic motors coupled with electric generators to supply electric power to the grid. The intermittent nature of wind speed results in the fluctuation on the wind turbine generator angular velocity [75], [76] and the power generation. To mitigate the effect of the output power fluctuations, an advanced control technique must be considered for the speed regulation of the generation units.

Nevertheless, the speed control of hydraulic wind power systems is challenging, since it is a nonlinear system under random disturbance inputs i.e. wind speed. The Nonlinearities in such systems are originated from nonlinear behavior of components such as check valves, directional valves and more importantly the proportional valve. These nonlinearities will cause behavioral changes and variations in the system.

Therefore, the speed control of the system would require an in-depth modeling. The controller's performance depends on states variables while the system is influenced by large input variations in a wide operating range.

The design of a single state observer for a given plant requires exact knowledge of the plant parameters and the disturbances on the system for superior performance. In practice, parameter uncertainty and disturbances will impact the performance and robustness of the observer. In fact, incorrect modeling in the observer design may lead to large estimation errors or even error divergence.

To mitigate this problem, adaptive estimation algorithms (where the adaptation is with respect to the disturbances and uncertainty in the plant parameters) have been proposed in the literature such as Newton-type adaptive estimation algorithms [77], and least squares adaptive algorithms [78]. Among these, the Multiple-Model Adaptive Estimation (MMAE) algorithm has received particular attention because of its functionality to deal with uncertainties and wide operating regimes systems [79], [80]. However, the use of multiple models for adaptive estimation goes back to the 1960s and 1970s when several authors studied Kalman filter based estimators as Kalman filter offers some advantageous such as its convenience form for online real time processing, Easy to formulate and implement given a basic understanding, Good results in practice due to optimality and structure, etc. [81]

Throughout past decade, a number of papers have made efforts to describe the use of multiple- model architectures for adaptive estimation and control, e.g. [82], [83], and [84]. While some have employed deterministic continuous-time methodologies [85], others utilized a discrete-time probabilistic approach [86]. All of these papers utilize

multiple-model architecture for the identification system. Multiple-model adaptive estimation (MMAE) was first proposed by Magill [87] and has been used in several papers obtaining numerous results on its properties such as state observers [88].

In the stochastic version of the MMAE [89], a separate discrete-time Kalman filter (KF) is developed for each selected model defined by a hypothesized parameter and disturbance vector in a wide range of system operating points. The resulting set of KFs forms a "bank" where each local KF generates its own state estimate and an output error (residual). The bank of KFs runs in parallel and at each sampling instant, the MMAE uses the measurement residuals to compute the conditional probability *p*. The higher probability will correspond the plant to a true plant model. The state estimation is a probabilistically weighted combination of all KF estimates. The rationale is that the highest probability should be assigned to the state estimation provided by the most accurate KF, and lower probabilities assigned to the remaining KFs [81], [90].

In this section, MMAE is utilized for state estimation of a nonlinear hydraulic wind power transfer system. The system is subject to multiple operating regimes which are initiated by external factors such as changes in control command or persistent plant disturbances (e.g., variations in wind speed).

6.1.1.2 Theory Overview

6.1.1.2.1 Kalman Filter

Kalman filters are used to estimate the states of linear systems. However, if inaccurate model parameters are used to construct the filter, the state estimate accuracy will degrade and may even diverge [91]. Consider a Kalman filter model associated with a particular hypothesized status of the hydraulic wind power transfer, which is denoted with the subscript *k*. Thus, the k^{th} model can be represented by [92]:

$$\begin{aligned} x_k(t_i) &= \Phi_k x_k(t_{i-1}) + B_k u(t_{i-1}) + G_k \omega_k(t_{i-1}) \\ z_k(t_i) &= H_k x_k(t_i) + \nu_k(t_i), \end{aligned} \tag{6.1}$$

where x_k is the Kalman filter model state vector, Φ_k is the state transition matrix, B_k is the control input matrix, u is the system input vector, G_k is the system noise matrix, z_k is the measurement noise, H_k is the output matrix, ω_k is an additive white discrete-time system noise with zero mean value and covariance Q_k as follows:

$$E\{\omega_k(t_i)\omega_k^T(t_i)\} = \begin{cases} Q_k, & t_i = t_j \\ 0, & t_i \neq t_j \end{cases} \tag{6.2}$$

and ν_k is an additive white measurement noise that is used in the Kalman filter model. This noise is independent from ω_k, with zero mean value and covariance R_k as follows:

$$E\{\nu_k(t_i)\nu_k^T(t_i)\} = \begin{cases} R_k, & t_i = t_j \\ 0, & t_i \neq t_j \end{cases} \tag{6.3}$$

In the hydraulic wind power system, the noise parameters Q and R are not accurately known, and can also change over time depending on operating conditions. To

derive these noise covariance matrices, the algorithm in [93] has been used and implemented in the Kalman filter.

The Kalman filter algorithm utilizes a discrete linearized model follows:

$$\begin{aligned}\hat{x}_k(t_i^-) &= \Phi_k \hat{x}_k(t_{i-1}^+) + B_k u(t_{i-1}) \\ \hat{z}_k(t_i^-) &= H_k \hat{x}_k(t_i^-),\end{aligned} \tag{6.4}$$

where $\hat{x}_k$ is state estimation vector, $\hat{z}_k(t_i^-)$is the output estimation at time $t_i^-$of the i^{th} time sample, $t_{i-1}^+$is the time after the measurement update at the $(i\text{-}1)^{\text{th}}$ time sample, and the state estimation covariance matrix propagation is:

$$P_k(t_i^-) = \Phi_k P_k(t_{i-1}^+)\Phi_k^T + G_k Q_k G_k^T \tag{6.5}$$

The state estimation will be updated using:

$$\hat{x}_k(t_i^+) = \hat{x}_k(t_i^-) + K_k(t_i) r_k(t_i), \tag{6.6}$$

where the Kalman gain is:

$$K_k(t_i) = P_k(t_i^-) H_k^T A_k(t_i)^{-1}, \tag{6.7}$$

and the Kalman filter-computed residual covariance matrix A_k is:

$$A_k(t_i) = H_k P_k(t_i^-) H_k^T + R_k. \tag{6.8}$$

The Kalman filter residual vector, shown in equation (6.6), is defined as:

$$r_k(t_i) = z(t_i) - H_k \hat{x}_k(t_i^-) = z_T(t_i) - H_k \hat{x}_k(t_i^-) \tag{6.9}$$

The covariance matrix is updated using as follows

$$P_k(t_i^+) = P_k(t_i^-) - K_k(t_i) H_k P_k(t_i^-), \tag{6.10}$$

$$\hat{x}_k(t_i^-) = \Phi_k \hat{x}_k(t_{i-1}^+) + B_k u(t_{i-1}). \tag{6.11}$$

Therefore, the steady state Kalman filter can be represented as

$$\hat{x}_k(t_i^+) = \hat{x}_k(t_i^-) + K_k r_k(t_i). \tag{6.12}$$

6.1.1.2.2 MMAE Structure

A block diagram of the MMAE scheme is shown in Figure 6.1. The input and output data of a plant with wide range of operating point is collected and passed to a bank of Kalman filters. The Kalman bank contains many parallel filters, called hypothesis filters where each is constructed using a model representing a different operating condition. The output of each filter is compared with that of the hydraulic wind power plant. The filter with the lowest residual represents the most accurate models.

The MMAE generates a weighted average of all Kalman estimated values. The weights are obtained by the *a posteriori* probability of the residual signals considering a history of input-output variations [94]. These weights can be calculated using:

$$p_k(t_i) = \frac{f_{z(t_i)|h,z(t_{i-1})}(z_i|h_k, Z_{i-1}).p_k(t_{i-1})}{\sum_{j=1}^{K} f_{z(t_i)|h,z(t_{i-1})}(z_i|h_k, Z_{i-1}).p_j(t_{i-1})}, \tag{6.13}$$

where

$$f_{z(t_i)|h,z(t_{i-1})}(z_i|h_k, Z_{i-1}) = \frac{1}{(2\pi)^{m/2}|A_k(t_i)|^{1/2}} \exp([-\frac{1}{2} r_k(t_i)^T A_k^{-1}(t_i) r_k(t_i)]). \tag{6.14}$$

In these equations, $f_{z(t_i)|h,z(t_{i-1})}(z_i|h_k, Z_{i-1})$ is the probability density function of the current measurement $Z(t_i)$ conditioned on the hypothesized status and measurement history $Z(t_{i-1})$, based on residual signal r_k and A_k. When actual residuals are inconsonance with filter-

computed covariance A_k, the exponential term in equation (6.14) is approximately [$-m/2$], where m is the measurement dimension.

The output of this block is a vector of probabilities which can be used to weight the state estimates as also shown in Figure 6.1. The output of the algorithm is a probability weighted state estimate [94], [95].

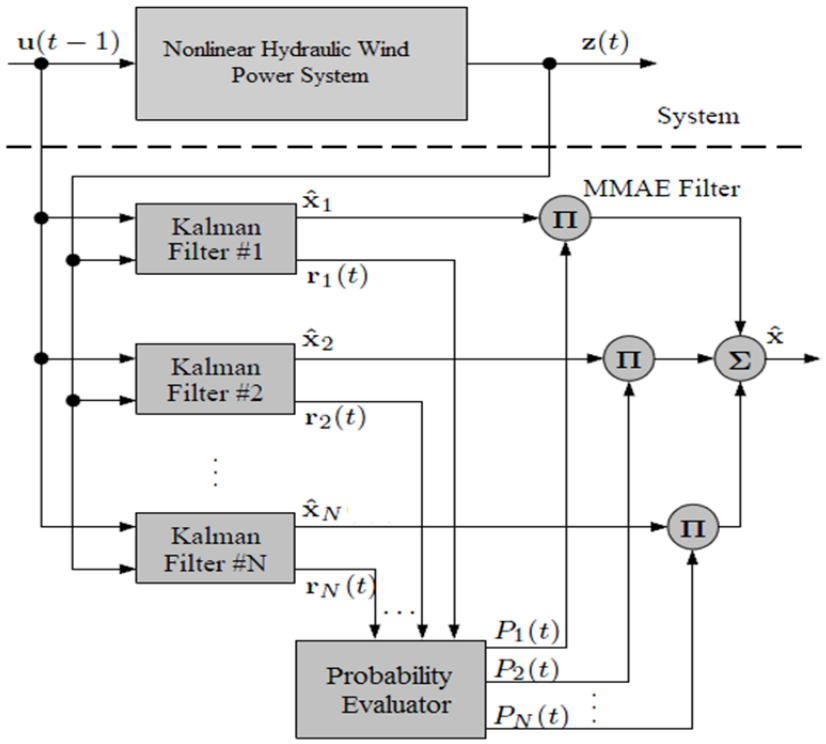

Figure 6.1 The MMAE filter block diagram

6.1.1.3 Main Results and Simulations

As mentioned earlier in modeling section of nonlinear hydraulic wind power system, it can be concluded that the system has 5 states which account for pressure of the pump and motors and speed of the motors. Reading the data from motors speed sensor,

they can be sent to the Kalman filters as a measurement for estimating the 3 other noisy pressures in different operating regimes.

Kalman filters and MMAE block diagram has been implemented using MATLAB/Simulink. The estimation of MMAE for the pressures is compared with the exact values from the nonlinear model of system in all possible operating points specified by control and disturbance input (valve position and wind speed respectively) to study the accuracy of implemented structure.

A comparison between MMAE and the nonlinear model is done by applying a arbitrary profile for wind speed as a disturbance input shown in Figure 6.2 to both systems with valve position of 0.35 inch. Figure 6.3 to Figure 6.5 depict the performance of state estimation of pressures comparing with the exact values from the nonlinear model.

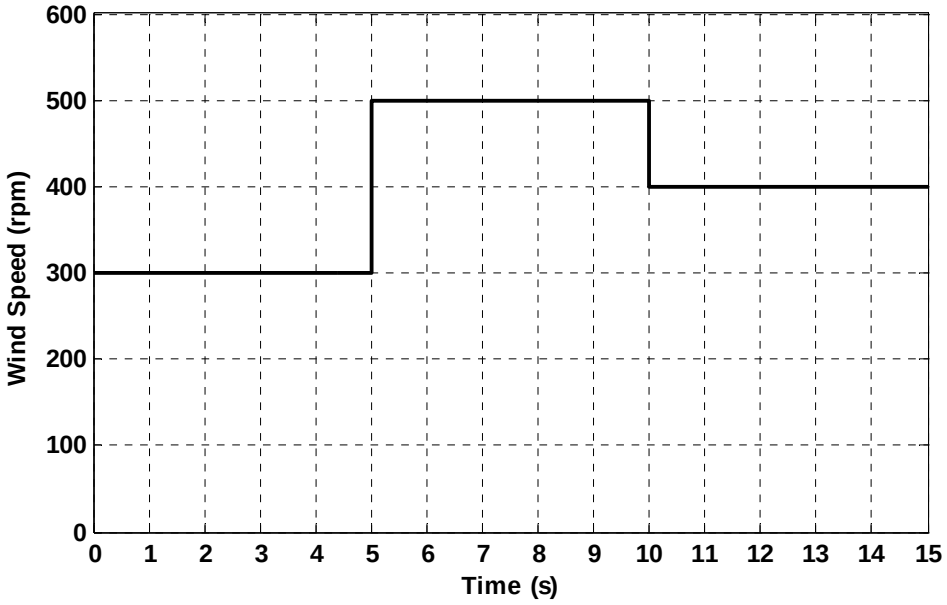

Figure 6.2 Wind speed profile applied to both systems

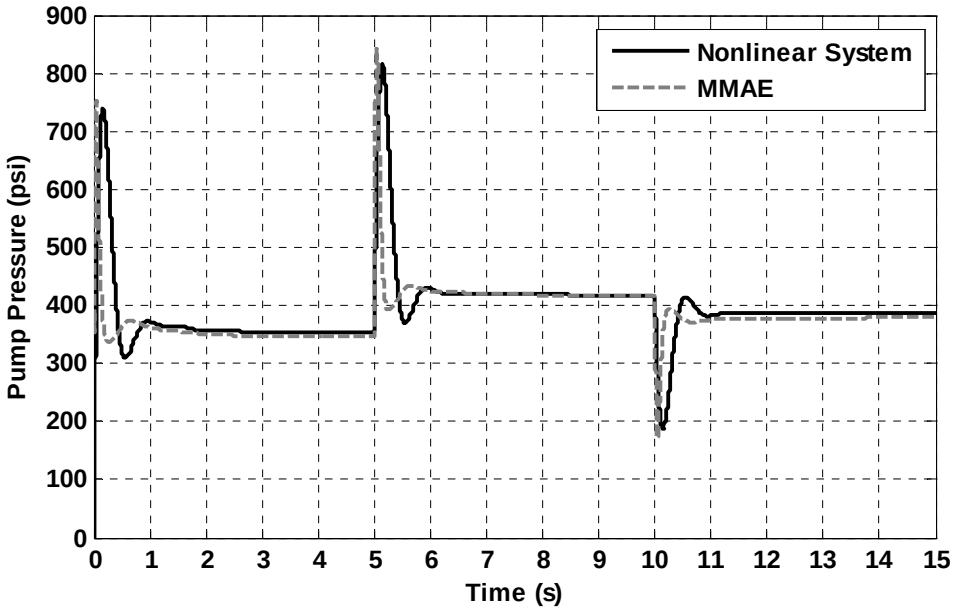

Figure 6.3 Pump pressure estimation, nonlinear system vs MMAE

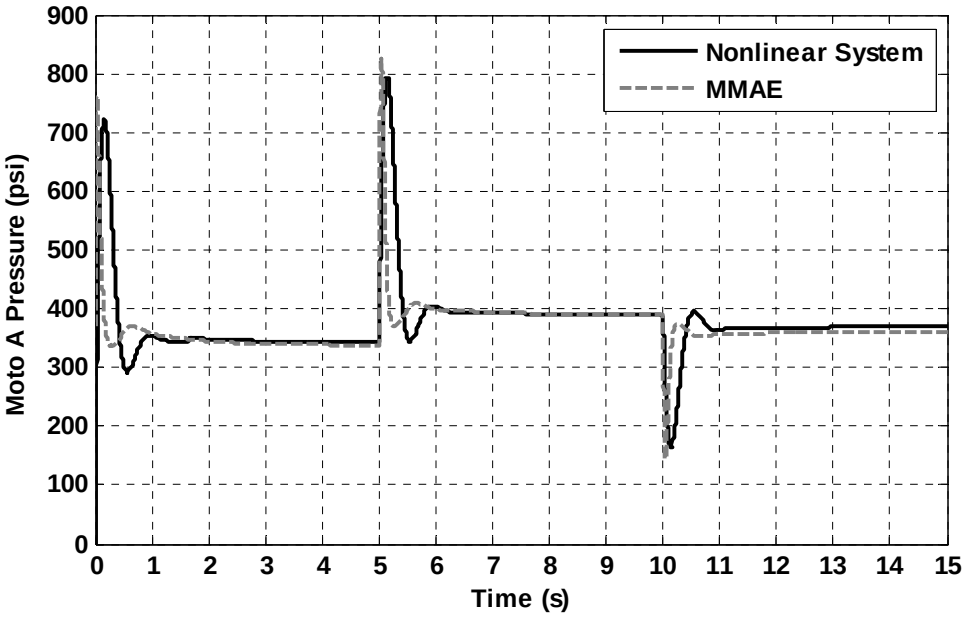

Figure 6.4 Motor A Pressure estimation, Nonlinear system vs MMAE

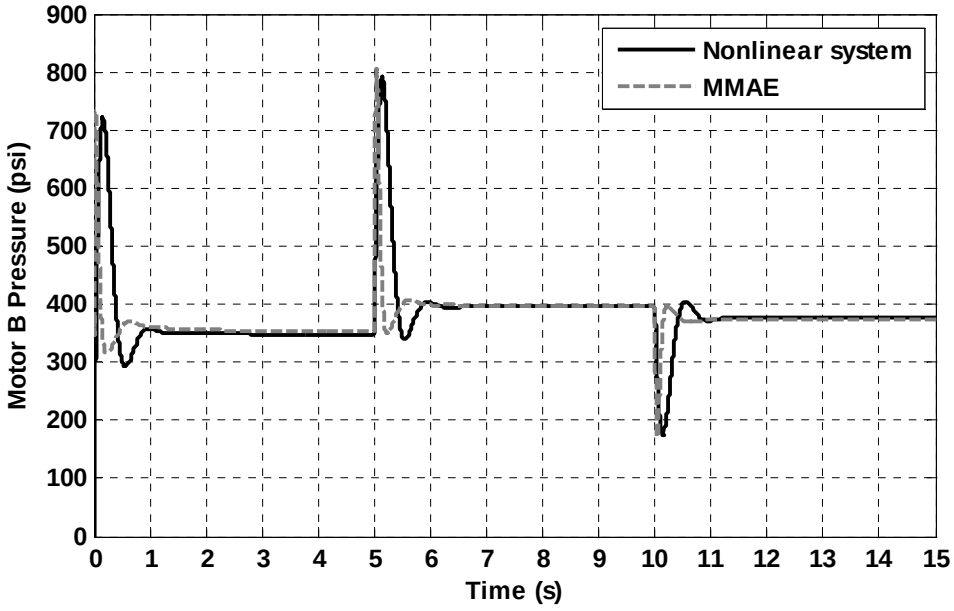

Figure 6.5 Motor B Pressure estimation, Nonlinear system vs MMAE

Figure 6.3 to Figure 6.5 confirm a close agreement between implemented MMAE and nonlinear system. It can be seen that the state estimation benefits from a good performance even in transients. As the MMAE estimation performance highly dependent on the Q and R noise covariance matrices, their precise estimation reduced their effects of disturbance analysis. In addition, precise operating point selection was essential in linearization and overall modeling performance improvement.

MMAE was applied to adaptively estimate states of a nonlinear hydraulic wind power system in wide operating conditions. This estimation technique uses a bank of Kalman filters, each of which represent a linear model for a specific range of operating point. In this section, MATLAB/Simulink was utilized for implementation of the MMAE structure. Accuracy of state estimation using MMAE was also verified by comparison with the nonlinear system [96].

6.1.2 Multiple-Model Adaptive Control

In this section a multiple model adaptive control (MMAC) strategy is used to mitigate the undesired effect of output power fluctuations in hydraulic wind power systems. This control structure is based on linear Kalman filters, probability block and PID controllers and aims to regulate the speed of generation unit. Nonlinearities and disturbances such as wind speed and valve position make the system work over a wide range of operating point which degrades the performance of the control loop. MMAC as an approach for these types of systems implemented and simulated to consider the control performance over the whole operating regimes.

6.1.2.1 Introduction and Literature Review

Adaptive control is a promising approach to estimate and control dynamic systems [97]. The study of multiple model adaptive control (MMAC) appeared around 1960'sto 1970's, where multiple Kalman filter-based models were studied to improve the accuracy of the state estimate in estimation and control problems [98], [99]. Soon after applications of MMAC were introduced [100]-[102].

Various approaches for the multiple model adaptive control have been established since the 90's. Balakrishnan's and Narenda's proposed several stability and robustness methods using classical switching and tuning algorithms. Later on, the perfection of the multi-model control concept was proved by further research. Magill and Lainiotis introduced the model representation through Kalman filters. Petridis', Kehagias' and Toscano's work focused on nonlinear systems with time variable. Landau and Karimi used several particular parameter adaptation procedures, Closed Loop Output Error, in MMAC. Additionally, Narenda utilized neural network to improve his multi-model control version. Finally, Dubois, Dieulot and Borne apply fuzzy procedures for switching and sliding mode control.

Progress in performance and stability of multiple models adaptive control soon made this approach applicable to various control problems where operating regimes cannot be determined a priori such as robotics, flight control, aerospace applications, and process control. Numerous results based on these methods can be found for example in Fekri et al. [103], Schiller and Maybeck [104], and Hespanha et al. [105]. Common to all these methods is the use of information obtained online to decide on appropriate control actions.

Multiple-model adaptive control is a promising approach to control complex, nonlinear, and time-variant systems with a wide range of operating points. In multiple model adaptive control, a bank of candidate models is designed to be used by the control structure. Then a supervisory controller selects the most appropriate model for the current conditions. For each model, a suitable controller can be designed off-line. The online controller switching is based on the performance evaluation of the bank of models. Control problems involving transitions between known operating regimes are readily handled by a multiple model approach [106]. This kind of multiple model adaptive control is always produced as the probability-weighted average of elemental controller outputs. As theoretical progress of MMAC, some convergence results on the probabilistic weighting algorithm have been obtained under suitable assumptions [107]-[110].

It is obvious that model bank significantly affects control performance. Thus, it is critical to have a model bank that considers all possible operating points. Since all possible operating points are not known a priori, increasing the number of model bank members may be a solution [111].

This section proposes a multiple models adaptive control structure for a hydraulic wind power system in order to maintain high performance over a wide range of operating points. These hydraulic systems run under fluctuating disturbances i.e. wind speed profile and valve position which influence on system operating regimes. Thus, there would be a crucial need for an advance control structure to eliminate negative effects of disturbance inputs.

6.1.2.2 Theory Overview

The nonlinear state space shown in equation (3.29) can be linearized around operating points. The linear model can be used for developing proper controller. However a linear model is valid for certain neighborhood of the operating points. If actual states of the system become far away from the points used for linearization, the behavior of the system would be totally different from the linearized. To cover all possible scenarios of the system operation, linearization of the model is needed at several set of operating points. As operation of the proportional valve descried in the modeling section, the valve plays a major role of nonlinearity in the system. The valve spool position can be varied from fully open to full closed and its performance at different operating points would differ to great extent. So that to derive multi linearized model, different valve spool positions are considered. Another input to the system that affects the system behavior is the pump speed. The pump speed is directly affected by wind speed. Wind speed varies widely. Therefore different pump speeds are used for deriving linearized models. The combination of the valve spool position and pump speed gives us multiple models and hence an appropriate controller should be design for each of them. Each of these controllers regulates the valve spool displacement to reach the desired primary motor speed.

Using multiple models is necessary because of physical uncertainties and disturbances in the hydraulic wind power system which causes a wide range of operating points. These variations and disturbances are well beyond the robustness of a single Kalman filter and correspondent controller [112]. MMAC is an adaptive technique that can overcome the robustness problems of a single filter/controller. In this method a

separate Kalman filter/PID controller is developed based on each different operating point [96].

Consider a Kalman filter model associated with a particular hypothesized status of the system, which was represented by equation (6.1) to equation (6.12). This set of Kalman filters forms a "bank," each filter based on a different system model and each outputting a residual as shown in Figure 6.6.

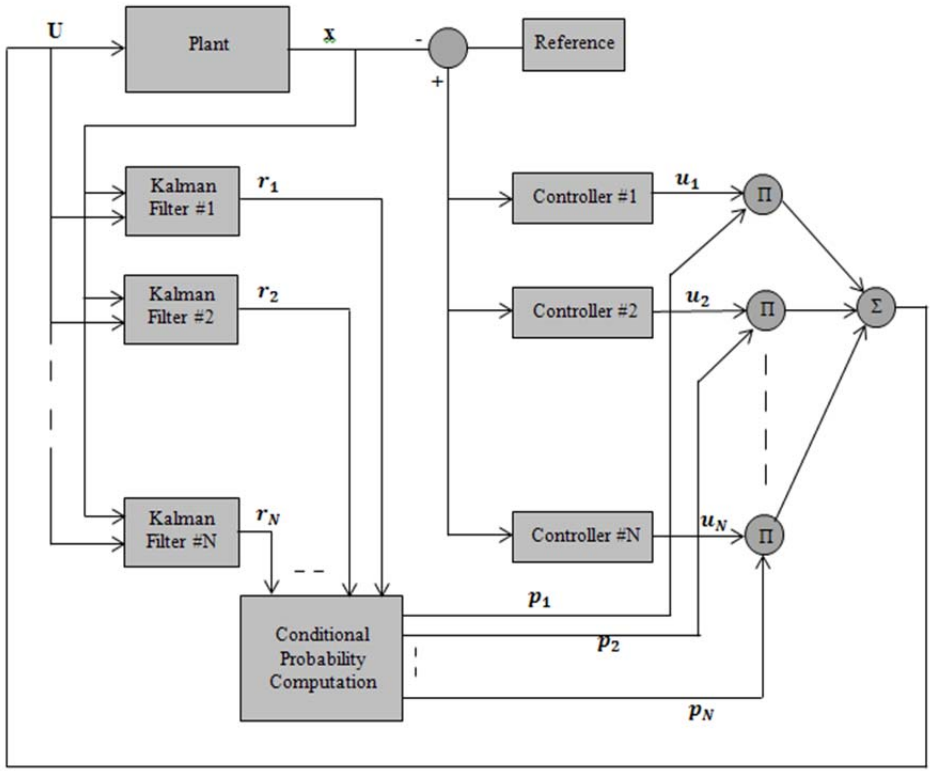

Figure 6.6 Multiple Model Adaptive Control (MMAC) structure

For each Kalman filter a PID controller is designed based on different tuning approaches in order to satisfy performance indices for that specific Kalman filter having the form of:

$$u(t) = K_p e(t) + K_i \int_0^t e(t)dt + K_d \frac{de(t)}{dt}, \tag{6.15}$$

where k_p, k_i, and k_d are proportional, integral and derivative gains, respectively and $e(t)$ is the error between desired output and system output.

The controller output based on the assumed operating point closest to the true operating point should be the most correct. The magnitude of the residual for this filter should be relatively small compared with the magnitudes of the residuals from the other filters. The residuals are used to compute conditional probabilities that each filter (and associated controller gain) is the one based on the correct operating point, and a weighting factor is determined for the corresponding controller output. The conditional probability is the probability that the parameter used in the system model for that filter is closest to the true operating point, conditioned on the entire measurement history observed up to that time. Thus, the highest probability should be assigned to the most correct filter, and lower probabilities assigned to other filters [113]. These probabilities can be calculated using equation (6.13) and equation (6.14). Each control input is then multiplied by its corresponding conditional probability to form a probabilistic weighted average final control input.

6.1.2.3 Control Structure Test

Going through the multiple model linearization approaches in chapter 5, it was concluded that 6 models can cover the whole range of operating regimes and constitute the model bank. The more precise a model bank represents the plant, the better the

control system performs. To come up with the Kalman filters, all linearized models (appendix A) are discretized and related Q and R covariance matrices are designed. Then, these Kalman filters are implemented in MATLAB/Simulink and used to feed the probability block with the residuals.

In this simulation, for each Kalman filter, a PI controller is designed using IMC tuning method to meet the performance indices such as overshoot and settling time. The input to the controllers is the error between desired output and the system output i.e. motor A speed.

Working on different operating points caused by control input and disturbance on the system, it is of high importance to create smooth transition among Kalman filters, eliminate parameter uncertainty effects, and minimize the tracking error in entire operating condition. As mentioned earlier, poor transition may lead to long periods of transient operation, usually accompanied by loss of information and instability [96]. The probability block is implemented in Simulink control loop to fulfill these expectations.

First, to simulate the bank of models, a sequence of events concerning the operating points is used as operation scenario. Then, to investigate the capability of the Kalman filters, identical operation points to what previously considered for linearizing the nonlinear model are included in the operation scenario. The operation scenarios are assumed to be as the following:

1. Pump speed *300* rpm and valve position *0.05* inch
2. Pump speed *300* rpm and valve position *0.125* inch
3. Pump speed *300* rpm and valve position *0.375* inch
4. Pump speed *300* rpm and valve position *0.45* inch

5. Pump speed *500* rpm and valve position *0.125* inch

6. Pump speed *500* rpm and valve position *0.375* inch

These series of events occur consecutively and cover common types of variations that the hydraulic wind system might undergo during their operation. Figure 6.7 depicts the conditional probability densities which are going to be multiplied by each controller output accordingly.

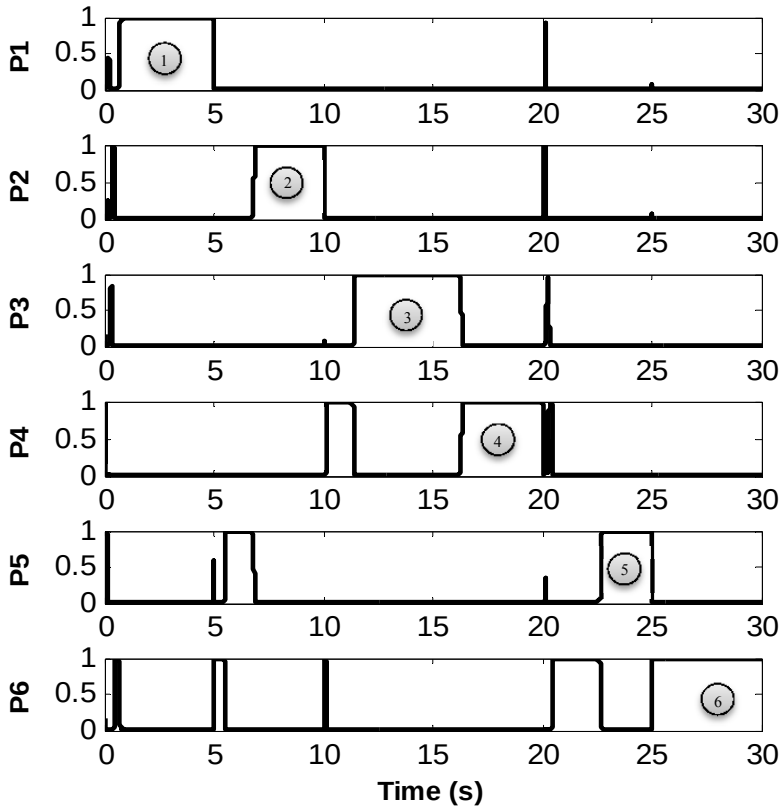

Figure 6.7 Conditional probability density function outputs over different cases of the operation scenario. Higher output values show the validity of the case and as a result the diagnosis of the change in operation. Numbers 1–6 show different steps of operation scenario

Applying probability density functions on operation scenario designates a weight between 0 and 1 to each system's output in each time instant. Higher probability numbers indicate validity of that particular system in that sample. Figure 6.7 shows the weight allocation computed by probability density functions in evaluation of the residual signal. As Figure 6.7 shows, the highest weight is allocated to a proper model (numbered according to the operation scenario) which accurately follows the scenario. Also, a quick transition is observed among steps. The control structure accurately identifies the change in operation points as designed in the scenario.

To clarify the overall performance of MMAC in speed tracking of nonlinear model of hydraulic wind power system, two different type of simulations are done by applying an arbitrary profile for wind speed (pump Speed) as a disturbance input.

6.1.2.4 Primary Motor Speed Regulation

In this simulation two different constant speeds are considered for motor A as a reference to evaluate the performance of the control system to generate fixed frequency power under variation of the wind speed as a disturbance.

6.1.2.4.1 2-Pole Generator

To generate 60 Hz electrical power by a 2 pole generator, the reference speed (motor A speed) needs to be 1800 rpm. Control system's goal is to maintain this reference under variation of the pump speed shown in Figure 6.8.

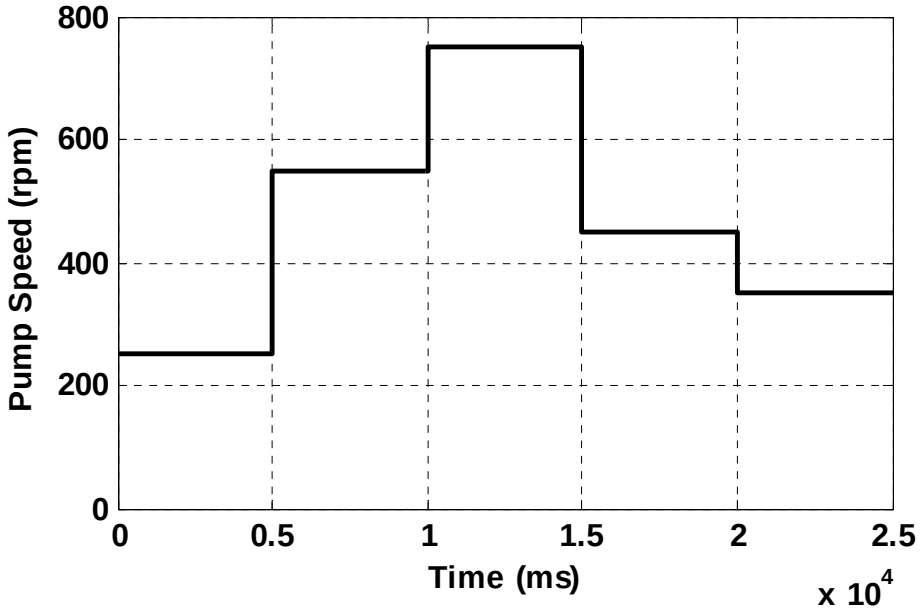

Figure 6.8 Applied pump speed variation as a disturbence on the system

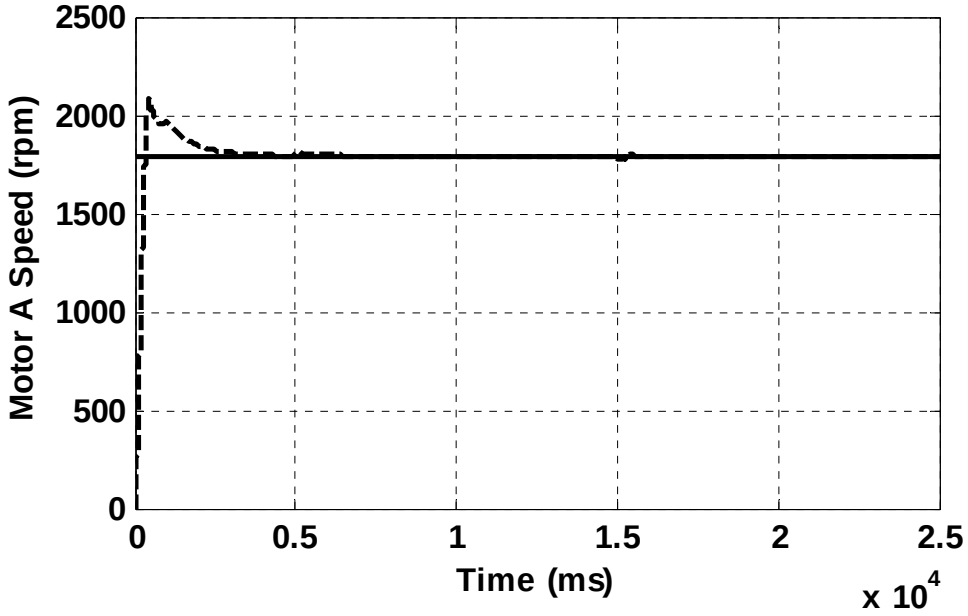

Figure 6.9 Regulation response of multiple models adaptive control with a 2 pole generator

Figure 6.9 shows the speed regulation of power generating achieved by MMAC. It can be seen that motor A speed remains constant under applied disturbances.

As it is depicted in Figure 6.10, control structure is selecting the best controllers by applying weights to their outputs according to instantaneous pump speed and valve position. It should be mentioned that control structure smooth transition between controllers has not affected control response.

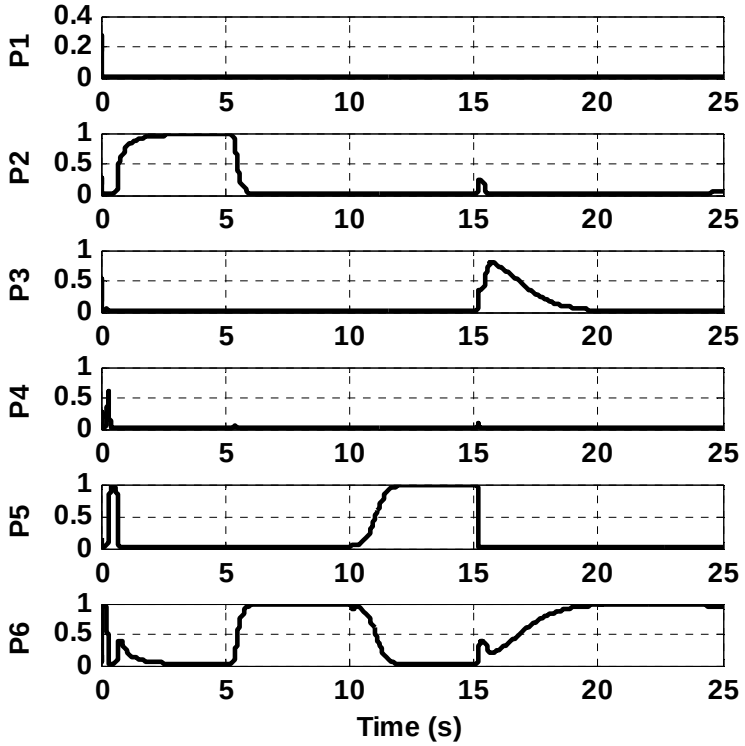

Figure 6.10 Weights of controllers output calculated by probability block

6.1.2.4.2 4-Pole Generator

In this section, the same simulation is considered for a system with 4 pole generator. In this case, motor A speed must be 900 rpm. Running the system under the

same disturbance profile shown in Figure 6.8, MMAC regulates the speed with a reasonable discrepancy, illustrated in Figure 6.11.

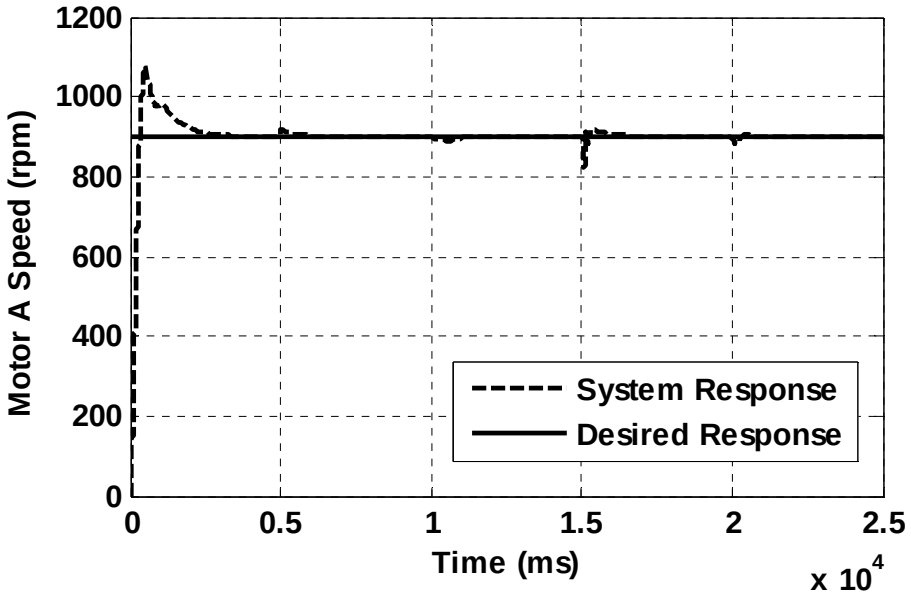

Figure 6.11 Regulation response of multiple models adaptive control with a 4 pole generator

Figure 6.12 shows the probability weights generated by MMAE unit to the controllers output. It can be seen that controllers number 3 and 4 are never utilized in MMAC. This indicates that system has not been run over those operation points correspondent to the controllers number 3 and 4.

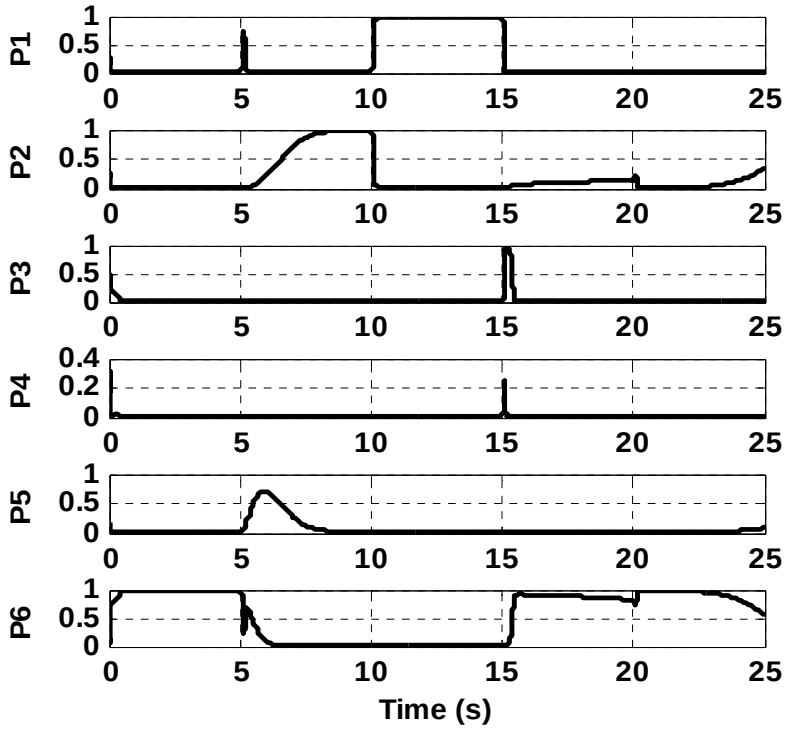

Figure 6.12 Weights of controllers output calculated by probability block

6.1.2.5 Primary Motor Speed Tracking

Challenging the utilized control approach, a fluctuating desired motor A speed is considered in order to run the system in different possible operating points. Figure 6.13 depicts the applied pump speed to the control system. Also, Figure 6.14 illustrates the desired output as well as tracking response of the MMAC.

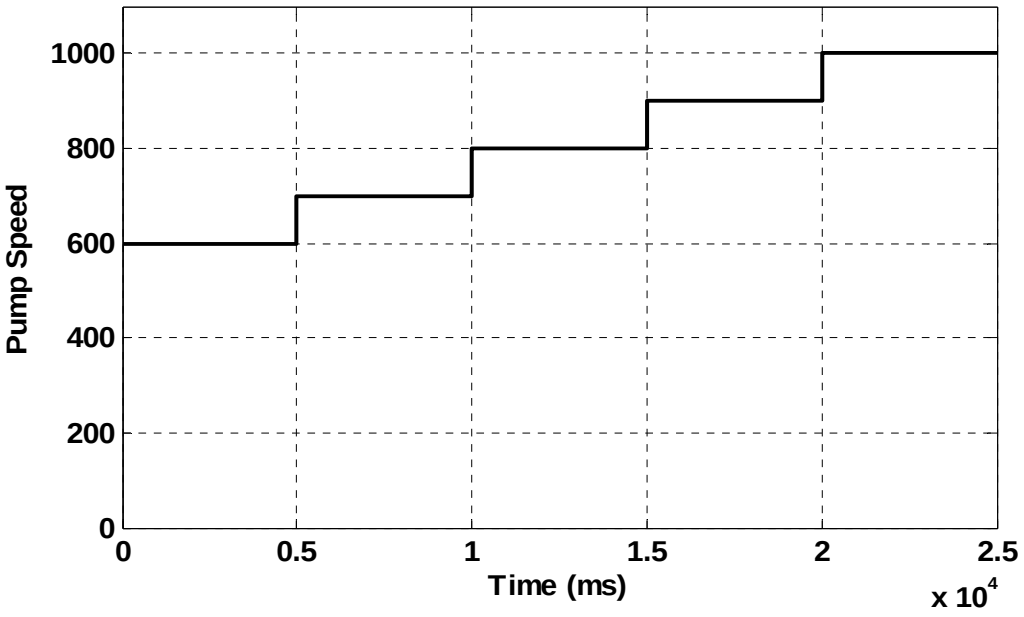

Figure 6.13 Applied pump speed variation as a disturbance on the system

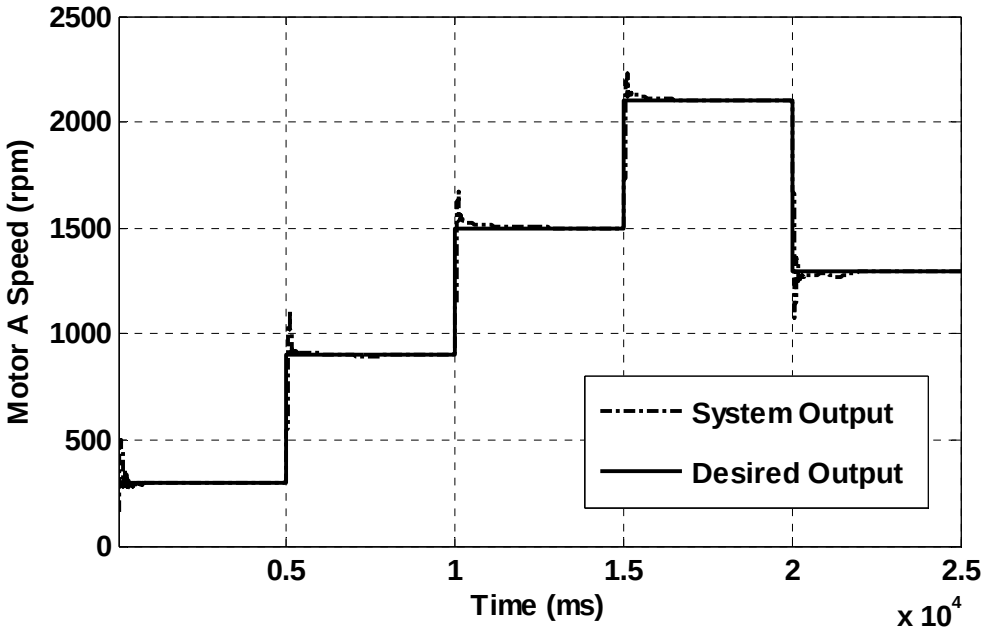

Figure 6.14 Tracking response of multiple models adaptive control

It can be seen that throughout all operating regimes, MMAC is working acceptable. Some discrepancies in the tracking response refer to the transition between Kalman filters which causes low overshoots to the system.

The control command (valve position), which is a summation of weighted controllers output, is shown in Figure 6.15. Smooth variation of valve position in this figure indicates the stability of the designed control structure.

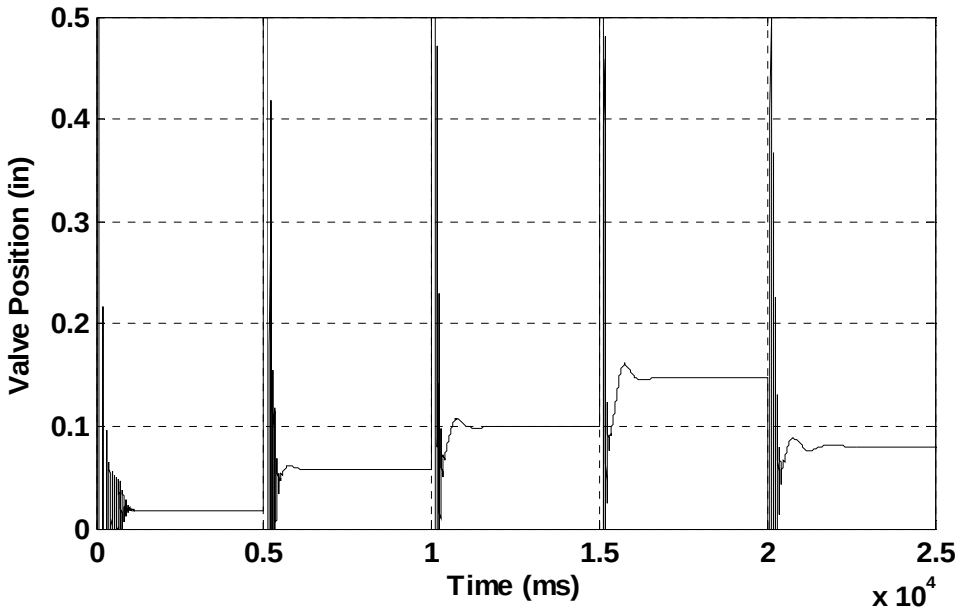

Figure 6.15 Control command of MMAC during simulation

During the simulation, probability block has been considering the residuals from Kalman filters to come up with the weight of each controllers output. Figure 6.16 shows the applied weights.

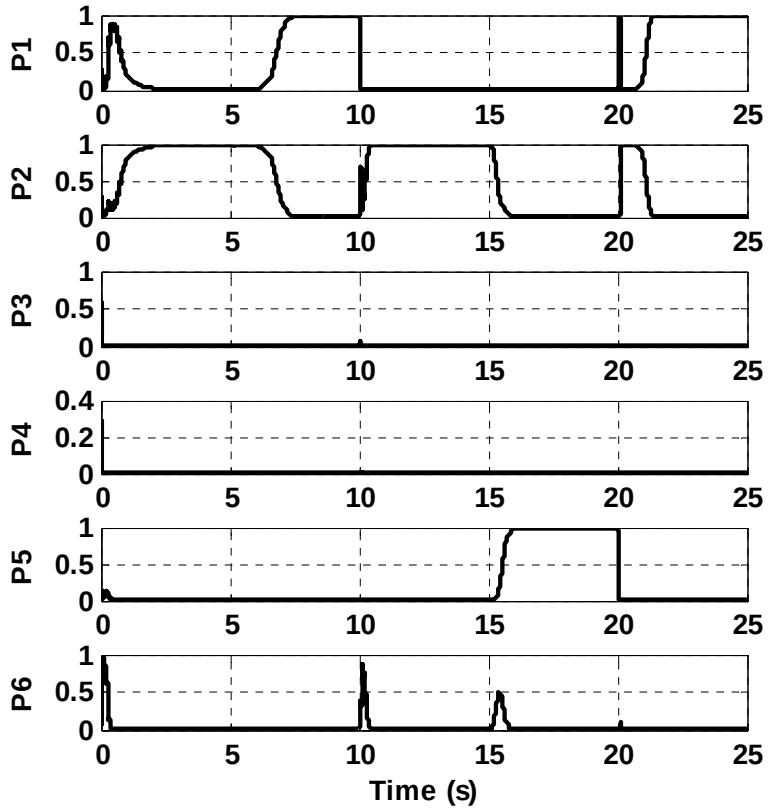

Figure 6.16 Weights of controllers output calculated by probability block

As shown above, each weight calculated by probability block varies from 0 to 1. Variation of these weights demonstrates model selection of probability block in each different operating point. Some models cover more operating points rather than the others. Therefore, their correspondent weights for the controller outputs are continuously high throughout the simulation.

Figure 6.17 shows the variation of residuals calculated by Kalman filters, input to the probability block, during the simulation. This figure illustrates the well match of each Kalman filter with the plant in its assumed operating regimes.

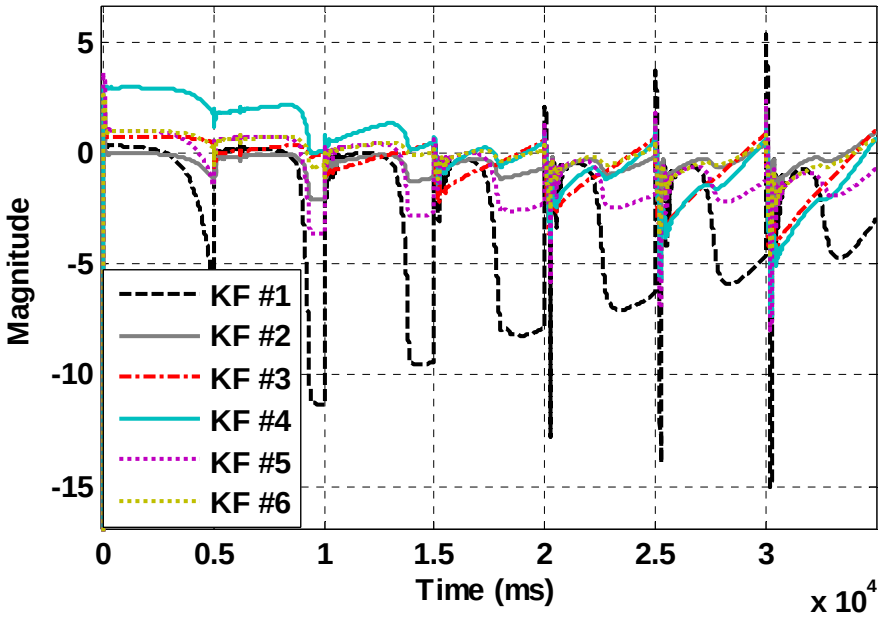

Figure 6.17 Residuals of the system calculated by Kalman filters

This simulation proved the high performance of multiple model adaptive control for a hydraulic wind power system which runs over a wide range of operating points.

Multiple model adaptive control of a hydraulic wind power system is presented in this section. The performance of this control approach is highly dependent on the number of models and also accuracy of the linearization and Kalman filters. Designing poor controllers for each Kalman filter will degrade the tracking response. Also, smooth transition between the Kalman filters requires well designed switching algorithm. In this section Kalman filters were designed by using linearized system in different reasonable operating points. Overall acceptable performance of MMAC indicates the functionality of tuned PI controllers in this structure [114].

6.2 Experimental System

It can be observed from equation (3.4) that even at constant flow the motor speed varies if the pressure fluctuates. As described, the differential pressure variation, inlet flow fluctuation and motor pressure variation are source of disturbances on motor speed, so that an appropriate controller is required for the valve to compensate for these disturbances.

This section represents a control system for the experimental hydraulic wind power transfer system. the primary goal of the control system is to maintain a constant speed for primary motor under the various disturbances such as pump shaft speed variations (wind fluctuation) and load variations (grid load fluctuation). The controller is challenged through different control experiments. First, the controller performance is shown in primary motor speed regulation under wind disturbance and load disturbance separately. Then, the control system runs to track a reference speed for primary motor. In each experiment, the response of the system is illustrated as well as all other states behavior during the run.

Addressing the primary goal of the design makes the control system single-input and single output (SISO). The control input to the system is a voltage profile to the proportional valve sent by the designed controller in MATLAB/Simulink. The more voltage is applied by the controller; the more flow deviates to the auxiliary motor. Also, the primary output of the system is the speed of primary motor. Finally, pump shaft speed and load on the motors are the disturbance inputs.

A PI controller is designed based on Ziegler–Nichols method in order to satisfy performance indices considered for the system having the form of:

$$u(t) = K_p e(t) + K_i \int_0^t e(t)dt \tag{6.16}$$

where k_p and k_i are proportional and integral gain, respectively and $e(t)$ is the error between desired output and system output. Figure 6.18 shows the step response of the system. Also, Figure 6.19 illustrates the circle area of the Figure 6.18 for better observation of step response. In Ziegler–Nichols method, studying the dynamic behavior of the system under the step input will result in PI gains. Table 6.1 provides the characteristic parameters of the systems.

Table 6.1 List of Characteristic Parameters of the System

Parameter	**value**
Final Speed	2482.57
Maximum Speed	2555.23
Overshoot Percentage	2.92
Natural Frequency	11.12 rad/s
Damping Frequency	7.39 rad/s
Damping ratio	0.7471
Time Constant	0.15s
Delay Time	0.63s
Setteling Time	1.73s

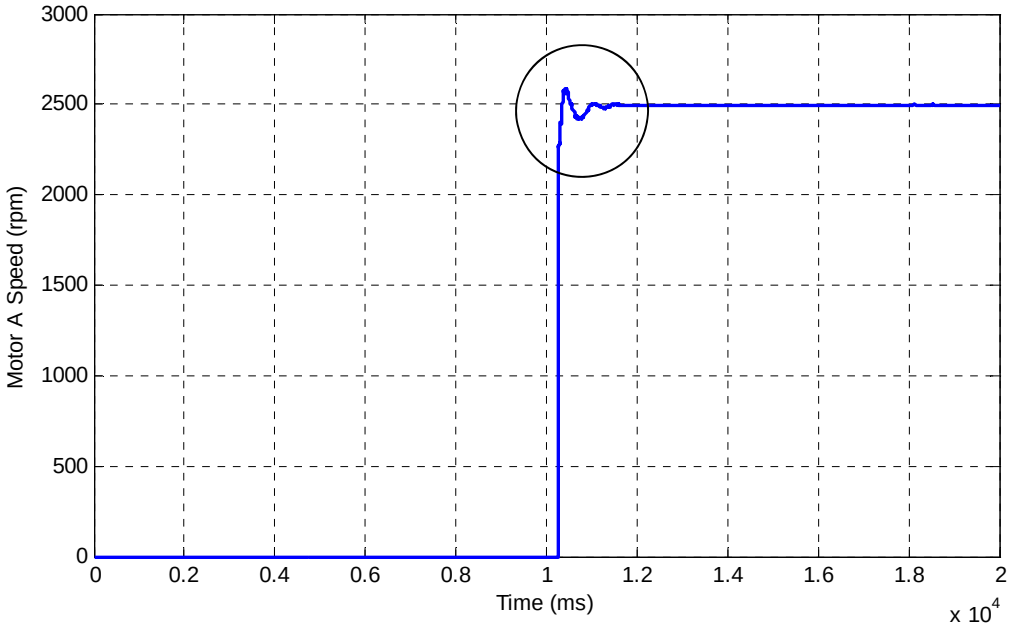

Figure 6.18 Step response of the experimental hydraulic wind power transfer system

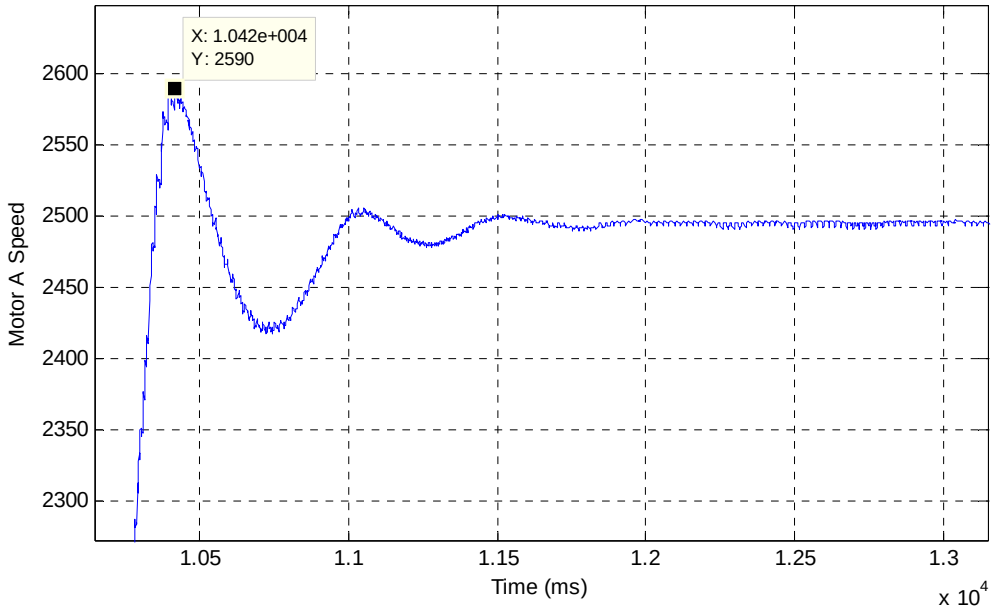

Figure 6.19 Zoomed circle area of step response of the experimental hydraulic wind power transfer system

Utilizing the step response characteristic parameters of the system in Ziegler–Nichols method, PI gains are listed in Table 6.2.

Table 6.2 List of PI Gains

Gain	value
Proportional	0.00013
Integral	0.0021

The gains in Table 6.2 are implemented in the PI controller in MATLAB/Simulink for further experiments in next sections.

6.2.1 Primary Motor Speed Regulation

6.2.1.1 Control under Wind Disturbances

In this section, the controller performance is tested under pump speed fluctuations. The system starts in closed loop and during the experiment a step variation for pump speed is applied to the system. The controller actuates the proportional valve properly to compensate for applied wind disturbance. Figure 6.20 depicts the pump speed fluctuations exerted to the control system. Regulation response of the system is shown in Figure 6.21 and Figure 6.22. Finally, Figure 6.23 illustrates the control command applied to the proportional valve by the controller. As it can be seen, the controller works flawlessly under wind speed disturbance.

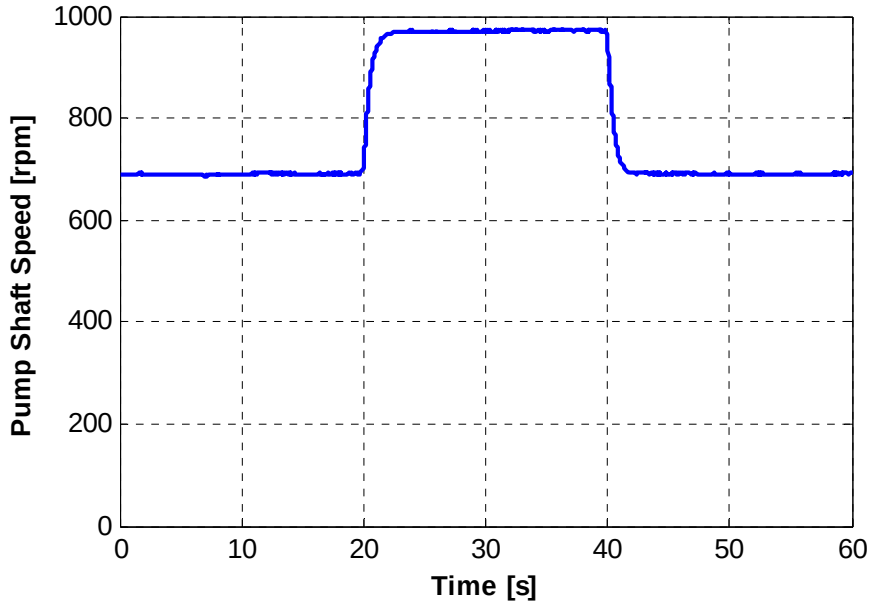

Figure 6.20 Pump speed variations applied to regulation under wind disturbance

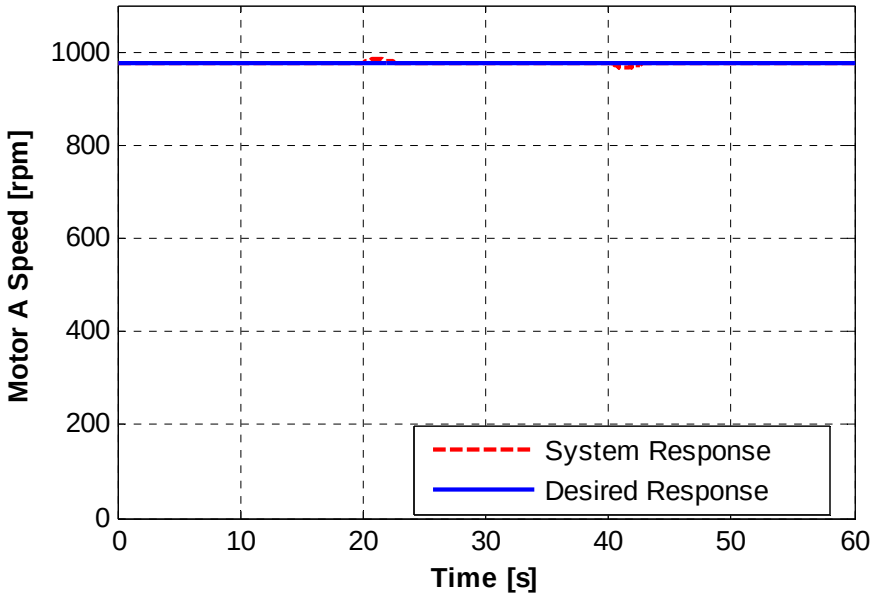

Figure 6.21 Regulation response of the system under wind disturbance

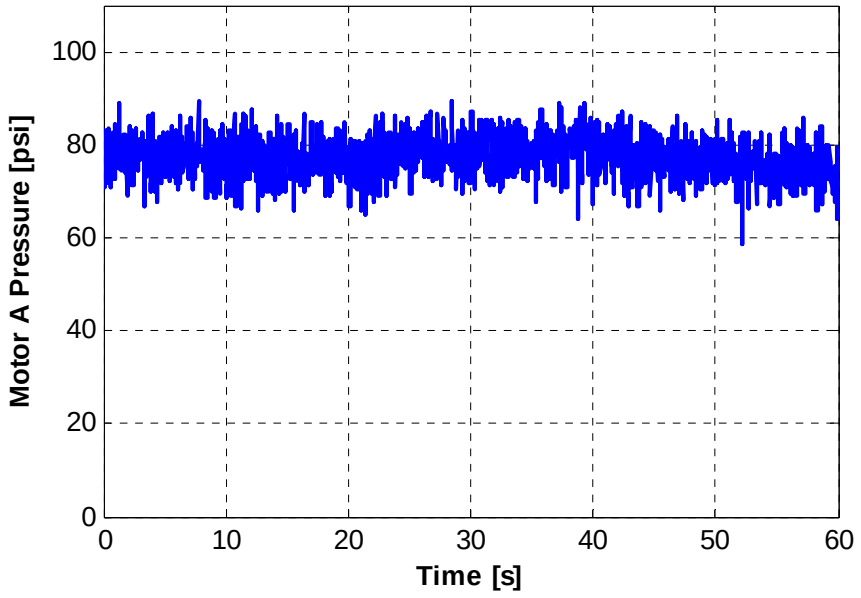

Figure 6.22 Motor A pressure in regulation under wind disturbance

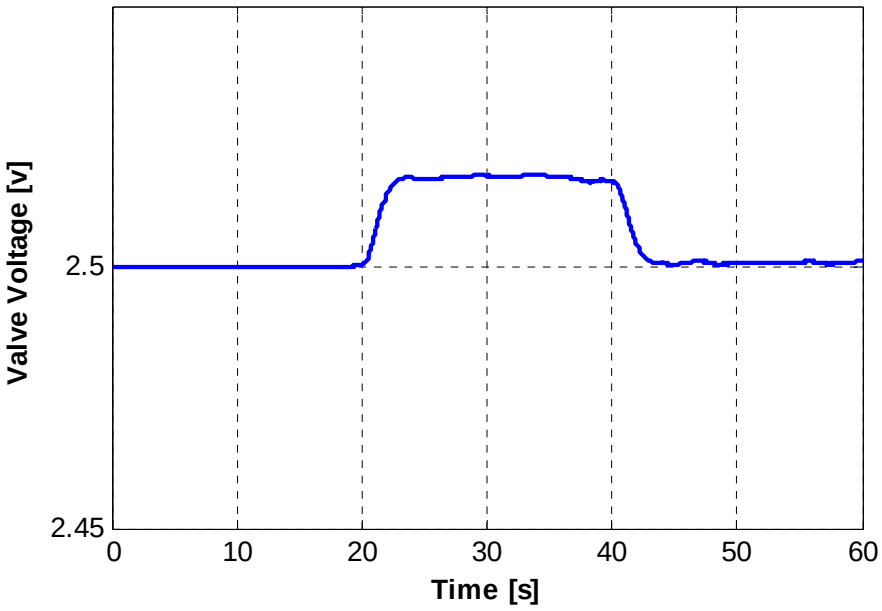

Figure 6.23 Controller command to the proportional valve in regulation under wind disturbance

6.2.1.2 Control under Load Disturbances

In this section, the controller performance is tested under load fluctuations. For this experiment, a load board is designed and implemented which includes capacitors and 100 Watt bulbs. Also, in this experiment, pump shaft is running at constant speed of 1600 rpm. The system starts in closed loop and during the experiment several step variations for the load are applied to the hydraulic motors. The controller actuates the proportional valve properly to compensate for applied load on the motor A. Figure 6.24 depicts the load fluctuations exerted to the control system. Regulation response of the system is shown in Figure 6.25 and Figure 6.26. Finally, Figure 6.27 illustrates the control command applied to the proportional valve by the controller. Reponses of this experiment shows a reasonable performance for the control system.

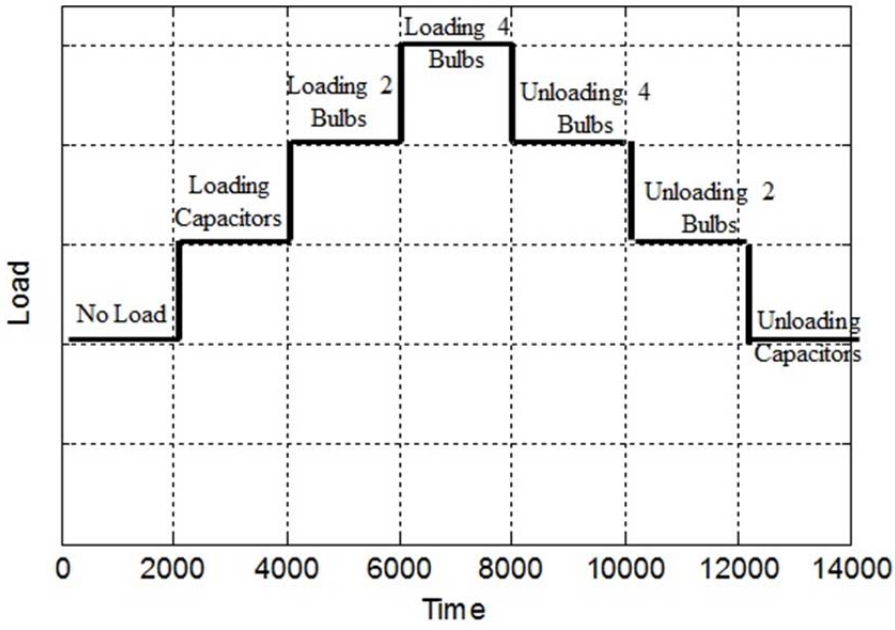

Figure 6.24 Load variations applied to the motor A in regulation under the load

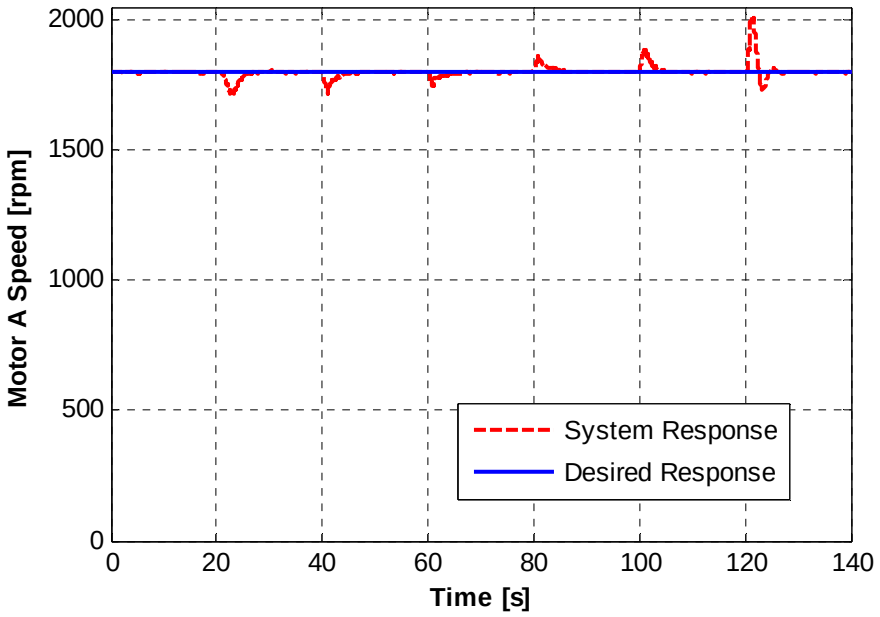

Figure 6.25 Regulation response of the system under load disturbance

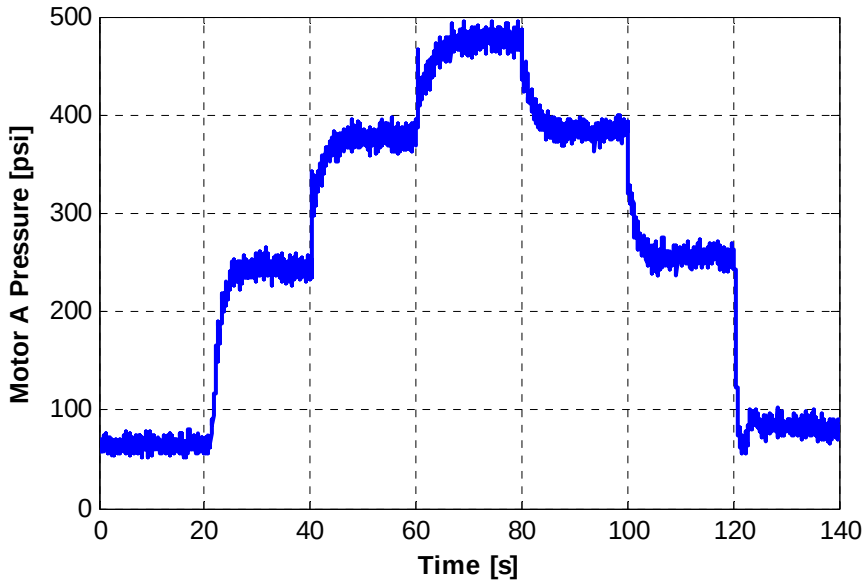

Figure 6.26 Motor A pressure in regulation under load disturbance

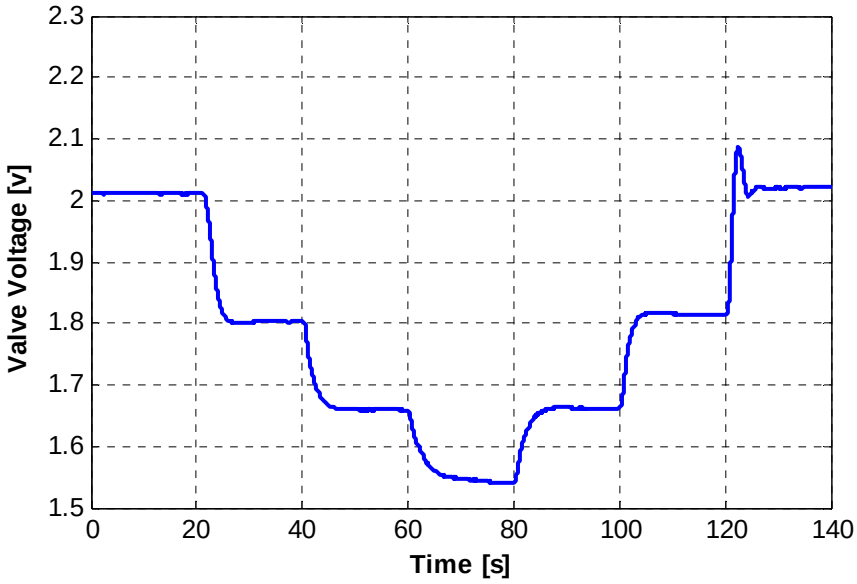

Figure 6.27 Controller command to the proportional valve in regulation under load disturbance

6.2.2 Primary Motor Speed Tracking

Finally, in this section, the controller performance is challenged by changing the speed reference. The system starts in closed loop and during the experiment speed reference of considered for motor A varies. In this experiment pump shaft is rotating at a constant speed of 600 rpm and the external load on the hydraulic motor A is negligible. The controller actuates the proportional valve properly to track the speed reference instantaneously. Regulation response of the system is shown in Figure 6.28 and Figure 6.29. Finally, Figure 6.30 illustrates the control command applied to the proportional valve by the controller. Reponses of this experiment shows a reasonable performance for the control system.

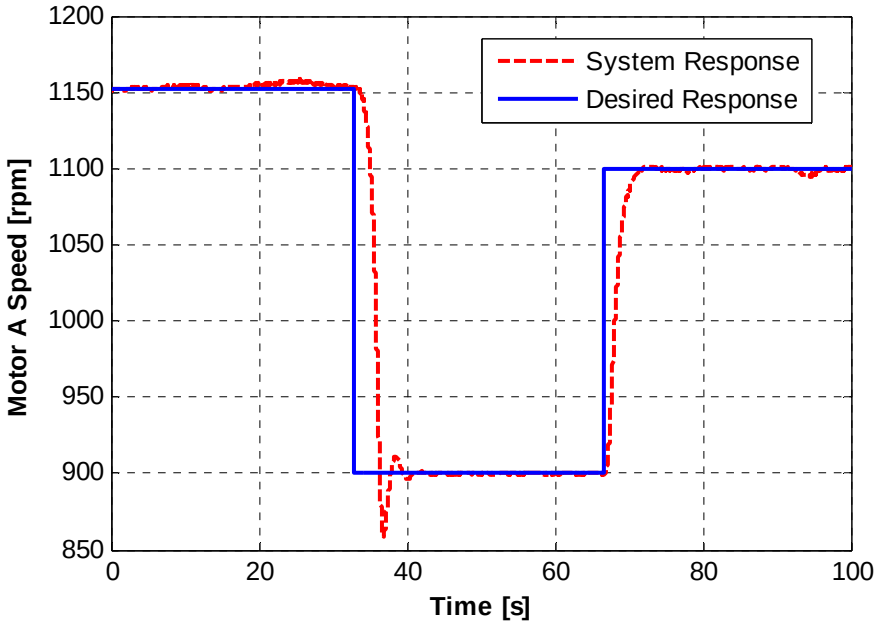

Figure 6.28 Tracking response of the system under constant load and wind speed

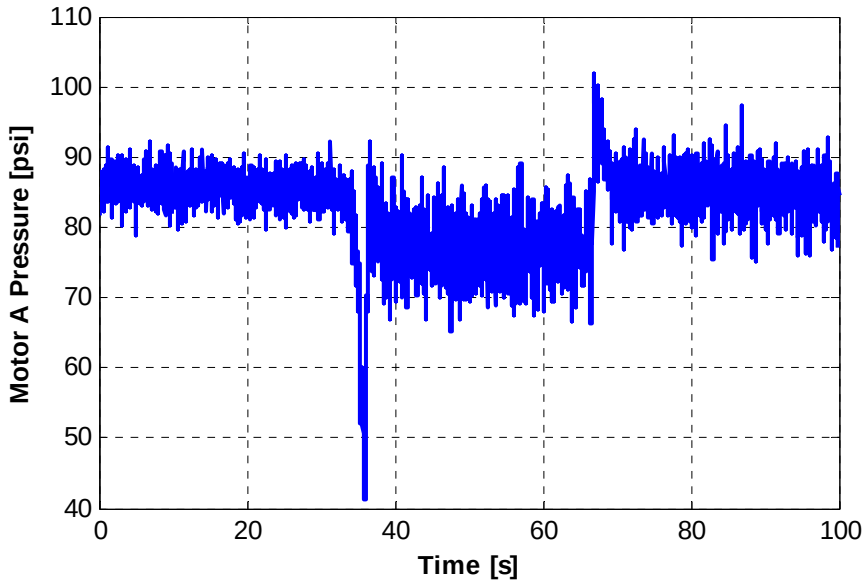

Figure 6.29 Motor A pressure in tracking system under constant load and wind speed

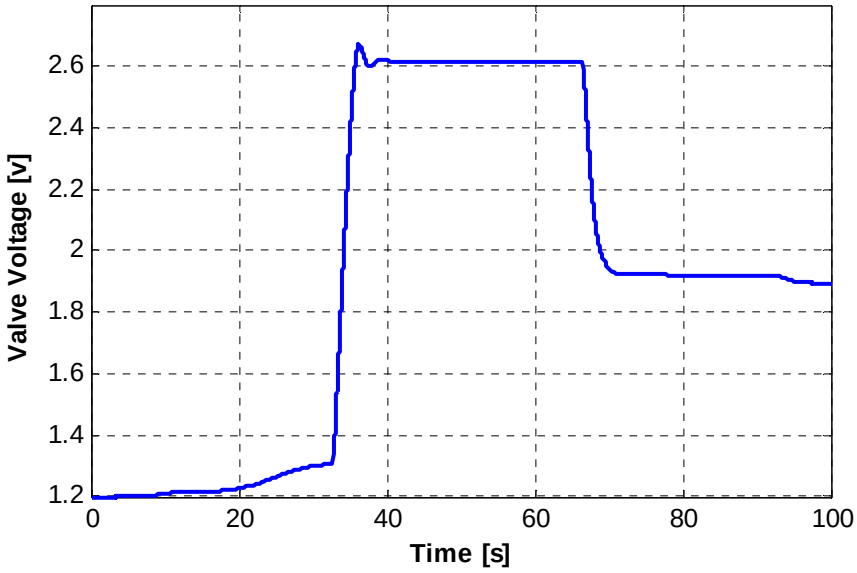

Figure 6.30 Controller command to the proportional valve in tracking system under constant load and wind speed

According to the results from the experimental responses of the hydraulic wind power transfer system, it can be concluded that the control system is working perfectly under load and wind speed fluctuations. However, increasing the number of the hydraulic components exert more nonlinearities to the system which may require for an advanced controller such as adaptive controller.

7. CONCLUSIONS AND FUTURE APPLICATIONS

This thesis studied the hydraulic wind power transfer systems. To get a better understanding, a mathematical model of the system was developed and studied utilizing the governing equations for all hydraulic components. The mathematical model embodies nonlinearities which are inherited from the hydraulic components such as check valves, proportional valves, pressure relief valves, etc.

An experimental prototype of the hydraulic wind power transfer systems was designed and implemented to study the system's dynamical behavior and operations. The provided nonlinear mathematical model was then validated by experimental result recorded from the prototype.

Moreover, this thesis developed a control system for the hydraulic wind power transfer systems. To maintain a fixed frequency of electrical voltage, the generator should remain at a constant rotational speed. The fluctuating wind speed from the upstream of the hydraulic pump, and the load variations from the downstream apply considerable disturbances on the generator coupled hydraulic pump. A controller was designed and implemented to regulate the flow in the proportional valve flowing towards the main pump to compensate load and wind turbine disturbances and consequently maintain the system frequency. The control system was applied to the mathematical model as well as

the experimental prototype by utilizing MATLAB/Simulink and dSPACE 1104 fast prototyping hardware and the results were compared.

Future applications of the hydraulic wind power transfer systems are very promising and require a great attention in engineering research. The hydraulic configuration in this generation of wind turbines allows for capturing the energy of multiple wind turbines into a single generator. Utilizing multiple wind turbines with one generation unit and attempting the transfer of energy of each wind turbine by a single closed loop hydraulic circuit. This will need a flawless hydraulic circuit design and implementation as well as the optimal number and allocation of wind turbines in wind farms. Also, adding the second and third wind turbines to the system will make the control system design much more challenging.

In addition, as mentioned earlier in the hydraulic systems description, in high wind speed operation of the wind turbines, the proportional valve is subject to send the excess flow to the auxiliary motor to maintain the reference speed for primary motor. The energy of the excess flow passing through the auxiliary motor can be captured by means of an energy storage system. This area can draw a great attention to study for the most efficient way to address this requirement. As a suggestion, a battery can collect the excess flow energy and send it back to the system in low wind speed operation. Thus, there would be a need to design a control system to manage the low wind speed and high wind speed operations.

Finally, the concept of transferring energy by means of a hydraulic circuit can be applied to various number of engineering fields. These hydraulic transmission systems offer the benefit of a continuously Variable Transmission (CVT), which is the infinite

effective gear ratio. These infinite shifting ratios of the power transmission system allow less energy losses and better fuel efficiency in vehicles. By improving the efficiency and design of hydraulic transfer systems, related engineering systems can utilize this novel idea. For instance, the regenerative hybrid vehicle system and gearless hydraulic transmission system are integrated to address both energy requirements of a hybrid vehicle and friction energy losses in the mechanical transmission system. A regenerative gearless HEV driveline can be introduced through a hydraulically connected power transmission system [12].

LIST OF REFERENCES

LIST OF REFERENCES

[1] R. Gasch and J. Twele, “Windkraftanlagen. Grundlagen, Entwurf, Planung und Betrieb”. Springer, Wiesbaden 2013, p 569 (German).

[2] G. Paul, "The Wind Industry's Experience with Aesthetic Criticism". Leonardo 26 (3), 1993, 243–248.

[3] F. thenakis, V. Kim, and H. Clon, "Land use and electricity generation: A life-cycle analysis". *Renewable and Sustainable Energy Reviews* 13 (6–7): 1465.

[4] A. Izadian and N. Girrens, "The U.S. and E.U. Renewable Energy Policies," *IEEE Industrial Electronics Magazine*, to appear 2013.

[5] A. Ragheb and M. Ragheb, “Wind Turbine Gearbox Technologies,” *Proceedings of the 1st International Nuclear and Renewable Energy Conference (INREC10)*, Amman, Jordan, March 2010.

[6] S. Hamzehlouia and A. Izadian, “Nonlinear State Space Modeling of Gearless Wind Power Systems,” *IECON* 2012, pp. 1098-1103.

[7] S. Eriksson, H. Bernhoff, and M. Leijon, “Evaluation of Different Turbine Concepts for Wind Power,” *Renewable and Sustainable Energy Reviews*, vol. 12, issue 5, pp. 1419-1434, June 2008.

[8] A. Izadian, “Central Wind Turbine Power Generation,” US Patent Application, US 20130127166, May 23, 2013.

[9] http://www.chapdrive.com/technology/5-mw-project. Last accessed July 2014.

[10] http://www.mhi.co.jp/en/news/story/1111291475.html. Last accessed July 2014.

[11] K. Dasgupta, "Analysis of a Hydrostatic Transmission System Using Low Speed High Torque Motor," *Mechanism and Machine Theory*, vol. 35, pp. 1481-1499, Oct 2000.

[12] S. Hamzehlouia, “Modeling And Control Of Hydraulic Wind Energy Transfers,” *Masters Thesis*, Purdue school of engineering and technology, IUPUI, Indianapolis, USA, 2012.

[13] P. H. Chang and S-J Lee, “A Straight-line Motion Tracking Control of Hydraulic Excavator System,” *Journal of Mechatronics*, vol. 12, pp. 119-138, 2002.

[14] [http://www.acadianahydraulic.com/apage/63976.php. Last accessed July 2014.

[15] K. Hulhatala, “Modeling of a Hydrostatic Transmission – Steady-State, Linear, and Non-Linear Models,” *Acta Polytechnica Scandinavica,* no. 123, pp. 9-101, 1996.

[16] F. P. Wijnheijmer, “Modeling and Hydraulic Servo System,” *Master’s Thesis, Eindhoven Technical University*, 2005.

[17] M. V. Gorbeshko. “Development of Mathematical Models for the Hydraulic Machinery of Systems Controlling the Moving Components,” *Hydrotechnical Constructio*, vol. 3, no. 12. 1997.

[18] S. Hamzehlouia and A. Izadian, “Modeling of Hydraulic Wind Power Transfers,” *Power and Energy Conference Illinois, PECI* 2012.

[19] S. Hamzehlouia, A. Izadian, A. Pusha, and S. Anwar, “Controls of Hydraulic Wind Power Transfer,” *IECON* 2011.

[20] L. Shi, Z. Xu, C. Wang, L. Yao, and Y. Ni, “Impact of Intermittent Wind Generation on Power System Small Signal Stability”, 2011 under CC BY-NC-SA 3.0 license.

[21] S. Gao and N. Zhang “A Review of Different Methodologies for Solving the Problem of Wind Power’s Fluctuation,” *International Conference on Sustainable Power Generation and Supply (SUPERGEN ’09)*, pp. 1-52009.

[22] P. Sorensen, N. A. Cutululis, A. V. Rodriguez, L. E. Jensen, J. Hjerrild, M. H. Donovan, and H. Madsen, “Power Fluctuations from Large Wind Farms,” *IEEE Transaction on Power Systems*, vol. 22, no. 3, August 2007.

[23] K. Wu, et al., "Modeling and identification of a hydrostatic transmission hardware-in-the-loop simulator," *International Journal of Vehicle Design*, vol. 34, pp. 52-64, 2004

[24] H. E. Merritt, “Hydraulic control systems”, New York, John Wiley Inc., 1967.

[25] E. C. Fitch and I. T. Hong, “Hydraulic component design and selection”, Oklahama, BarDyne Inc, 1998.

[26] J. F. Reethof and J. L. Shearer, “Fluid Power Control”, The M.I.T. Press, Cambridge, MA, 1960.

[27] A. Pandula and G. Halasz, “Dynamic Model for Simulation of Check Valves in Pipe Systems.” *Periodica Polytechnica*, Mech. Eng. Series, vol 46/2, pp. 91-100, 2002.

[28] M. Deldar, A. Izadian, and S. Anwar, “Modeling of a Hydraulic Wind Power Energy Transfer System Utilizing a Proportional Valve,” *IEEE Energy Conversion Congress and Exposition, ECCE* 2013, Colorado, September 2013.

[29] S. Hamzehlouia and A. Izadian, "State-space representation of a hydraulic wind power transfer," *IEEE International Conference on Electro-Information Technology*, EIT 2012.

[30] M. Vaezi, A. Izadian, and M. Deldar, "Hydraulic Wind Power Plants: Nonlinear Model of Low Wind Speed Operation", submitted as a journal paper for review, 2013.

[31] A. Izadian, S. Hamzehlouia, M. Deldar, and S. Anwar, "Hydraulic Wind Power Transfer System: Operation and Modeling," *IEEE Transactions on Sustainable Energy*. Accepted, 2014.

[32] S. Hamzehlouia and A. Izadian, "Adaptive Control of a Gearless Wind Energy Transfer System," In *Proceeding of IEEE Industrial Electronic Conference, IECON*, 2012.

[33] C. Y. Lai, C. Xiang, and T. H. Lee, "Identification and control of nonlinear systems using piecewise affine models," in Proc. *IEEE Conf. Decis. Control*, Atlanta, GA, Dec. 2010, pp. 6395–6402.

[34] C. Wen, S. Wang, X. Jin, and X. Ma, "Identification of dynamic systems using piecewise-affine basis function models,"*Automatica*, vol. 43,no. 10, pp. 1824–1831, 2007.

[35] O. Suntharasantic, P. Rungtweesuk, and M. Wongsaisuwan, "Piecewise Affine Model Approximation for Unmanned Bicycle", *SICE Annual Conference* 2011.

[36] H. Nakada, K. Takaba, and T. Katayama, "Identification of piecewise affine systems based on statistical clustering technique," *Automatica*, vol. 41, no. 5, pp. 905–913, 2005.

[37] J. Thomas, S. Olaru, J. Duisson, and D. Dumur, "Robust model predictive control for piecewise affine systems subject to bounded disturbances," in Proc. *IFAC Conf. Anal. Design Hybrid Syst.*, 2006,pp. 329–334.

[38] M. Athans, D. A. Castanon, et all. "The stochastic control of theF-8C aircraft using a multiple model adaptive control (MMAC) method-Part I: equilibrium flight". *IEEE Transactions on Automatic Control* 1977.

[39] A. D. Buchan, D. W. Haldane, and R. S. Fearing, "Automatic Identification of Dynamic Piecewise Affine Models for a Running Robot", *IEEE/RSJ International Conference on Intelligent Robots and Systems* (IROS) 2013.

[40] A. Banerjee, Y. Arkun, B. Ogunnaike, and R. Pearson, "Estimation of Nonlinear Multiple Systems Using Linear Models", *AIChE Journal*, Vol.43, No. 5, May 1997.

[41] S. H. Zak, "Systems and Control", *Oxford University Press*, 2003.

[42] E. D. Sontag, "Nonlinear regulation: the piecewise linear approach," *IEEE Trans. Automatic Control*, vol. 26, no. 2, 1981, pp. 346-358.

[43] A. Juloski, W. P. Heemels, G. Ferrari-Trecate, R. Vidal, S. Paoletti, and J. H. G. Niessen, "Comparison of four procedures for the identification of hybrid systems," in *Hybrid systems: computation and control*, M. Morari and L. Thiele Eds. Springer Verlag, 2005, pp. 354-369.

[44] S. Paoletti, A. Lj. Juloski, G. Ferrari-Tracate, and R. Vidal, "Identification of hybrid systems: a tutorial," *European Journal of Control*, vol.513, no. 2-3, 2007, pp. 242-260.

[45] W. Heemels, B. De Schutter, and A. Bemporad, "Equivalence of hybrid dynamical models," *Automatica*, vol. 37, 2001, pp. 1085-1091.

[46] L. Rodrigues and J. P. How, "Automated control design for a piecewise affine approximation of a class of nonlinear systems," *in Proc. American Control Conference*, 2001, pp. 3189-3194.

[47] S. Paoletti, "Identification Of Piecewise affine Models," Ph.D. dissertation, Dipartimento di Ingegneria dell'Informazione, Univ. Siena, Siena, Italy, 2003.

[48] M. Vaezi, A. Izadian, and M. Deldar, "A Model Linearization Technique for Hydraulic Wind Power Systems," *Proceeding of IEEE PECI conference*, 2014.

[49] B. Zhang, M. Hsu, and U. Dayal, "Harmonic Average Based Clustering Method and System," US Patent 6,584,433, 2000.

[50] V. Kathiresan and Dr. P Sumanthi, "An Efficient Clustering Algorithm based on Z-Score Ranking method," *International Conference on Computer Communication and Informatics* (ICCCI-2012), Jan. 10-12, 2012.

[51] M. Yedla, R. Pathakota, and T. M. Srinivasa "Enhancing K-means Clustering Algorithm with Improved Initial Center", *International Journal of Computer Science and Information Technologies(IJCSIT)*, Vol. 1 (2) ,2010, 121-125.

[52] M. Vaezi and A. Izadian, "Piecewise Affine System Identification of a Hydraulic Wind Power Transfer System", *IEEE Transactions on Control Systems Technology*, Under Review, 2014

[53] L. Xiaofeng and Y. Ye, "Nonlinear System Modeling and Application Based on System Equilibrium Manifold and Expansion Model", *Journal of Computational and Nonlinear Dynamics* 2013.

[54] A. Isidori, "Nonlinear Control Systems." Springer-Verlag, New York, NY, 1989.

[55] J. K. Hedrick and A. Girard, "Control of Nonlinear Dynamic Systems: Theory and Applications", Berkeley University, 2010.

[56] M. A. Henson and D. E. Seborg, "Feedback linearizing control,"inNonlinear Process Control, M. A. Henson and D. E. Seborg,Eds. Englewood Cliffs, NJ: Prentice-Hall, 1997, ch. 4, pp. 149–232.

[57] M. Ababneh, M. Salaha, and K. Alwidyan, “Linearization of Nonlinear Dynamical Systems: A Comparative Study”, *Jordan Journal of Mechanical and Industrial Engineering*, Pages567-571, 2011.

[58] J. Yaochu, Z. Jing, and J. Jingping, “Fuzzy linearization for nonlinear systems: a preliminary study”, *IEEE Conference on Fuzzy Systems*, 1994.

[59] W. Kang, “Approximate linearization of nonlinear control systems”. *Syst. Contr. Lett*. 23, 43–52, 1994.

[60] I. Bonis, W. Xie, and C. Theodoropoulos, “Multiple Model Predictive Control of Dissipative PDE Systems”, *IEEE Transactions on Control Systems Technology*, Volume:PP, 2013.

[61] M. Lin, J. Gunnar, et all “A Review of Piecewise Linearization Methods” *Hindawi Publishing Corporation* – Nov 6, 2013.

[62] Y. Zhang, S. Sankaranarayanan, and F. Somenzi, , “Piecewise Linear Modeling of Nonlinear Devices for Formal Verification of Analog Circuits,” *Proceedings of the 12th Conference on Formal Methods in Computer-Aided Design*, pp. 196–203, 2012.

[63] T. Hatanaka, K. Uosaki, and M. Koga. Evolutionary computation approach to Wiener model identification. *In Proc. Congress on Evolutionary Computation. CEC ’02*, volume 1, pages 914–919, 2002.

[64] J. K. Cavers. “Optimum table spacing in predistorting amplifier lineariz-ers”, *IEEE Trans. Veh. Technol*., 48(5):1699–1705, 1999.

[65] F. Belkhouche. “Trajectory-based optimal linearization for nonlinear autonomous vector fields”, *IEEE Trans. Circuits Syst*. I, Reg.

[66] M. Storace and O. De Feo. “Piecewise-linear approximation of nonlinear dynamical systems”. *IEEE Trans. Circuits Syst*. I, Reg. Papers, 51(4):830–842, 2004.

[67] R. Rossi, S. A. Tarim, S. Prestwich, and B. Hnich. “Piecewise lin-ear approximations of the standard normal first order loss function” arXiv:1307.1708, 2013.

[68] P. Julian, A. Desages, and O. Agamennoni. “High-level canonical piecewise linear representation using a simplicial partition”, *IEEE Trans.Circuits Syst*. I, Fundam. Theory Appl., 46(4):463–480, 1999.

[69] T. Hatanaka, K. Uosaki, and M. Koga, "Evolutionary computation approach to Wiener model identification," In *Proc. oj CEC'02,Honolulu*, HI , USA, May 2002.

[70] T. Arte, "Wiener system identification with four-segment and analytically invertible nonlinear model," *American Control Conference*, Jul 2007, pp. 4339-4344.

[71] S. Ghosh, A. Ray, D. Yadav, and B. Karan, “A Genetic Algorithm Based Clustering Approach for Piecewise Linearization of Nonlinear Functions,” *Devices and Communications (ICDeCom), 2011 International Conference on. IEEE*, pp. 1–4, 2011.

[72] Z. Xie and L. Guan, ”Multimodal Information Fusion of Audio Emotion Recognition Based on Kernel Entropy Component Analysis”, *In IEEE Int. Symp. on Multimedia*, pages 1–8, 2012.

[73] R. Bellman and R. Roth. “Curve fitting by segmented straight lines”, *Journal of the Amer. Stat. Assoc*., 64(327):1079–1084, 1969.

[74] M. Vaezi and A. Izadian, “Optimum Adaptive Piecewise Linearization: An Estimation Approach in Wind Power”, *IEEE Transactions on Control Systems Technology*, Under Review, 2014.

[75] T. Senjyu, R. Sakamoto, N. Urasaki, H. Higa, K. Uezato, and T. Funabashi , H. Hideki, and H. Sekine, “Output Power Leveling of Wind Turbine Generator for All Operating Regions by Pitch Angle Control”, *IEEE Transaction on Energy Conversion*, vol. 21, no.

[76] E. Abdin and W. Xu, “Control Design and Dynamic PerformanceAnalysis of a Wind Turbine-Induction Generator Unit,” *IEEE Transaction on Energy Conversion*, vol. 15,no. 1, March 2000.

[77] P. Mavridis and P. Moustakides, ” Simplified Newton-type adaptive estimation algorithms”, Signal Processing, *IEEE Transactions*, pp 1932 – 1940, Aug 1996.

[78] G. Glentis, K. Berberidis, and S. Theodoridis, "Efficient least squares adaptive algorithms for FIR transversal filtering", *Signal Processing Magazine, IEEE*, On page(s): 13 - 41 Volume: 16, Issue: 4, Jul 1999.

[79] B. D. O. Anderson and J. B. Moore, Optimal Filtering. New Jersey, USA: Prentice-Hall, 1979.

[80] A. P. Aguiar, V. Hassani, A. M. Pascoal, and M. Athans, “Identification and convergence analysis of a class of continuous-time multiple-model adaptive estimators,” *in Proc. of The 17th IFAC World Congress*, Seoul.

[81] V. Hassani, A. P. Aguiar, M. Athans, and A. M. Pascoal, “Multiple Model Adaptive Estimation and Model Identification using a Minimum Energy Criterion”, *American Control Conference Hyatt Regency Riverfront*, USA, pp 518-523, June 2009.

[82] S. Fekri, M. Athans, and A. Pascoal, “Issues, progress and new results in robust adaptive control,” *Int. J. of Adaptive Control and Signal Processing*, 2006, in press.

[83] B. D. O. Anderson, T. S. Brinsmead, F. de Bruyne, J. Hespanha, D. Liberzon, and A. S. Morse, "Multiple model adaptive control: Part 1: Finite controller coverings," *Int. J. of Robust and Nonlinear Control*, vol. 10, pp. 909–929, 2000.

[84] A. Morse, "Supervisory control of families of linear set-point controllers-part 1: Exact matching," *IEEE Trans. on Automat. Contr.*, vol. 41, pp. 1413–1431, 1996.

[85] J. Hespanha, D. Liberzon, A. S. Morse, B. D. O. Anderson, T. S. Brinsmead, and F. de Bruyne, "Multiple model adaptive control: Part 2: Switching," *Int. J. of Robust and Nonlinear Control*, vol. 11, pp. 479–496, 2001.

[86] M. Athans, S. Fekri, and A. Pascoal, "Issues on robust adaptive feedback control," in *Preprints 16th IFAC World Congress, Invited Plenary paper*, Prague, Czech Republic, July 2005, pp. 9–39.

[87] D. Magill, "Optimal adaptive estimation of sampled stochastic processes," *IEEE Trans. on Automat. Contr.*, vol. 10, pp. 434–439, 1965.

[88] A. Pedro Aguiar, M. Athans, and A. M. Pascoal, "Convergence Properties of a Continuous-Time Multiple-Model Adaptive Estimator", *In Proc. of ECC-European Control Conference*, Greece, 2007

[89] Y. Baram and N. Sandell, "An information theoretic approach todynamical systems modeling and identification," *IEEE Trans. On Automat. Contr.*, vol. 23, pp. 61–66, 1978.

[90] X. R. Li and Y. Bar-Shalom, "Multiple-model estimation with variable structure," *IEEE Trans. on Automat. Contr.*, vol. 41, pp. 478–493,1996.

[91] H. Stearns and M. Tomizuka, "Multiple Model Adaptive Estimation of Satellite Attitude using MEMS Gyros", *American Control Conference*, USA, , pp 3490-3495, June, 2011.

[92] P. D. Hanlonpeter and S. Maybeck, "Multiple-Model Adaptive Estimation Using a Residual Correlation Kalman Filter Bank", *Aerospace and Electronic Systems IEEE Transactions*, pp 393 – 406, 2000.

[93] J. Valappil and C. Georgakis, "Systematic Estimation of State Noise Statisticsfor Extended Kalman Filters", *AIChE Journal*, Vol. 46, No. 2, 2000.

[94] P. K. Eide and Maybeck, "An MMAE failure detection system for the F-16", *IEEE Transactions of Aerospace and Electronic Systems*,32, 3, pp1125—113, 1996.

[95] S. Fekri Asl, M. Athans, and A. Pascoal, "Identification of Mass-Spring-Dashpot Systems using Multiple-Model Adaptive Estimation (MMAE) Algorithms", Conference paper, 2003.

[96] M. Vaezi and A. Izadian, "Multiple-Model Adaptive Estimation of a Hydraulic Wind Power System," In *proceedings of IEEE Industrial Electronics Conference, IECON* 2013, Vienna, Austria.

[97] A. Edalatnoor, A. Izadian, and M. Vaezi, “Indirect Adaptive Control of Droplet Dispensing in Digital Microfluidic Systems,” In *proceedings of IEEE Industrial Electronics Conference, IECON* 2013, Vienna, Austria.

[98] DG. Lainiotis “Partitioning: aunifying framework for adaptive systems I: Estimation; II: Control”, *Proceedings of the IEEE* 1976; pp 1126–1143 and 1182–1197.

[99] M. Athans, D. A. Castanon, et all. “The stochastic control of the F-8C aircraft using a multiple model adaptive control (MMAC) method-Part I: equilibrium flight”, *IEEE Transactions on Automatic Control* 1977; pp 768–780.

[100] C. Yu, R. J. Roy, H. Kaufman, and B. W. Bequette. “Multiple-model adaptive predictive control of mean arterial pressure and cardiac output”. *IEEE Transactions on Biomedical Engineering* 1992; pp 765–778.

[101] R. L. Moose, Van Landingham, and D. McCabe, “Modeling and estimation for tracking maneuvering targets”. *IEEE Transactions on Aerospace and Electronic Systems* 1979;pp 448–456.

[102] L. XR and Y. Bar-Shalom “Design of an interacting multiple model algorithm for air traffic control tracking”. *IEEE Transactions on Control Systems Technology* 1993; pp 186–194.

[103] S. Fekri, M. Athans, and A. Pascoal "Issues, progress and new results in robust adaptive control", *Int. J. Adaptive Control Signal Processing*, vol. 20, no. 10, pp.519 -579 2006.

[104] G. Schiller and P. S. Maybeck (1997). “Control of a large space structure using MMAE/MMAC techniques”, *IEEE Trans. on Aerospace and Electronic System* 33(4), 1122-1130.

[105] J. Lee , S. Bohacek , J. P. Hespanha, and K. Obraczka "Modeling communication networks with hybrid systems", *IEEE/ACM Trans. Networking*, vol. 15, no. 3, pp.630 -643 2007.

[106] T. A. Johanson and R. Murray-Smith, "Operating regime approach to nonlinear modeling and control", *Multiple Model Approaches to Modeling and Control*,pp.3 -72.

[107] Y. Baram “Information, consistent estimation and dynamic system identification”. *Ph.D. Dissertation*, MIT, Cambridge, MA, U.S.A., November 1976.

[108] Y. Baram and N. R. Sandell “An information theoretic approach to dynamical systems modeling and identification”. *IEEE Transactions on Automatic Control* 1978; 23(1):61–66.

[109] Y. Baram and N. R. Sandell “Consistent estimation on finite parameter sets with application to linear systems identification”. *IEEE Transactions on Automatic Control* 1978; pp 451–454.

[110] A. Kehagias, “Convergence properties of the Lainiotis partition algorithm”. *Control and Computers* 1991; pp 1–6.

[111] E. Peymani, A. Fatehi, and A. Khaki-Sedigh, “The Effect of Tuning in Multiple-Model Adaptive Controllers: A Case Study”. *International Symposium on Advanced Control of Chemical Processes, IFAC-ADCHEM*, Istanbul, Turkey.

[112] P. S. Maybeck, “Stochastic Models, Estimation and Control”, Vol. 1.*New York, Academic Press*, 1979; republished Arlington,VA: Navtech, 1994.

[113] G. C. Griffin, “Control of a large flexible space structure using multiple model adaptive estimation and control techniques”. *MS thesis, AFIT/GE/ENG/94D-14, School of Engineering, Air Force Institute of Technology*, Wright-Patterson AFB, OH, Dec. 1994.

[114] M. Vaezi and A. Izadian, “Adaptive Control of a Hydraulic Wind Power System Using Multiple Models”, In *proceedings of IEEE Industrial Electronics Conference, IECON* 2014, Dallas, USA.

APPENDIX

APPENDIX LIST OF LINEAR MODELS

Here all 6 models are shown by their state space matrices. *A* and *B* matrices represent the dynamics of the system.

$$A_1 = \begin{bmatrix} 0.6503 & 0.0187 & 0.0187 & -0.0003 & -0.0047 \\ 0.0374 & 0.9398 & 0.0135 & -0.0261 & -0.0001 \\ 0.6449 & 0.0135 & 0.3329 & -0.0002 & -0.0085 \\ 0.0001 & 0.0057 & 0.0000 & 0.9984 & -0.0000 \\ 0.0041 & 0.0000 & 0.0037 & -0.0000 & 0.9989 \end{bmatrix}$$

$$A_2 = \begin{bmatrix} 0.6142 & 0.0677 & 0.3095 & -0.0010 & -0.0046 \\ 0.1355 & 0.8043 & 0.0511 & -0.0241 & -0.0004 \\ 0.6189 & 0.0511 & 0.3212 & -0.0006 & -0.0082 \\ 0.0004 & 0.0053 & 0.0001 & 0.9992 & -0.0000 \\ 0.0041 & 0.0002 & 0.0036 & -0.0000 & 0.9994 \end{bmatrix}$$

$$A_3 = \begin{bmatrix} 0.5758 & 0.2660 & 0.1496 & -0.0051 & -0.0016 \\ 0.5320 & 0.3721 & 0.0870 & -0.0155 & -0.0007 \\ 0.2992 & 0.0870 & 0.6048 & -0.0010 & -0.0140 \\ 0.0023 & 0.0034 & 0.0002 & 0.9994 & -0.0000 \\ 0.0014 & 0.0003 & 0.0062 & -0.0000 & 0.9977 \end{bmatrix}$$

$$A_4 = \begin{bmatrix} 0.6445 & 0.3092 & 0.0377 & -0.0062 & -0.0004 \\ 0.6185 & 0.3489 & 0.0238 & -0.0141 & -0.0002 \\ 0.0755 & 0.0238 & 0.8915 & -0.0003 & -0.0170 \\ 0.0027 & 0.0031 & 0.0001 & 0.9995 & -0.0000 \\ 0.0003 & 0.0001 & 0.0075 & -0.0000 & 0.9963 \end{bmatrix}$$

$$A_5 = \begin{bmatrix} 0.6515 & 0.0511 & 0.2889 & -0.0008 & -0.0036 \\ 0.1023 & 0.8612 & 0.0274 & -0.0250 & -0.0002 \\ 0.5778 & 0.0274 & 0.3860 & -0.0003 & -0.0105 \\ 0.0003 & 0.0055 & 0.0001 & 0.9995 & -0.0000 \\ 0.0032 & 0.0001 & 0.004 & -0.0000 & 0.9987 \end{bmatrix}$$

$$A_6 = \begin{bmatrix} 0.6565 & 0.2338 & 0.1012 & -0.0040 & -0.0010 \\ 0.4677 & 0.4835 & 0.0398 & -0.0184 & -0.0003 \\ 0.2023 & 0.0398 & 0.7487 & -0.0004 & -0.0156 \\ 0.0018 & 0.0041 & 0.0001 & 0.9995 & -0.0000 \\ 0.0009 & 0.0001 & 0.0069 & -0.0000 & 0.9963 \end{bmatrix}$$

$$B_1 = \begin{bmatrix} -102.5000 & 0.0520 & 0.0000 & 0.0000 \\ 291.8000 & 0.0014 & 0.0000 & 0.0000 \\ -86.9500 & 0.0372 & 0.0000 & 0.0000 \\ 0.8762 & 0.0000 & -0.0001 & 0.0000 \\ -0.3226 & 0.0001 & 0.0000 & -0.0002 \end{bmatrix}$$

$$B_2 = \begin{bmatrix} -54.7100 & 0.0502 & 0.0000 & 0.0000 \\ 160.2000 & 0.0054 & 0.0000 & 0.0000 \\ -50.8700 & 0.0370 & 0.0000 & 0.0000 \\ 0.4987 & 0.0000 & -0.0001 & 0.0000 \\ -0.1991 & 0.0001 & 0.0000 & -0.0002 \end{bmatrix}$$

$$B_3 = \begin{bmatrix} 6.6090 & 0.0511 & 0.0000 & 0.0000 \\ 39.9800 & 0.0274 & 0.0000 & 0.0000 \\ -53.1900 & 0.0130 & 0.0000 & 0.0000 \\ 0.1436 & 0.0001 & -0.0001 & 0.0000 \\ -0.2340 & 0.0000 & 0.0000 & -0.0002 \end{bmatrix}$$

$$B_4 = \begin{bmatrix} 43.4700 & 0.0533 & 0.0000 & 0.0000 \\ 52.4100 & 0.0332 & 0.0000 & 0.0000 \\ -139.3000 & 0.0030 & 0.0000 & 0.0000 \\ 0.1645 & 0.0001 & -0.0001 & 0.0000 \\ -0.5667 & 0.0000 & 0.0000 & -0.0002 \end{bmatrix}$$

$$B_5 = \begin{bmatrix} -85.5300 & 0.0549 & 0.0000 & 0.0000 \\ 253.3000 & 0.0040 & 0.0000 & 0.0000 \\ -82.3400 & 0.0288 & 0.0000 & 0.0000 \\ 0.7762 & 0.0000 & 0.0001 & 0.0000 \\ -0.3254 & 0.0001 & 0.0000 & -0.0002 \end{bmatrix}$$

$$B_6 = \begin{bmatrix} 13.9200 & 0.0566 & 0.0000 & 0.0000 \\ 86.2700 & 0.0212 & 0.0000 & 0.0000 \\ -114.1000 & 0.0082 & 0.0000 & 0.0000 \\ 0.2892 & 0.0000 & -0.0001 & 0.0000 \\ -0.4795 & 0.0000 & 0.0000 & -0.0002 \end{bmatrix}$$